Synthesis and Characterization of Functional Inorganic Materials with a Layered Structure

（層状構造を持つ機能性無機材料の合成と評価）

Synthesis and Optical Property of Alkali Rare-earth Molybdate Nanoscroll from Layered precursor via H^+ Exchange Method without Organic Compound

2017

Mizuki Watanabe

Doctoral Program in Advanced Materials Science and Technology

Graduate School of Science and Technology, Niigata University

8050 Ikarashi 2-nocho, Niigata 950-2181, Japan 81, Japan

Preface

The works of this thesis have been carried out under the guidance of Associate Professor Dr. Kenji Toda at Graduate School of Science and Technology, Niigata University,8050 Ikarashi 2-nocho,Niigata 950-2181, Japan.

This thesis intendeds to synthesize new kind of nanoscroll material from layered molybdnium oxides by ion-exchange method at room temperature, to reveal their emission properties, and to build a new effective and useful design concept for nano materials obtained by H^+-exchange method.

The author wishes that the achievements obtained from this work provide positive information for the further development of luminescent materials.

Mizuki Watanabe

Graduate School of Science and Technology, Niigata University

8050 Ikarashi 2-nocho, Niigata 950-2181, Japan

Feb, 2017

Contents

Chapter 1

General Introduction

1.1 Background

Many functional ceramics are synthesized by the oldest and simplest method, the solid state reaction (SSR) method. The method is to mix solid starting materials (constitute metal oxides or carbonates) and then heat in furnace. The solid starting materials do not react together at room temperature over normal time scales and it is necessary to heat them at high temperatures, around or higher than 1000℃, in order for reaction to occur at an appreciable rate. Although the SSR method suit mass production, they offers a limited control of the final microstructure. The high-temperature synthesis is requited in order to promote sintering and, eventually, crystal growth of the solid. Therefore, it is difficult for the SSR method to reduce dimension (i.e. from three dimensions to one dimension) of the inorganic material and obtain inorganic materials with unique morphologies and tunable size.

Solution method at low temperature, such as sol-gel method [1, 2], hydrothermal method [3, 4], and co-precipitation method [5, 6] are used as size or morphology controllable method. The particles with various sizes and morphology can be homogeneously obtained by liquid-phase reaction, because the reaction need not high temperature operating resulting in the growth of particle, as compared with the SSR method. The particles, ranging from 1 nm to 100 nm, are generally called as “nano” particles. Nanoparticle shows various unique features in the morphological/structural

properties, thermal properties, electromagnetic, mechanical properties, and optical properties, as compared to miroro-scale crystals [7-12]. Inorganic nano materials with unique morphologies and tunable size or dimension have attracted much attention in chemistry and materials science.

Among of solution method, “soft-chemical method” using the principles of soft chemistry, or *chimie douce*—the French have coined the term firstly—has been investigated actively over the last few decades for the following two features:

1. Soft-chemical method requires lower energy than other method. It has advantage that reaction takes place at much lower temperatures than when using the SSR method. The SSR method have problem to be solved such as high energy cost due to heating operations and special conditions or equipment, such as high pressure furnace. Although solution method requires lower temperatures than the SSR method, it involves a higher cost and difficulty to handle on a large scale, because it requires special resolvable reagents, acid/base treatment, or waste liquid treatment.

2. Soft-chemical method is in the synthesis of new, metastable phases, which cannot be obtained by other routes; the metastable phases are kinetically stable to quite high temperature. The final metastable phase retained structural features of the precursor phase. For example, a new polymorpho of titanium dioxide, TiO_2(B) has been synthesized from the precursor phase $K_2Ti_4O_9$ with layered structure obtained by the SSR method [13]. The interlayer potassium ion in $K_2Ti_4O_9$ is exchanged to proton, forming $H_2Ti_4O_9 \cdot H_2O$. Finally, the new TiO_2(B) polymorph is obtained by heating and

dehydration. The crystal structure of TiO_2(B) phase retained feature of precursor phase $K_2Ti_4O_9$. The product materials obtained by the soft-chemical method often have the precursor-related structure—such reaction is called *topotactic reaction*.

Therefore, we focus on the soft-chemical method as a potentially powerful method in order to new functional inorganic nanomaterial controlling thermodynamically structural and morphological features at kinetic level.

1.2 Nanosheet obtained by soft-chemical method

"Nanosheet" is one of most interesting nanomaterials obtained by soft-chemical method. It is well-known that some clay compounds exfoliate to single layer in water and the colloidal suspensions are obtained [14-16]. With technology improvement, layered compound except clay compounds can exfoliate to single layer, such as, chalcogenides [17-19], phosphate [20-22] and oxides [23-33]—this is nanosheet. Nanosheet is two-dimensional materials which derived as a single layer from layered precursor material by exfoliation of layered compounds via soft-chemical procedure; it is the single crystal, because it preserves the structure of the layer in precursor compound. Exfoliation of various layered compounds with exchangeable cation interlayer has been reported, as listed in Table 1.1. Nanosheet has high anisotropic aspect morphology, whose thickness is about single nano meters and lateral size range from several hundred square nanometers to several square micrometers. It, therefore, is expected to behave as a new class of inorganic macromolecules. The interesting

properties of nanosheet have been reported, such as unique optical property differing from those of bulk materials [34, 35], luminescence property [36-38], dielectric property [39, 40], liquid crystallinity [41-42], and photocatalytic property with high activity due to their large surface area [43-48]. Especially, the nanosheet has attracted great attention as a well-defined *building block* to construct self-assembled nanostructure for designed catalyst, photonic band gap materials, and nanoscale electronic devices.

Table 1.1 Kind of nanosheet

Clay compounds	$Na_x(Al_{2-x}Mg_2)Si_4O_{10}(OH)_2 \cdot nH_2O$
Chalcogenides	TaS_2, NbS_2, MoS_2, WS_2
Phosphates	α-$Zr(HPO4)_2 \cdot H_2O$, $VOPO_4 \cdot 2H_2O$,
Ti oxides	$Cs_{0.7}Ti_{1.825}\square_{0.175}O_4$, $K_2Ti_4O_9$, $Na_2Ti_3O_7$
Nb oxides	$K_4Nb_6O_{17}$, KNb_3O_8
Ti-Nb oxides	$KTiNbO_5$, KTi_2NbO_7
Mn oxides	$K_{0.45}MnO_2$, $NaMnO_2 \cdot nH_2O$
Layered perovskites	$KCa_2Nb_3O_{10}$, $KLa_2Nb_2O_7$, $Bi_2W_2O_9$, $K_2NaCaTa_2O_{10}$, $K_2La_2Ti_3O_{10}$
Layered double hydroxides	$[Mg_{1-x}Al_x(OH)_2][(NO_3)_x \cdot nH_2O]$
Grapheme	—
Boron nitride	—

1.3 Nanorscroll

1.3.1 Kind of nanotube

Some of nanosheets roll up spontaneously and transform into one-dimensional morphology—this is nanoscroll. The thin film composed of nanosheets is possible to create novel materials. They, however, can be used as a building block only for thin film and substrate is required to build up nanosheet, as shown in Fig.1.2 (a). In contrast, one-dimensional materials, nanoscroll can be used as a building block more widely, ranging from one dimension to three dimensions without substrate, as shown in Fig. 1.2 (b).

One-dimensional materials are categorized to broad types—*nesting* and *scroll*—depending on the structure, as shown in Fig.1.1. One-dimensional materials with tubular

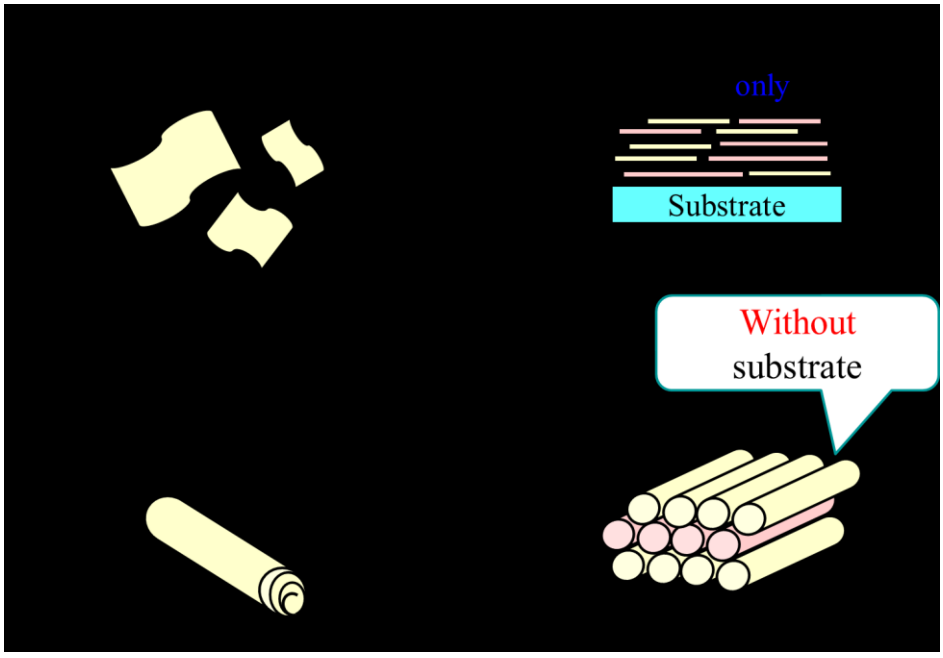

Fig. 1.1 Image of the application forms of nanosheet and nanoscroll as building blocks.

nesting structure such as layered chalcogenide WS_2 and MoS_2 nanotube [49, 50] and carbon nanotube [51] and boronnitride nanotube [52] have been reported increasingly. However, it is difficult to be prepared the single-crystalline nanotube doped a small amount of metal-ion such rare-earth ions exhibiting various excellent functions, because they are usually synthesized by the hydrothermal method based on resolution/reprecipitation reaction and a small amount of dopant ion are excluded from the crystal lattice. On the other hand, it is easy to be prepared single-crystalline nanoscroll—*scroll-type* oxide nanotube—doped a small amount of metal-ion such rare-earth ions. They are usually synthesized by the soft-chemical method based on topotactic reaction. Therefore, single-crystalline layer and nanoscroll could be easily obtained by doping metal-ions in the precursor structure, because the layer preserves the structure of the layer in the precursor. We, therefore, focused on oxide nanoscrolls, because nanoscroll has both advantages of nanosheet (single crystal) and nanotube (1D material).

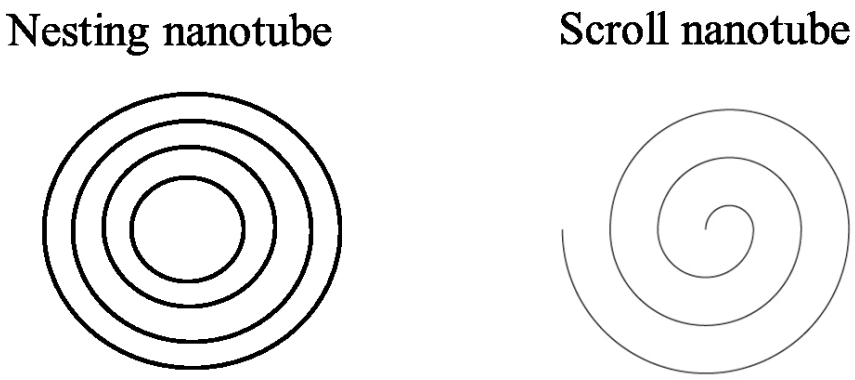

Fig. 1.2 Image of two type nanotube.

Although some nanotube like TiO_2 [53-55], V_2O_5 [56 -58] were obtained by the hydrothermal method, they could be obtained as nanoscroll or nanotube preserving the layered structure. In this study, we view these materials as to be nanotube.

1.3.2 Problem of nanoscroll: the type of oxide nanoscroll is limited.

However, nanoscroll is actually quite rare, such as $H_{0.70}Ti_{1.825}\square_{0.175}O_4 \cdot H_2O$ (□: vacancy) [59], $H_{0.13}MnO_2 \cdot 0.7H_2O$ [59], $HCa_2Nb_3O_{10} \cdot 1.5H_2O$ [59], Ruddlesden-Popper pahses $H_2[A_{n-1}B_nO_{3n+1}]$ (A= Na, Ca, Sr, La; B= Ta, Ti) [60], and $K_{4-x}H_xNb_6O_{17}$ (x= 3) [61]. In particular, the type of elements constructing matrix is limited. The oxide nanoscroll only with Ti, Ta, and Nb, up to now, have been reported, probably because many oxide with these transition metals form layered structure. Consequently, the property is also limited to photocatalystic properties [62, 63].

1.3.3 Problem of nanoscroll: Synthetic method

Nanocsroll are usually synthesized by two step processing, as shown in Fig. 1.3 : 1) H^+ exchange of the layered structure materials, and then 2) exfoliation of single layer using large amine i.e. tetrabutylammonium hydroxide (TBA^+OH^-). However, the adsorbed organic ions on the surface of nanoscroll usually result in the reduction of the opto-electric properties of nanoscroll materials. A new type environment-friendly synthetic method without organic solvent is necessary in order to efficiently use the nanoscrolls in optical and opto-electric devices and characterize optical and electric properties of pure nanoscroll themselves.

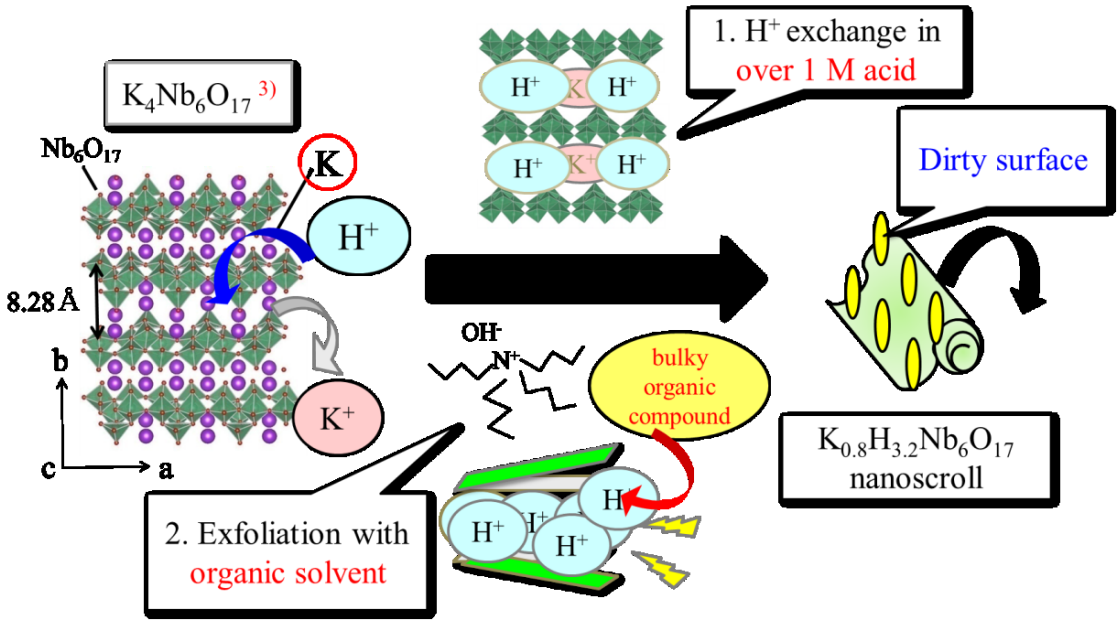

Fig. 1.3 Image of process for synthesis of nanoscroll.

1.3.4 What kind layer rolls up?

$H_xK_{4-x}Nb_6O_{17}$ nanoscrolls, which were obtained by exfoliation of layered niobate, $K_4Nb_6O_{17}$, are reported by Mallouk et al. and they explained that $(-Nb_6O_{17}-)_n$ sheets spontaneously rolled up by the difference of stress originating in asymmetric structure of the top and bottom of $(-Nb_6O_{17}-)_n$ sheets [61]. However, the similar behaviors have also been reported for layered structure materials having symmetric layers, such as $H_2CaNaTa_2O_{10}$ [60], $H_2SrTa_2O_7$ [60] and $H_{0.7}Ti_{1.825}\square_{0.175}O_4 \cdot H_2O$ [59]. It is possible, therefore, that there is no relationship between symmetry of layer sheets and rolling-up mechanism because not only asymmetric layer but also some symmetric sheets also rolled up—the rolling up mechanism is *still* unclear. In this study, therefore, we also investigated the relationship between the rolling up phenomena and symmetry of the layers.

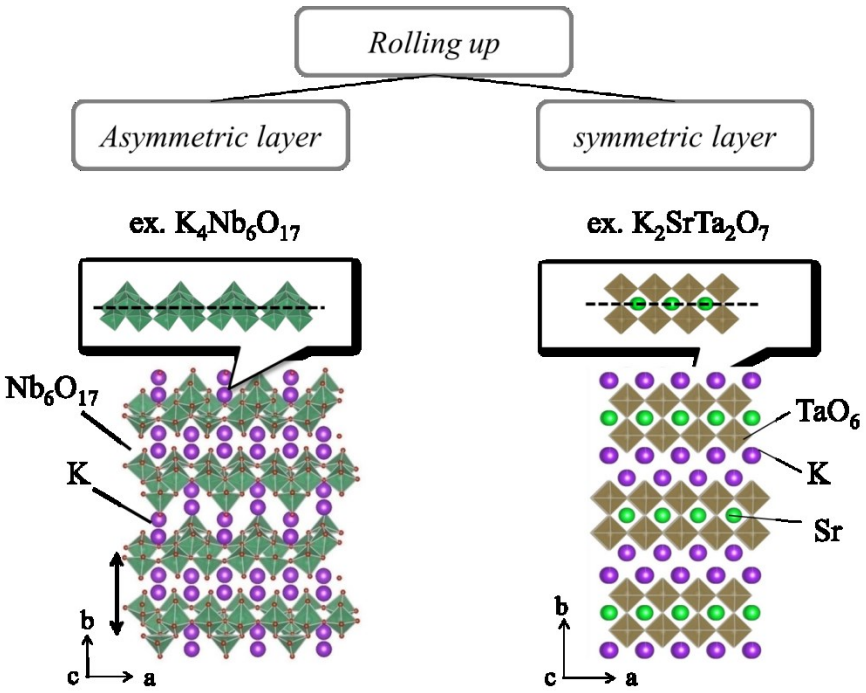

Fig. 1.4 Two type layer rolling up spontaneously.

1.4 Our suggestion of precursor

We focus on alkali metal rare-earth molybdate with general composition $ALn(MoO_4)_2$ (A: Alkali metal ion, Ln: rare earth ion) with layered structure as a new precursor for synthesis of nanoscroll, because of their structures and versatile properties, such as catalytic properties [64], photoluminescence properties [65, 66], and laser properties [67, 68]. Therefore, nanosheet and nanoscroll are expected as high-performance nanomaterials. Especially, we focus their photoluminescence property because rare earth molybdates show excellent photoluminescence and there are no reports of nanoscroll phosphor with rare-earth element in the crystal structure.

1.4.1 $ALn(MoO_4)_2$ with layered structure

The structure of the double rare-earth molybdates $ALn(MoO_4)_2$ are determined by the ionic radius of alkali metal ion and rare-earth ion; the structure was summarized in several investigations [69-71]. $ALn(MoO_4)_2$ (A= Li, Na) have the scheelite-type structure for all rare-earth elements, as shown in Fig. 1.5 (a) They have MoO_4 tetrahedra and the REO_8 units with an eight-coordination number. $KLn(MoO_4)_2$ forms $KLn(MoO_4)_2$ phases with the $KY(MoO_4)_2$-type structure observed only for RE= Dy–Lu. For RE= Eu, Gd, Tb, triclinic α-$KEu(MoO_4)_2$-type structure with the space group of *P*-1 [72] can be observed in $KLn(MoO_4)_2$ [69]. Fig. 1.5 (b) shows crystal structure of triclinic $KLn(MoO_4)_2$ with the space group of *P*-1. $KLn(MoO_4)_2$ contains $(Ln(MoO_4)_2)_n$ layers stacked along *c*-axis and exchangeable potassium cations between $(Ln(MoO_4)_2)_n$ layers. This is indicates that K^+ ion in the $KLn(MoO_4)_2$ was easily exchanged with another ions by the ion-exchanging method. In $(Ln(MoO_4)_2)_n$ layers, additionally, two MoO_4 tetrahedra situated in two Mo^{6+} site, respectively are unsymmetrically located on top and bottom of LnO_8 polyhedron. The lack of inversion symmetry $(Ln(MoO_4)_2)_n$ layers is expected to cause rolling up, if there is the relationship between symmetry of layer sheets and rolling-up mechanism. By confirming whether the $KLn(MoO_4)_2$ can roll up to nanoscroll via exfoliation, it, therefor, is possible to suggest a useful example for the elucidation of rolling-up mechanism.

In addition, other $ALn(MoO_4)_2$ layered structures have been reported: orthorhombic $KY(MoO_4)_2$-type structure with the space group of *Pbcn* [70], as described in Fig. 1.5 (c), and monoclinic $CsLu(SO_4)_2$-type structure with the space

group of *P*12/*c* 1 [71], as described in Fig. 1.5 (d), respectively. These type structures have something in common with α-$KEu(MoO_4)_2$-type structure. The affinity is that they are composed of $(Ln(MoO_4)_2)_n$ layers stacked along axis having two MoO_4 tetrahedra unsymmetrically located on top and bottom of LnO_8 polyhedron and exchangeable potassium cations between $(Ln(MoO_4)_2)_n$ layers, although two MoO_4 tetrahedra situated in only one Mo^{6+} site. Because of lack of inversion symmetry in their layers, therefore, $ALn(MoO_4)_2$ with those type structure is also expected to be protonated, to be exfoliated, and to roll up.

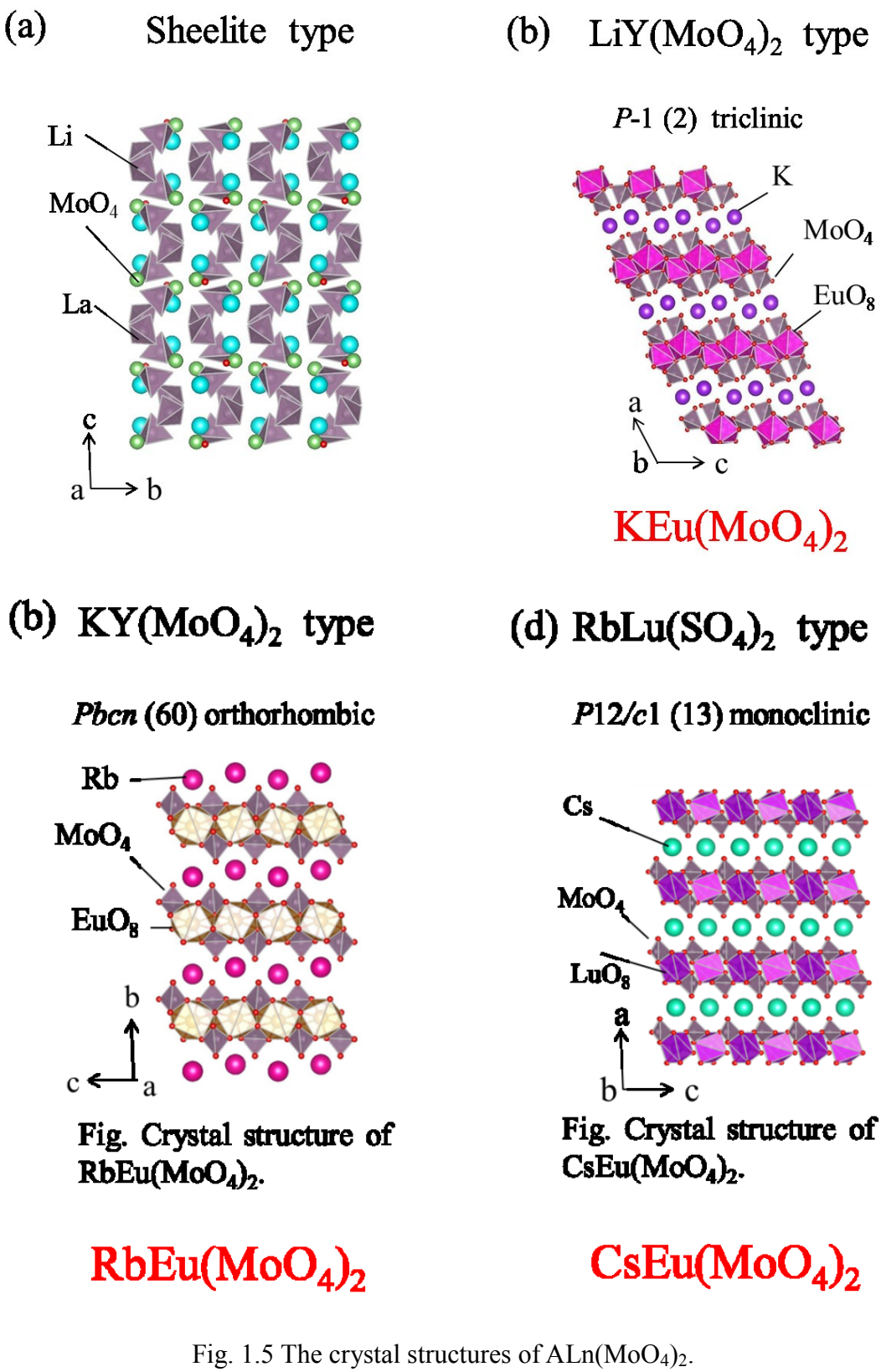

Fig. 1.5 The crystal structures of $ALn(MoO_4)_2$.

1.4.2 Approach for H^+ exchange and exfoliation of $ALn(MoO_4)_2$

However, there was no success in exchanging interlayer alkali metal ions by protons, exfoliating $ALn(MoO_4)_2$ into $Ln(MoO_4)_2$ nanosheet, and rolling up into $Ln(MoO_4)_2$ nanoscroll. Why are there no reports despite to layered structure with ion-exchangeable alkali ions? The reason is simple—It's because they *dissolve* in over 1 M concentrated acid which were used for conventional H^+ exchange method! As solution for this problem, we used *dilute acid*, one hundredth of concentration of conventional acid.

1.5 Objectives and scope of this thesis

Main goal of this study are states as follows;

1. Synthesis of a novel nanoscroll via soft-chemical procedure without organic solvent
2. Protonated and transformation of the layered oxides with rare-earth ions acting as emissive center, except Ti, Nb, and Ta containing oxides—$ALn(MoO_4)_2$
3. Characterization of luminescence property of obtained samples themselves without organic compounds
4. Development of luminescence properties of obtained samples

1.6 Composition of this thesis

This study is composed of seven chapters as follows;

In chapter 2, synthesis of H^+-exchanged $ALn(MoO_4)_2$ (Ln= K, Rb, Cs), detail observation of the morphology, and the photoluminescence property of the protonated

are described. Both *photoluminescence property* and *liquid crystallinity* of the solution dispersed $HEu(MoO_4)_2$ nanoscroll derived from $KEu(MoO_4)_2$ in de-ionized water are explained.

In chapter 3, red-emissive triclinic $KEu(MoO_4)_2$:Gd^{3+} were synthesized in order to suppress *concentration quenching* of the matrix by substitute Eu^{3+} with Gd^{3+}. The morphological and ptoluminescence properties of precursor powder and protonated powder are characterized.

In chapter 4, green-emissive triclinic $KEu(MoO_4)_2$:Gd^{3+} by substitute Gd^{3+} with Tb^{3+} were synthesized in order to obtained green-emissive phosphor nanoscroll and broaden the area of application. The morphological and ptoluminescence properties of precursor powder and protonated powder are characterized.

In chapter 5, synthesis of other nanoscrolls from orthorhombic $RbLn(MoO_4)_2$ (Ln = Pr, Nd, Sm, Eu), are discussed.

Finally, we summarize the morphological, structural, and photoluminescence properties of $Ln(MoO_4)_2$ nanoscroll in Chapter 6.

Reference

[1] J. Dhanaraj, R. Jagannathan, T. R. N. Kutty, and C.-H. Lu, *J. Phys. Chem. B*, **105** (2001) 11098–11105.

[2] M. Yu, J. Lin, Z. Wang, J. Fu, S. Wang, H. J. Zhang, and Y. C. Han, *Chem. Mater.*, **14** (2001) 2224–2231.

[3] R. Yan and Y. Li, *Adv. Funct. Mater.*, **15** (2005) 763–770.

[4] Z. Xu, X. Kang, C. Li, Z. Hou, C. Zhang, D. Yang, G. Li, and J. Lin, *Inorg. Chem.*, **49** (2010) 6706–6715.

[5] H. Lai, A. Bao, Y. Yang , Y. Tao, H. Yang, Y. Zhang, and L. Han, *J. Phys. Chem. C*, **112** (2008) 282–286.

[6] Y. Tian, X. Qi, X. Wu, R. Hua, and B. Chen, *J. Phys. Chem. C*, **13** (2009) 767–10772.

[7] K. Uchino. E. Sadanaga, and T. Hirose, *J. Am. Ceram. Soc.*, **72** (1989) 1555-1559.

[8] M. Takashige, T. Nakamura, *Jpn. J. Appl. Phycs.*, **20** (1981) 43-46.

[9] K. Ishikawa, K. Yoshikawa, and N. Okada, *Phys. Rev.*, **B37** (1988) 5852-5855.

[10] S. Sato, N. Asai, and M. Yonese, *Colloid Polym. Sci.*, **274** (1996) 889-893.

[11] K. Niihara, *J. Ceram. Soc. Japan*, **99** (1999) 974-982.

[12] F. Wakai, Y. Kodama, S. Sakaguchi, N. Murayama, K. Izaki, and K. Niihara, *Nature*, **344**, (1990) 421-423.

[13] R. Marchand, L. Brohan, and M. Tournoux, Mater. Res. Bull., **15** (1980) 1129-1133.

[14] G.F. Walker *Nature,* **187** (1960) 312-313.

[15] P.H. Nadeau, *Appl. Clay Sci.*, **2** (1987) 83-93 .

[16] A.J. Jacobson, *Mater. Sci. Forum*, **1** (1994) 152–153.

[17] A. Lerf, R. Schöllhorn, *Inorg. Chem.*, **16** (1977) , 16 , 2950–2956.

[18] P. Joensen, R.F. Frindt, S.R. Morrison, Mater. Res. Bull., **21** (1986) 457-461.

[19] F. Nazar, A. J. Jacobson , *Chem. Commun.*, (1986), 570 .

[20] G. Alberti, M. Casciola, U. Costantino, *J. Colloid Interface Sci.*, **107** (1985) 256-263

[21] G. Alberti, M. Casciola, U. Costantino, and R. Vivani, *Adv. Muter.*, **8** (1996), 291–303

[22] N. Yamamoto, T. Okuhara , and T. Nakato , *J. Mater. Chem.*, **11** (2001) 1858.

[23] H. Rebbah, M. M. Borel, and B. Raveau, *Mater. Res. Bull.*, 15 (1980), 317

[24] H. Rebbah, J. Pannetier, and B. Raveau, *J. Solid State Chem.*, **41** (1982), 57-62.

[25] L.F. Nazar, S. W. Liblong, and X.T. Yin, *J. Am. Chem. Soc.*, **113** (1991) 5889-5890.

[26] M. M.J. Treacy, S.B. Rice, and A.J. Jacobson, J.T. Lewandowski, *Chem. Mater.*, **2** (1990) 279-286.

[26] T. Sasaki and M. Watanabe, *J. Phys. Chem. B*, **101** (1997) 10159–10161.

[27] T. Sasaki and M. Watanabe, *J. Am. Chem. Soc.*, **120** (1998) 4682–4689.

[29] M. Fang, C. H. Kim, T. E. Mallouk, Chem. Mater., **11** (1999) , 1519–1525.

[30] T. Sasaki, M. Watanabe, H. Hashizume, H. Yamada, and H. Nakazawa, *J. Am. Chem. Soc.*, **118** (1996) 8329–8335.

[31] R.E. Schaak and T.E. Mallouk, *Chem. Mater.*, **12** (2000), 2513-3434.

[32] R.E. Schaak and T.E. Mallouk , *Chem. Mater.* **14** (2002) 1455–1471.

[33] J.-Y. Kim, I. Chung, J.-H. Choy, G.-S. Park, *Chem. Mater.*, **13** (2001) 2759–2761

[34] Q. Gao, O. Grialdo Wei Tong , and Steven L. Suib, *Chem. Mater.*, **13** (2001), 778–786.

[35] Y. Omomo , T. Sasaki, Lianzhou , and M. Watanabe, *J. Am. Chem. Soc.*, **125** (2003) 3568–3575.

[36] S. Ida, C. Ogata, M. Eguchi, W.J. Youngblood, T. E. Mallouk and Y. Matsumoto, *J. Am. Chem. Soc.*, **130** (2008) 7052–7059.

[37] S. Ida, C. Ogata , U. Unal , K. Izawa, T. Inoue, O. Altuntasoglu, and Y. Matsumoto, *J. Am. Chem. Soc.*, **129** (2007) 8956–8957.

[38] T. C. Ozawa, K. Fukuda, K, Akatsuka, Y. Ebina, and T. Sasaki, *Chem. Mater.*, **19** (2007) 6575–6580.

[39] B.-W. Li†, M. Osada, Y. Ebina, K. Akatsuka, K. Fukuda, and T. Sasaki, *ACS Nano*, **8** (2014,) 5449–5461.

[40] M. Osada, K. Akatsuka, Y. Ebina, H. Funakubo, K. Ono, K.Takada, and T.Sasaki, *ACS Nano*, **4** (2010) 5225–5232.

[41] N. Miyamoto and T. Nakato, *Adv. Mater.*, **14** (2002) 1267–1270.

[42] T. Nakato, N. Miyamoto, A. Harada, and H. Ushiki, *Langmuir*, **19** (2003) 3157–3163.

[43] N. Miyamoto and T. Nakato, *J. Phys. Chem. B*, **108** (2004) 6152–6159.

[44] K. Domen, A. Kudo, M. Shibata, A. Tanaka, K. Maruya, and T. Onishi, *J. Chem. Soc.*, *Chem. Commun.*, (1986) 1706–1707.

[45] A. Kudo, A. Tanaka, K. Domen, K. Maruya, Ken-ichi Aika, and T. Onishim, *J. Catal.*, **111** (1988) 67–76.

[46] Y. Ebina, T. Sasaki, M. Harada, and M. Watanabe, *Chem. Mater.*, **14** (2002) 4390–4395.

[47] Y. Okamoto, S. Ida, J. Hyodo, H. Hagiwara, and T. Ishihara, *J. Am. Chem. Soc.*, **133** (2011) 18034–18037.

[48] S. Ida, Y. Okamoto, M. Matsuka, H. Hagiwara, and T. Ishihara, *J. Am. Chem. Soc.*, **134** (2012) 15773–15782.

[49] R. Tenne, L. Margulis, M. Genut, and G. Hodes, *Nature*, **360** (1992) 444 – 446.

[50] Y. Feldman, E. Wasserman, D.J. Srolovitz, and R. Tenne *Science*, **267** (1995) 222–225.

[51] S. Iijima and T. Ichihash, *Nature*, **363** (1993) 603 – 605.

[52] N.G. Chopra, R.J. Luyken, K. Cherrey, V.H. Crespi, M.L. Cohen, S.G. Louie, and A. Zettl, *Science*, **269** (1995) 966-967.

[53] T. Kasuga, M. Hiramatsu, A. Hoson, T. Sekino, and K. Niihara, *Adv. Mater.*, **11** (1999) 1307–1311.

[54] C.-C. Tsai and H. Teng, *Chem. Mater.*,**18** (2006) 367–373.

[55] Y.Q. Wang, G.Q. Hua, X.F. Duana, H.L. Sunc, and Q.K. Xuec, Chem. Phys. Lett., **365** (2002) 427–431.

[56] B.D. Yao, Y.F. Chan, X.Y. Zhang, W.F. Zhang, Z.Y. Yang, and N. Wang, *Adv. Mater.*, **82** (2003) 281-283.

[57] F. Krumeich, H.-J. Muhr, M. Niederberger, F. Bieri, B. Schnyder, and R. Nesper,

J. Am. Chem. Soc., **121** (1999) 8324–8331.

[58] H.-J. Muhr, F. Krumeich, U. P. Schönholzer, F. Bieri, M. Niederberger, L. J. Gauckler, and R. Nesper, *Adv. Mater.*, **12** (2000) 231–234.

[59] R. Ma, Y. Bando, and T. Sasaki, *J. Phys. Chem. B*, **108** (2004) 2115–2119.

[60] R. E. Schaak and T. E. Mallouk, *Chem. Mater.*, **12** (2000) 3427–3434.

[61] G.B. Saupe, C.C. Waraksa , H.-N. Kim , Y.J. Han , D.M. Kaschak , D. M. Skinner, and T.E. Mallouk, *Chem. Mater.*, **12** (2000) 1556–1562.

[62] K. Maeda, M. Eguchi, S.-H. A. Lee, W.J. Youngblood, H. Hata, and T.E. Mallouk, *J. Phys. Chem. C*, **113** (2009) 7962–7969.

[63] K. Maeda, M. Eguchi, W.J. Youngblood, and T.E. Mallouk, *Chem. Mater.*, **20** (2008) 6770–6778.

[64] S.S. Liu, D.P. Yang, D.K. Ma, S. Wang, and T.D. Tang, *Chem. Commun.*, **47** (2011) 8013–8015.

[65] Z Wang, H Liang, M Gong, Q Su J. Alloy. Compd., **432** (2007) 308–312.

[66] S. Neeraja, N, Kijima, A.K Cheetham, Chem. Phys. Lett., **387** (2004) 2–6.

[67] S.B. Stevens, C.A.Morrison, T.H. Allik, A.L. Rheingold, and B.S. Haggerty *Phys. Rev. B*, **43** (1991) 7386 – 7394.

[68] V. Volkov, C. Cascales, A. Kling, and C. Zaldo, *Chem. Mater.*, **17** (2005) 291–300.

[69] P. V. Klevtsov and R. F. Klevtsva, *J. Struct. Chem.*, **18** (1977) 419– 439.

[70] O.D. Chimitova, V.V. Atuchin, B.G. Bazarova, M.S. Molokeev, and Z.G. Bazarova, *Proc. of SPIE*, **3771** (2013) 87711A-1– 9.

[71] V.V. Atuchin O.Y. Khyzhun, O.D. Chimitova, M.S. Molokeev, T.A. Gavrilova, B.G. Bazarov, and J.G. Bazarova, *J. Phys. Chem. Solids*, **77** (2015) 101–108.

[72] R.F. Klevtsova, L.P. Kozeeva, and P.V. Klevtsov, *Kristallografiya*, 19 (1974), 89– 94.

Chapter 2

Synthesis and Photoluminescence Properties of $HEu(MoO_4)_2$ Derived from Layered Molybdate $AEu(MoO_4)_2$ (A=K, Rb, Cs) by H^+-exchange Method

2.1 Introduction

Nanophosphors, recently, were actively investigated due to their potential applications in the flat panel displays, solar energy converters, optical amplifiers, electroluminescenct devices, photodiodes, bio-detectors, sensors, and color display. They are also significantly important material in the field of luminescence because they exhibit excellent optoelectronic properties [1-5]. Among these applications, solar energy converters have been received much attention during the last few decades [6-8]. The crystal Si solar cells were widely used on an industrial scale, because of its low cost and high electrical conversion efficiency. However, the efficiency limit of crystal Si solar cells was approximately 30%, which is considered to be the mismatch between the incident solar photon spectrum and the energy band gap of silicon. In particular, silicon has low optical absorption below 400 nm (Fig. 2.1). Therefore, various schemes have been proposed to overcome this fundamental efficiency limit for the crystal Si solar cells [9-16]. Among these schemes, one way to surpass this limit is using a luminescence down-shifting process to absorb high-energy photons and re-emit them at longer wavelengths such that the photovoltaic device exhibits a significantly better

response. Therefore, investigations have been devoted to search for new high efficiency down-conversion nanophosphors, which can show excellent optical absorption below 400 nm.

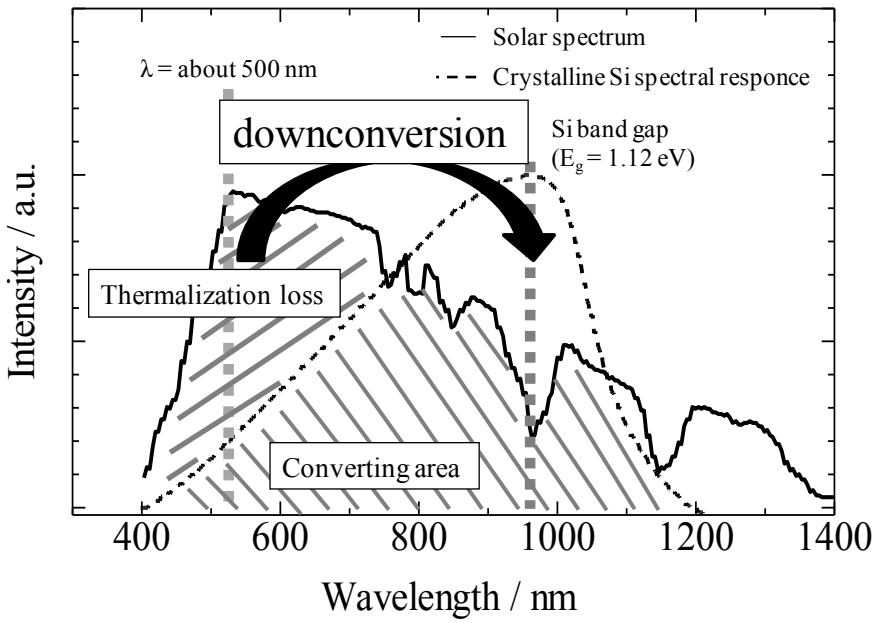

Fig. 2.1 Downconversion for crystalline Si solar cell.

The triclinic $KEu(MoO_4)_2$ with α-$KEu(MoO_4)_2$-type layered structure [17] exhibits red emission (over 600 nm) attributed to f-f transition of Eu^{3+}[18-20]. The optical property—optical absorption (below 400 nm) and red emission (around 614 nm)—is suitable for a spectral-converter phosphor for crystalline Si solar cells, enhancing the energy conversion efficiency. The nanoparticle of $KEu(MoO_4)_2$ is a good candidate for spectral-converter phosphor. This study, therefor, is aimed at synthesis of nanomaterial of $KEu(MoO_4)_2$ originated to precursor layered structure by soft-chemical H^+ exchange method. In addition, $RbEu(MoO_4)_2$ and $CsEu(MoO_4)_2$ have layered

structures; they have orthorhombic $KY(MoO_4)_2$-type structure with the space group of *Pbcn*, and monoclinic $CsLu(SO_4)_2$-type structure with the space group of *P*12/*c*1, respectively [21-23]. Although they contain Eu^{3+} acting as emission center in the crystalline lattice, there are few reports of their luminescence properties; detail structural and luminescence property of $CsGd_{1-x}Eu_x(MoO_4)_2$ solid-solution phosphor, recently [21], has been reported. Thus, their nanoparticle is also expected as novel nanophosphor by soft-chemical H^+ exchange method.

In this chapter, we confirm whether alkali metal cations in the layered molybdates $AEu(MoO_4)_2$ (A=K, Rb, Cs) are exchanged by protons in dilute (0.01 M) HNO_3 aqueous solution or not. The morphology and luminescence properties of protonated powders are also investigated. In addition, re-dispersibility—this property is required to apply for practical thin film in display or wavelength converter of crystalline Si solar cell—dried $HEu(MoO_4)_2$ powder and the photoluminescence property solution dispersed $HEu(MoO_4)_2$ to deionized water was investigated.

2.2 Experimental

2.2.1 Synthesis of materials

Precursor powder, $AEu(MoO_4)_2$ was synthesized by a conventional solid-state reaction method. A mixture of K_2CO_3 (purity 99.95%; Kanto Chemical Co. Inc.), Rb_2CO_3 (purity 97%; Wako Pure Chemical Industies, Ltd.), and Cs_2CO_3 (purity 99.99%; Kanto Chemical Co. Inc.), Eu_2O_3 (purity 99.99%; Shinetsu Chemical Co. Inc.), and MoO_3 (purity 99.99%; Kojundo Chemical Co. Inc.) was mixed using a mortar with acetone for 15 min, and then the mixture was calcined at 700°C for 6 h in air. $HEu(MoO_4)_2$ powders were obtained by stirring of $AEu(MoO_4)_2$ (0.5 g) in 0.01 M aqueous HNO_3 solution (100 mL) at room temperature for 7 days in order to exchange alkali metal ions to proton. The acid solution was refreshed once several days to complete H^+ exchange. After stirring, the solution was isolated suction filtration with membrane filter (ADVANTEC MFS, INC., mixed cellulose ester, pore size: 0.45μm, diameter: 47 mm). The sample was washed with deionized water for 24 h and then dried at 50 °C for 24 h.

2.2.2 Materials characterization

The obtained samples were characterized by X-ray powder diffraction (XRD; Mac Science Ltd., MX-Labo) to identify the crystal structure and the sample composition was analyzed by X-ray fluorescence analysis (XRF; Seiko Instruments Inc., SEA 1200VX). Morphology of the samples was characterized by means of scanning electron microscopy (SEM; 5310MVB, JEOL Ltd.) and transmission electron microscopy (TEM; JEM-1200EX, JEOL Ltd.). The emission (PL) and excitation (PLE)

spectra were measured at room temperature with a spectrofluorometer (Jasco Corp., FP-6500/6600), where the emission spectra were obtained for excitation at 396 nm, and excitation spectra were obtained for emission at 612 nm. The Raman spectrum in the range of 50-1200 cm^{-1} was investigated using a 532 nm laser as an excitation source (LabRAM, Horiba). Polarized-light microscopy observation of liquid crystal phase of $HEu(MoO_4)_2$ in a capillary was performed with a Olympus BX60.

2.3 Result and discussion

Structural and Morphological properties

To synthesize nanophosphors, the obtained $AEu(MoO_4)_2$ phosphors were stirred in HNO_3 aqueous solution at room temperature. The $AEu(MoO_4)_2$ powders, however, were completely dissolved in highly concentrated HNO_3 solution above 0.05 M during the stirring process for several hours. In contrast, for the samples stirred in 0.01 M aqueous HNO_3 solution for 7 days, the alkali metal ions of the $AEu(MoO_4)_2$ phosphors were successfully exchanged by H^+ without particle dissolution. The composition of $AEu(MoO_4)_2$ before and after H^+ exchange was analyzed by XRF. The compositions are based on amount of Mo. In all sample powder, the amount ratios of Mo and Eu maintain after H^+ exchange procedure. On the other hand, there was remarkable change of amount of alkali metal ions. Fig. 2.2 shows the amount of alkali metal ions in the phosphors before and after H^+ exchange procedure. Fig. 2.2 (a), (b), and (c) revealed that the composition of $KEu(MoO_4)_2$ and after-protonated $KEu(MoO_4)_2$, $RbEu(MoO_4)_2$ and after-protonated $RbEu(MoO_4)_2$, and $CsEu(MoO_4)_2$ and after-protonated $CsEu(MoO_4)_2$. The precursor powders of $KEu(MoO_4)_2$, $RbEu(MoO_4)_2$, and $CsEu(MoO_4)_2$ are described K-form, Rb-form, and Cs-form, respectively; the protonated powders are described HK-form, HRb-form, and HCs-form, respectively. In all samples, the ratio of Eu and Mo basically retains after H^+ exchange, suggesting the framework of the precursor structure preserves. On the other hand, the ratio of remaining K^+, Rb^+, and Cs^+ in protonated powders is 3.5, 0.1, and, 4.2 %, respectively, as summarized in Fig. 2.2 (d). In all sample, the amount of alkali metal ions in the

protonated powders was reduced less 5%. This result indicates that K ion, Rb ion, and Cs ion in $KEu(MoO_4)_2$, $RbEu(MoO_4)_2$, and $CsEu(MoO_4)_2$, respectively were successfully exchanged by H^+, retaining their framework.

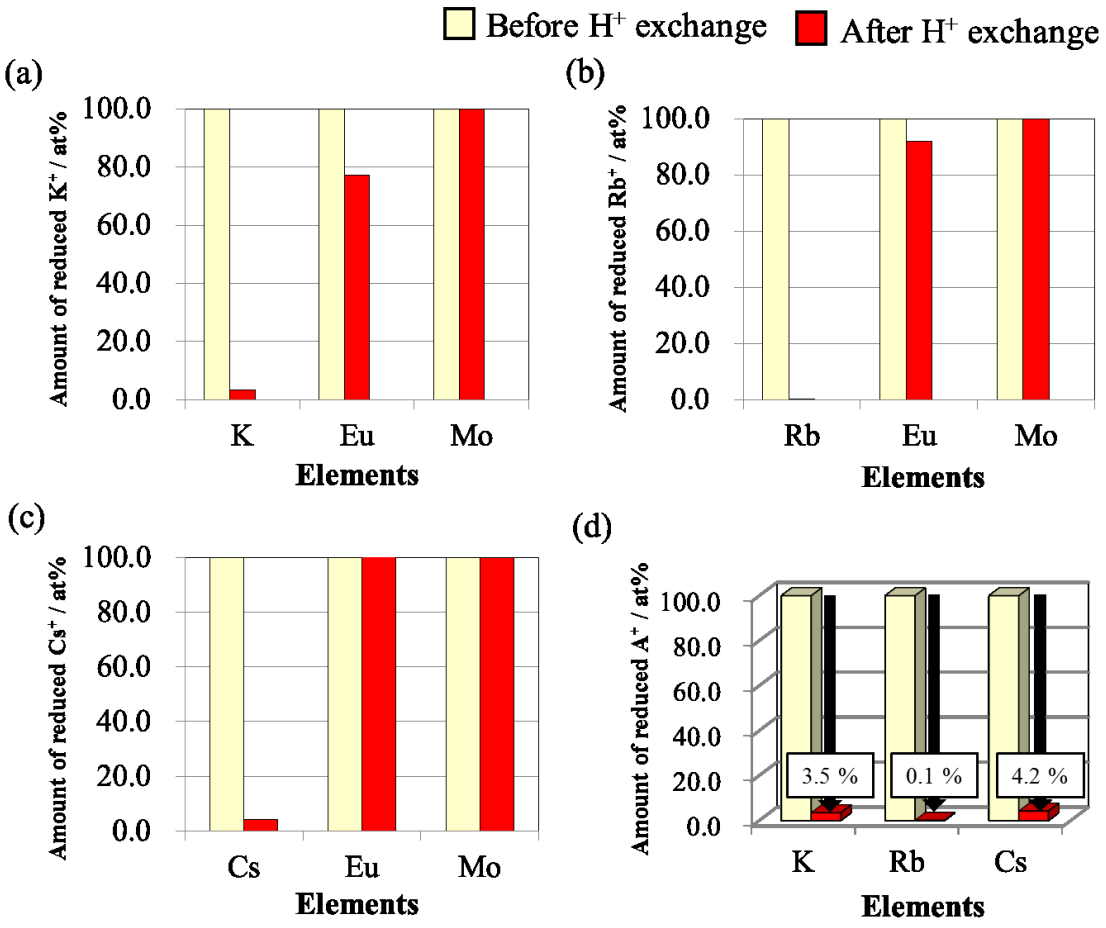

Fig. 2.2 XRF results of before and after (a) $KEu(MoO_4)_2$ (b) $RbEu(MoO_4)_2$, and (c) $CsEu(MoO_4)_2$ powder. The precursor powders were synthesized by a conventional solid state method and dried protonated powder were obtained by H^+-exchange method using 0.01 M HNO_3 for 7 d.

Table 1 summarizes the condition of H^+ exchange method in the previous works of nanoscrolls. It's noteworthy that H^+ exchange of $AEu(MoO_4)_2$ proceeded in the diluter acid, compared with the previous works—the concentration of the acid solution which was used for H^+ exchange of $AEu(MoO_4)_2$ is about one-hundredth of the previous works—although the H^+-exchange reaction time of $AEu(MoO_4)_2$ was similar to that of the previous works. This result suggests that $AEu(MoO_4)_2$ have the faster proton exchange rate than other layered oxide containing Ta, Nb, and Ti. Probably, the difference of the proton exchange rate between $AEu(MoO_4)_2$ and other layered oxide containing Ta, Nb, and Ti is due to the difference in H^+ conductivity, causing from the difference in the charge density of the interlayer contributed by the central ions (Mo^{6+}, Ta^{5+}, Nb^{5+}, and Ti^{4+}) of the MoO_4, TaO_6, NbO_6, and TiO_6 polyhedra; the charge density of the central ions are proportional to the valence (Mo^{6+}, Ta^{5+}, Nb^{5+}, and Ti^{4+}).

Table 1 The condition of H^+ exchange method in the this work and previous works of nanoscrolls

	acid	Concentration	Time	Temperature	Ref.
$K_{4-x}H_xNb_6O_{17}$	HCl	1-3 M	7 d	40℃	[24]
$Ti_{0.91}O_2$	HCl	1 M	several-time change of the acid solution	room temperature	[25, 26]
MnO_2	HCl	1 M	10 d	room temperature	[25, 27]
$Ca_2Nb_3O_{10}$	HNO_3	4 M	12 h	room temperature	[25, 28]
$La_2Ti_3O_{10}^{2-}$	HNO_3	1 M	5 d	room temperature	[29]
$TBA_xH_{2-x}SrTa_2O_7$	HNO_3	0.1 M	5 d	room temperature	[29]
$HEu(MoO_4)_2$	HNO_3	**0.01 M**	**7 d**	room temperature	this study

Fig. 2.3 shows the powder XRD patterns of the precursor $AEu(MoO_4)_2$ powder and $HEu(MoO_4)_2$ powder prepared by the H^+ exchange of $AEu(MoO_4)_2$. As shown in Fig. 2.3 (a), (b), and (c), all observed diffraction patterns of the precursor powder were well indexed the standard XRD pattern of triclinic α-$KEu(MoO_4)_2$-type structure with the space group of *P*-1, orthorhombic $KY(MoO_4)_2$-type structure with the space group of *Pbcn*, and monoclinic $CsLu(SO_4)_2$-type structure with the space group of *P*12/*c*1, respectively; the standard diffraction patterns were obtained from the inorganic crystal structure database (ICSD). In contrast, the XRD patterns of protonated powders were different from those of the precursor powders. This result indicates that the structures changed by H^+ exchange. The detail crystal structures, unfortunately, have not been revealed yet. Fig. 2.3 (d) shows the summarized XRD patterns of protonated powder derived from $AEu(MoO_4)_2$. All protonated powders have the new diffraction peaks (in blue area) which are not detected in the precursor powders; the new peaks are situated the similar area in all protonated powders. This result indicates that all protonated powders have similar structure by H^+ exchange.

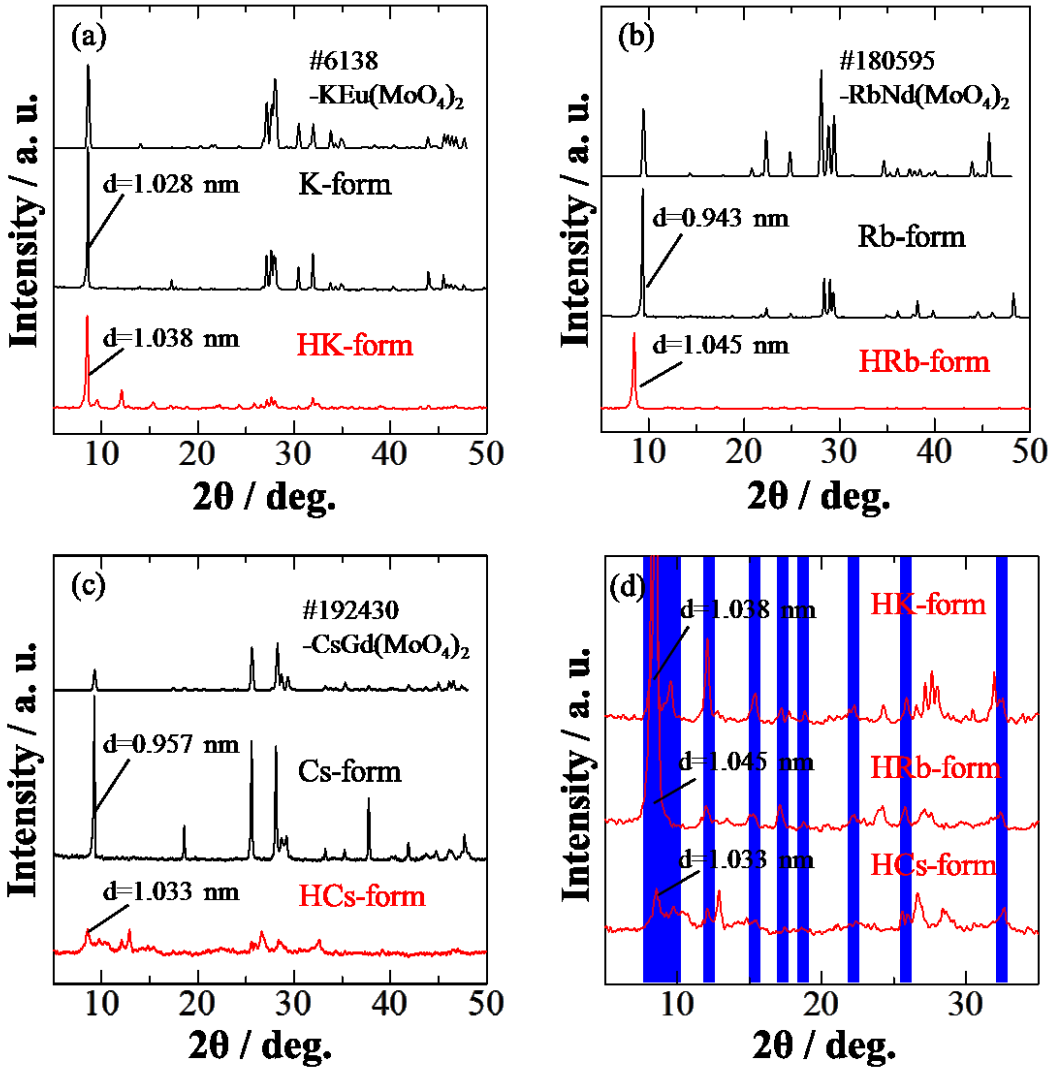

Fig. 2.3 The XRD patterns of (a) precursor $KEu(MoO_4)_2$ (K-form) powder and protonated (H-form) powder, (b) precursor $RbEu(MoO_4)_2$ (Rb-form) powder and protonated (H-form) powder, (c) precursor $CsEu(MoO_4)_2$ (Cs-form) powder and protonated (H-form) powder, and (d) all protonated powders. All A-form (A=K, Rb, Cs) powders were synthesized by a conventional solid state method. All dried H-form powders were obtained by stirring in 0.01 M HNO_3 at room temperature for 7 d and drying.

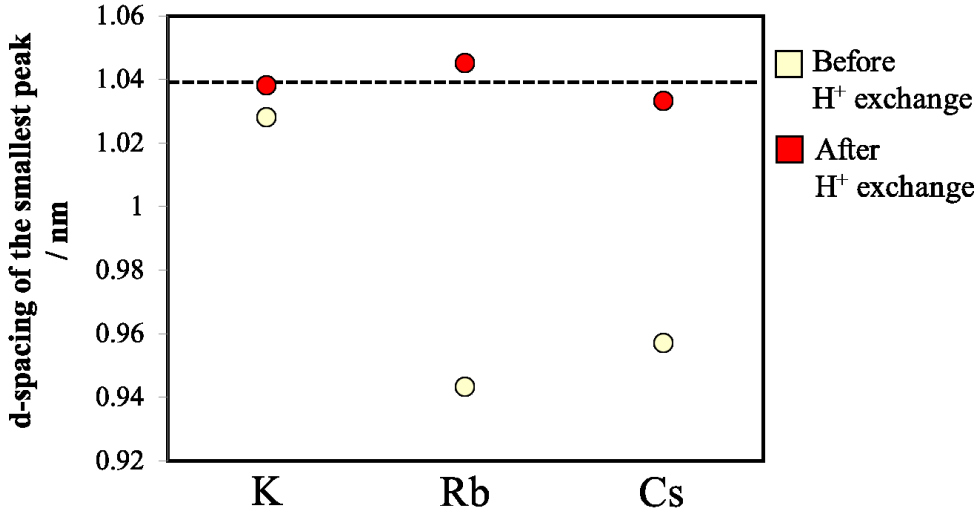

Fig. 2.4 The d-spacing of the smallest peak in the precursor and protonated powders, indicating the interlayer distance. The broken line shows the average d-spacing after H^+ exchange.

The *d*-spacing of peaks at the smallest angle reflect the interlayer distances of precursor powders with layered structure. Fig. 2.4 shows the value of *d*-spacing of the smallest peak in the precursor (between *d*=0.94 and 1.03 nm) and protonated (around *d*=1.04) powders. Although the *d*-spacing of the smallest peak of precursor powders were different, those of protonated powders were similar, indicating that all protonated powders form similar large-distance structure by H^+ exchange regardless of that of precursors.

Fig. 2.5 shows the SEM images of the precursor $AEu(MoO_4)_2$ powders and $HEu(MoO_4)_2$ powder prepared by the H^+ exchange of $AEu(MoO_4)_2$. The particles of precursor K-form, Rb-form, and Cs-form have a granular particle morphology; the particle sizes in all samples were over 10 μm. On the contrary, the protonated powders

show different result from the precursor powders. HK-from, HRb-form, and HCs-form have rod-like particle morphology, as shown in Fig. 2.5 (a-c). The high-magnification images inserted in Fig. 2.5 (d-f) revealed that the rod-like particles contained smaller rod-like particles and formed bundles. The rod-like particle in bundles are 10 - 30 μm in average length, and most have outer average diameters ranging from 270 to 300 nm. These results indicate that the particle size and morphology of $AEu(MoO_4)_2$ were successfully changed by the H^+-exchanging in the alkali metal site, although the sample after H^+-exchanging was maintain layered crystal structure.

To gain a better understanding of the mechanism of morphological change, we have studied the time course of the reaction by TEM. Fig. 2.6 depicts TEM images of protonated powder obtained after different reaction times. After reacting for 12 h, intermediate which thin sheet are kinking and spontaneously rolling up—as a *spill* formed by twisting of paper—can be seen shown in Fig. 2.6 (a). The rolling-up transformation occurred at the same time as exchanging K^+ into H^+; exfoliation phenomena also occurred at same time. This result suggests that the nanoscrolls of HK-form powder was successfully obtained by H^+ exchange procedure. Eventually, uniformly sized nanoscrolls with an outer diameter of 20 nm were obtained. The nanoscrolls spontaneously gathered and lined up, as shown in Fig. 2.6(d); the outer diameter of bundled nanoscrolls was coincided with that of rod-like particles in Fig. 2.5(d). It is noteworthy that $HEu(MoO_4)_2$ nanoscrolls formed self-assemble bundles under the condition which no organic compound with positive charge exist; it's very rare case, because self-assembly of the particles are used organic compound and

polymer [30-39]. In this study, $HEu(MoO_4)_2$ nanoscrolls probably gathered using H^+/H_3O^+ ions as counter cations and formed H^+/H_3O^+ bridging bond like Mo-O-H^+/H_3O^+-O-Mo. Unfortunately, the condition of H^+/H_3O^+ in H-form powders remain incompletely understood.

In previous study, the exfoliation of layer parts from precursors and rolling up of the layers is observed via not only H^+ exchange but also reaction with organic compound, because electrostatic interaction between layers is strong in most precursors of nanosheet and nanoscroll, transition metal oxide [40, 41]. Why exfoliation of $(Eu(MoO_4)_2)_n$ layers from $KEu(MoO_4)_2$ occurs only by H^+ exchange? We consider the answer in terms of the difference in electronegativities of elements contained in the precursor structures. In Nb-containing precursor $K_4Nb_6O_{17}$, for instance, the difference between the electronegativities of Nb^{5+} (1.6) [42] and O^{2-} (3.44) [42] in $(Nb_6O_{17})_n$ layers is 1.84 and that of inter layer K^+ (0.8) [42] and O^{2-} (3.44) [42] shared with NbO_8 polyhedra in $(Nb_6O_{17})_n$ layers is 2.62. On the other hand, in case of $KEu(MoO_4)_2$, the difference between the electronegativities of Mo^{6+} (2.16) [42] and O^{2-} (3.44) [42] in $(Eu(MoO_4)_2)_n$ layers is 1.36 and that between inter layer K^+ (0.8) [42] and O^{2-} (3.44) [40] shared with MoO_4 tetrahedra and EuO_8 polyhedra in $(Eu(MoO_4)_2)_n$ layers is 2.62. The difference between the electronegativities of Mo-O, obviously, is smaller than that of Nb-O, indicating that Mo-O is more covalently bound than Nb-O. As a result, the difference of combinative capability between Mo-O and K-O in $KEu(MoO_4)_2$ is clearer than that of combinative capability between Nb-O and K-O in $K_4Nb_6O_{17}$. Consequently, electrostatic interaction between ion-exchangeable alkali metal ion interlayers and the

$(Eu(MoO_4)_2)_n$ layers in is weaker than that between ion-exchangeable alkali metal ion interlayer and $(Nb_6O_{17})_n$ layers. In case of other nanosheet or nanoscroll precursors with Ti, and Ta, the difference between the electronegativities of Ti-O and Nb-O is 1.9 and 1.94, respectively; the value is larger than that of Mo-O, 1.36. The weaker electrostatic interaction between interlayer K ions and the $(Eu(MoO_4)_2)_n$ layers caused exfoliation only by H^+ exchange. However, the detail of rolling-up mechanism of $AEu(MoO_4)_2$ are not clear.

Furthermore, $(Eu(MoO_4)_2)_n$ layers spontaneously rolled up only by H^+ exchange. The rolling-up behaviors mechanism might be similar to that of nanoscroll derived from $K_4Nb_6O_{17}$. The spontaneous rolling up caused by lack of inversion symmetry of $(Eu(MoO_4)_2)_n$ layers, as shown in Fig. 1.(b). MoO_4 tetrahedrons are located one above the other unsymmetrically in $Eu(MoO_4)_2$ single layer and a space-filling of the top and the bottom of a shingle sheet are different. The rolling-up phenomena of $RbEu(MoO_4)_2$ and $CsEu(MoO_4)_2$, as in case with $KEu(MoO_4)_2$, could be accounted for in terms of their crystal structure with asymmetric layer. Additionally, the pH is important in controlling the rolling-up/unrolling-up equilibrium. Below about pH 7, the particles begin to aggregate, and consequently form tubular morphology, because the solution conditions are unsuitable to attain well-dispersed colloids [43, 44]. The rolling up of $AEu(MoO_4)_2$ after exfoliation, therefore, is prompted by not only the symmetric layer morphology but also the acidic condition.

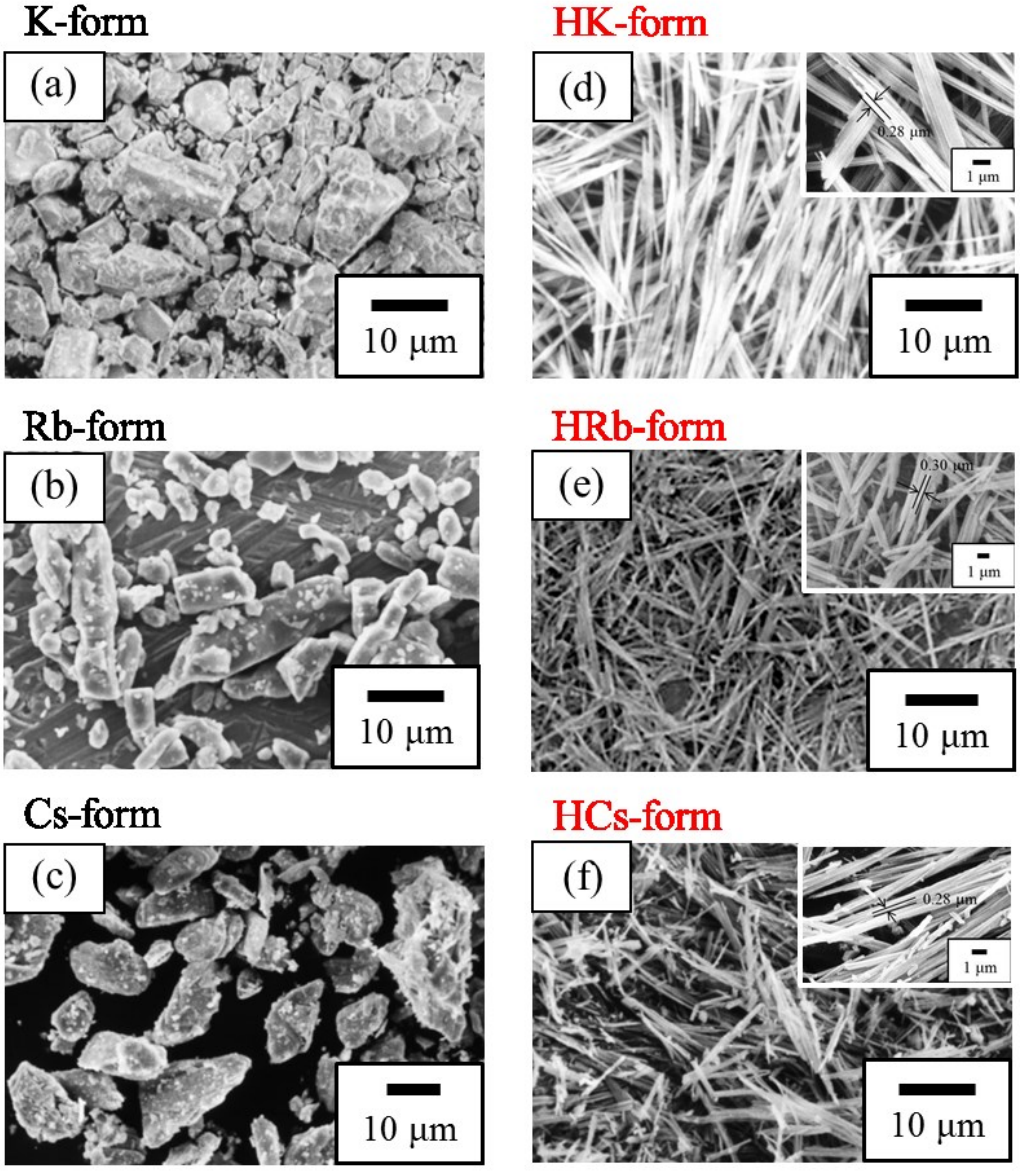

Fig. 2.5 The SEM images of precursor powder (a) $KEu(MoO_4)_2$ (K-form), (b) $RbEu(MoO_4)_2$ (Rb-form), and $CsEu(MoO_4)_2$ (Cs-form) and protonated powder (d) HK-form, (e) HRb-form, and (f) HCs-form. All precursor A-form (A=K, Rb, Cs) powders were synthesized by a conventional solid state method. Inset in (d)-(f) are high-magnification SEM images. All dried H-form powders were obtained by stirring in 0.01 M HNO_3 at room temperature for 7 d and drying.

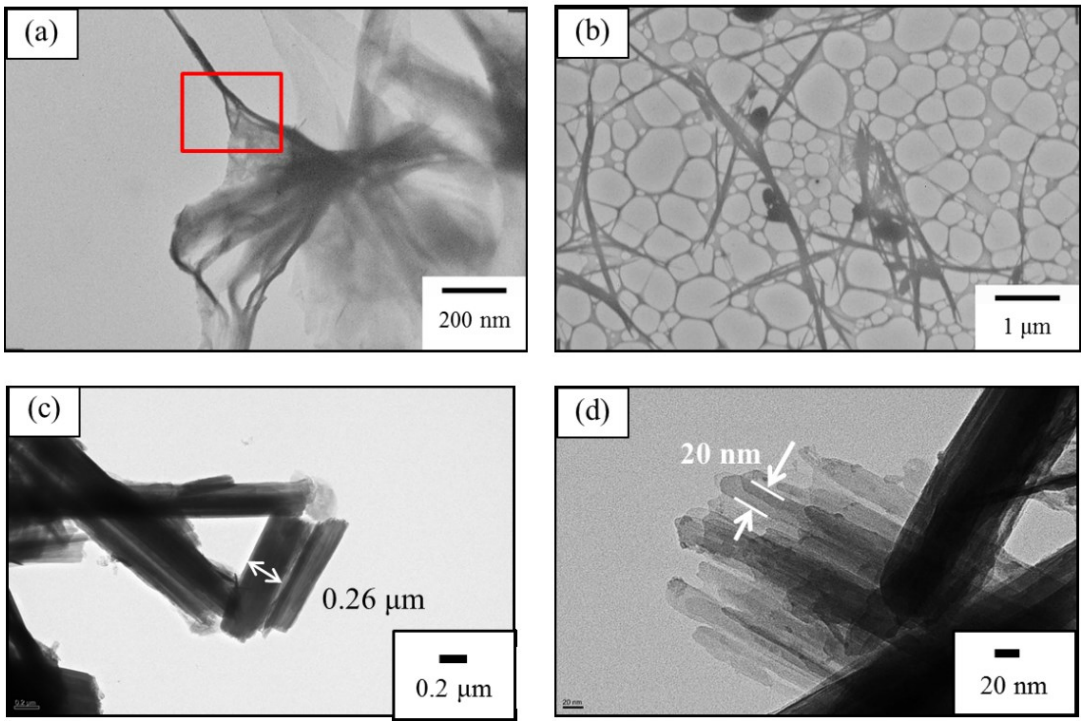

Fig. 2.6 The TEM images of protonated HK-form powder obtained after reacting for (a) 12 hours, (b) 2 days, and (c) 7 days and (d) the high-resolution TEM images of protonated powder obtained after reacting for 7 days.

Optical properties

Fig. 2.7 shows the excitation and emission spectra of the precursor $AEu(MoO_4)_2$ powder and $HEu(MoO_4)_2$ powder prepared by the H^+ exchange of $AEu(MoO_4)_2$. The excitation spectra of K-form, Rb-form, and Cs-form powders shows a broad O^{2-}-Mo^{6+} charge transfer (CT) band and some strong narrow peaks were observed between 360 and 500 nm, and were attributed to the 4f-4f transitions of the Eu^{3+} ion; the emission spectra of them show some strong narrow peaks were observed, coincided to the 4f-4f transitions of the Eu^{3+} ion. the emission peak intensity corresponding to the $^5D_0$–$^7F_2$ electric dipole transition at 614 nm is higher than that of the $^5D_0$–$^7F_1$ magnetic dipole transition at 592 nm, suggesting that the Eu^{3+} ions occupy sites in the $KEu(MoO_4)_2$ lattice without inversion symmetry. In addition, it is noted that the CT band of Eu^{3+}-O^{2-} is not clearly observed in the excitation spectra due to the possible overlap of the CT band with that of molybdate group [45-47]. On the order hand, the excitation absorption band of the CT transition of O^{2-}-Mo^{6+} of HK-form, HRb-form, and HCs-form shifts to the longer wavelength side with H^+-exchanging and the excitation absorption band of the CT band of Eu^{3+}-O^{2-} is clearly observed in the excitation spectra. The excitation peak shift with H^+ exchanging can be explained by the change of the interaction with the environment around the Mo^{6+} ion in the host lattice. The position of the excitation band of MoO_x groups depends on the coordination number x. With increasing the coordination number of Mo ions in the host matrices, the position of CT band shifts to longer wavelength, because higher coordination number of Mo ion leading to a longer and weaker Mo^{6+}-O^{2-} bond [48]. The CT band edge of H-form powders (450 nm) is

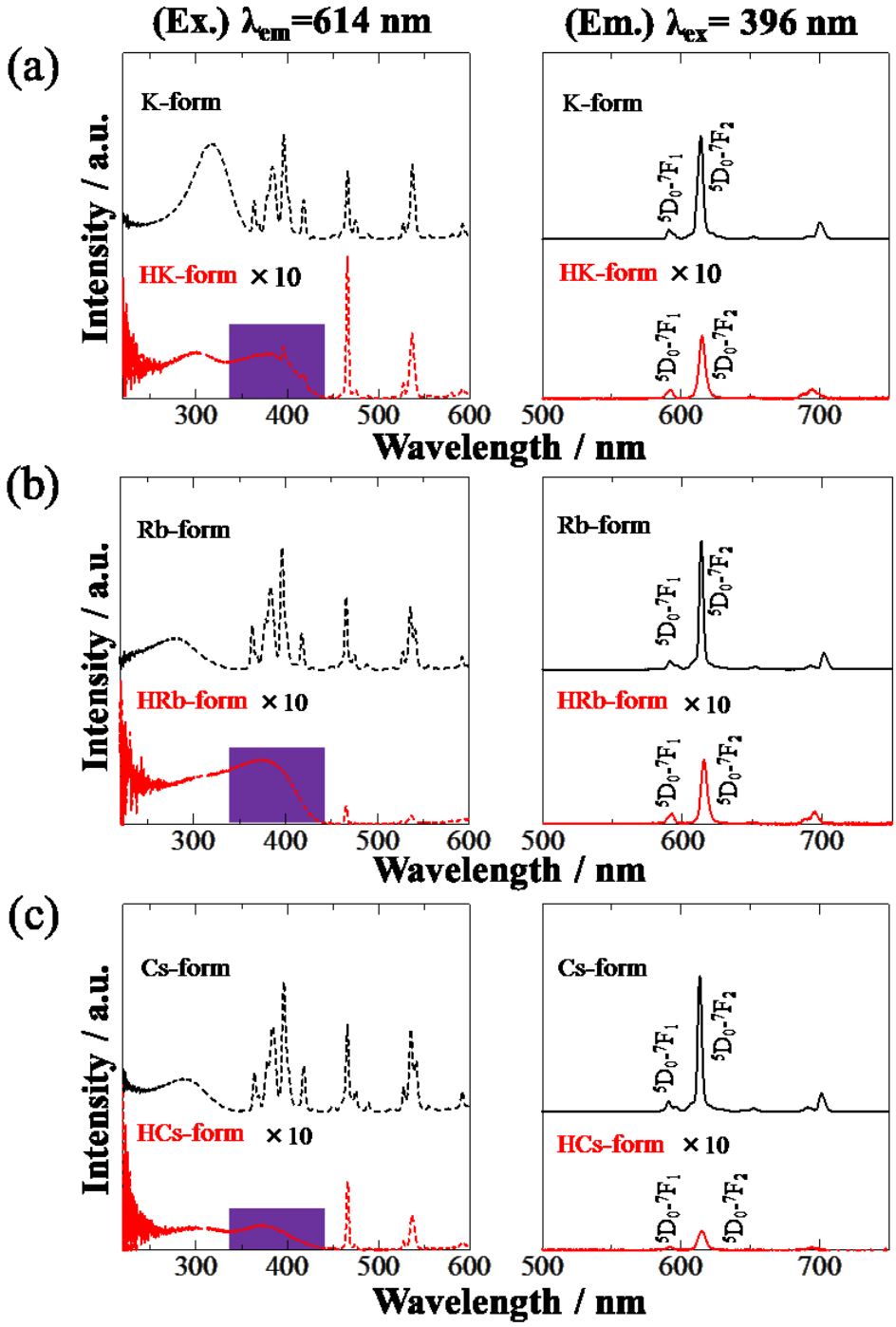

Fig. 2.7 The excitation (broken line) and emission (solid line) spectra (a) precursor $KEu(MoO_4)_2$ (K-form) powder and protonated (HK-form) powder, (b) precursor $RbEu(MoO_4)_2$ (Rb-form) powder and protonated (HRb-form) powder, (c) precursor $CsEu(MoO_4)_2$ (Cs-form) powder and protonated (HCs-form) powder.

similar to that of molybdate phosphors with MoO_6 group (420-480 nm) [48]. This result indicates that the coordination environment around Mo ions in $AEu(MoO_4)_2$ changes higher-coordination environment by H^+ exchange and consequently forming nanoscroll. In the emission spectra, meanwhile, all peaks corresponded to the Eu^{3+} 4f-4f transition, and the emission peak profiles of these sample before or after H^+-exchanging were essentially the same and there is no spectral shift due to the H^+-exchanging because the symmetric environment around the Eu^{3+} ion in the $(Eu(MoO_4)_2)_n$ layers is the same in the samples.

To investigate change of environment around Mo ions, we performed Raman spectrometry. The Raman spectra of the precursor $AEu(MoO_4)_2$ powder and $HEu(MoO_4)_2$ powder prepared by the H^+ exchange of $AEu(MoO_4)_2$ is shown in Fig. 2.8. The Raman spectra of precursor K-form, Rb-form, and Cs-form powders consist of characteristic Raman mode of alkali rare-earth molybdates with isolated MoO_4 structure: the stretch vibration of MoO_x polyhedra in higher frequency area (800-1000 cm^{-1}) and wide empty gap in the range 500-700 cm^{-1} [49-58]. After H^+ exchange procedure, new Raman peaks were observed in H-form powders which are not observed in the Raman spectra of the precursors, although some peaks corresponding to those of precursors remained. The observed exotic Raman peaks in the three H-form materials which are not observed in the Raman spectra of the precursors are listed in Table. 2.2. The Raman peaks of H-form powders were located at similar area. This result indicates that the all H-form powders have similar bonding structure, despite the difference of the crystal structure of precursors. The Raman bands (blue-color font) at 150 (HK-form),

156 (HRb-form), 157 (HCs-form) and 817 (HK-form), 816 (HRb-form), 819 (HCs-form) cm^{-1} are assigned to infinite layered sheets in α-MoO_3: the associated Mo-O-Mo bending mode and asymmetric vibration of the bridging Mo-O-Mo bonds [52/58-55/61]. The Raman band (green-color font) at 960 (HK-form), 961 (HRb-form), 956 (HCs-form) cm^{-1} is attributed to the symmetric stretching vibration of isolated MoO_6 and band at 702(HK-form), 703 (HRb-form), 706 (HCs-form) cm^{-1} are coincided with asymmetric stretching vibration of isolated MoO_6 [53, 58, 62]. This result indicates that MoO_6 formed by H^+ exchange and consequently the excitation absorption band shift to the longer wavelength side in the excitation spectra of protonated powders. The Raman band (red-color font) at 883(HK-form), 874 (HRb-form), 881 (HCs-form) cm^{-1} corresponds to asymmetric stretching vibration of MoO_4 in dimeric O_3Mo-O-MoO_3 unit [58]. These results indicate H-form powders forms isolated MoO_6 structure and bridging Mo-O-Mo bonds, while the precursor, originally, have only isolated MoO_4 in the crystal structure by H^+ exchange and rolling up.

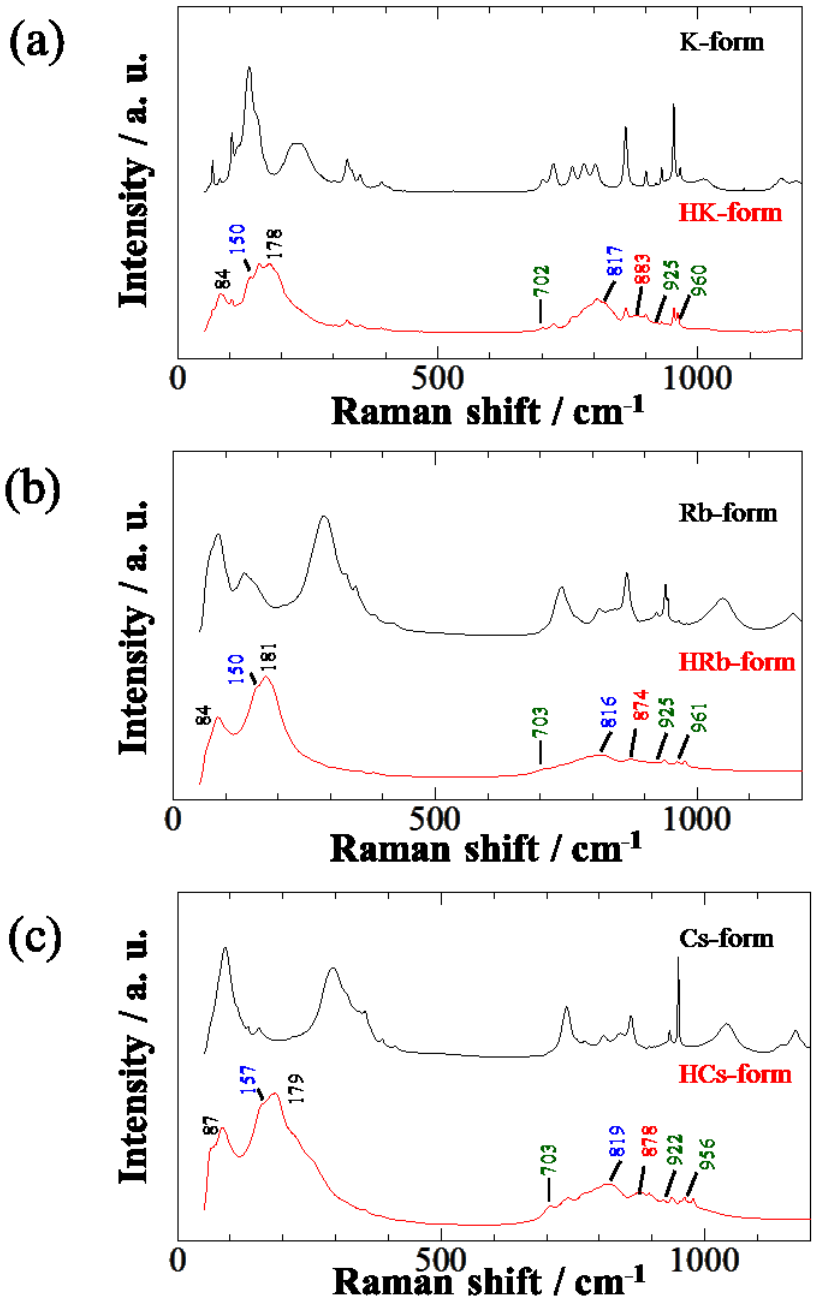

Fig. 2.7 The Raman spectra (a) precursor $KEu(MoO_4)_2$ (K-form) powder (black line) and protonated (HK-form) powder (red line), (b) precursor $RbEu(MoO_4)_2$ (Rb-form) powder (black line) and protonated (HRb-form) powder (red line), (c) precursor $CsEu(MoO_4)_2$ (Cs-form) powder (black line) and protonated (HCs-form) powder (red line).

Table. 2.2 Raman peaks observed in H-form powders at ordinary temperatures and pressures.

HK-form ν (cm^{-1})	HRb-form ν (cm^{-1})	HCs-form ν (cm^{-1})	Assignment	reference
84	84	87		48
150	156	157	associated Mo-O-Mo bending mode of infinite layered sheet in α-MoO_3	42-45
178	181	179	External mode	48
702	703	706	asymmetric stretching vibration of isolated MoO_6	37, 42, 46
817	816	819	asymmetric vibration of Mo-O-Mo linkage of infinite layered sheet in α-MoO_3	42-45
883	874	881	asymmetric stretching vibration of MoO_4 in dimeric O_3Mo-O-MoO_3 unit	42
925	925	922	asymmetric stretching vibration of isolated MoO_6	37, 42, 46
960	961	956	symmetric stretching vibration of isolated MoO_6	37, 42, 46

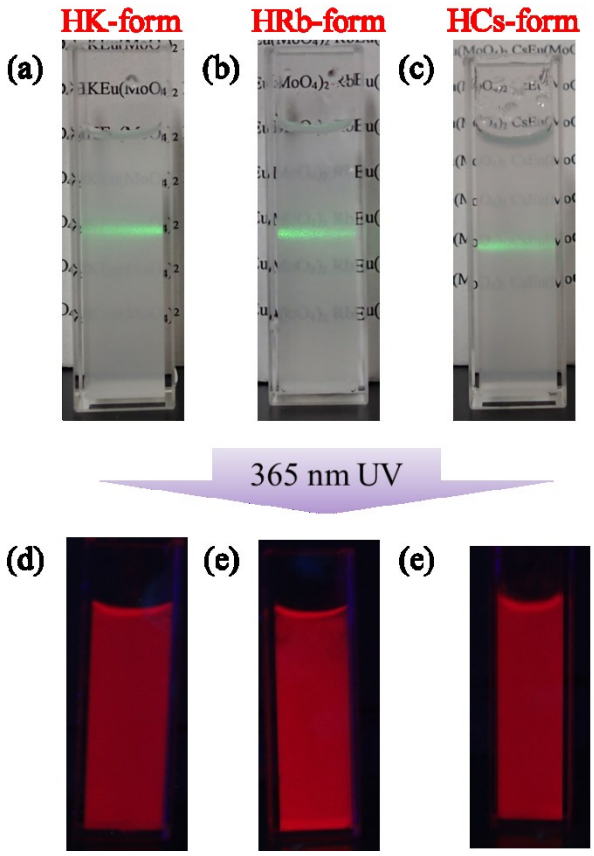

Fig. 2.8 The photograph of the suspension re-dispersed dried (a) HK-form, (b) HRb-form, and (c) HCs-form nanoscrolls into deionized water after 1 h (The concentration of the H-form powder was adjusted to 1.0×10^{-3} mol/dm^{-3}) and their Tyndall effect and emission under UV light of 365 nm.

We investigated re-dispersibility of H-form powders, because it is important in order to use as phosphor-disperse films. Fig. 2.8 shows the photograph of the suspension re-dispersed dried H-form nanoscrll powders into deionized water after 1 h. The concentration of the H-form powders was adjusted to 1.0×10^{-3} mol/dm^{-3}. The Tyndall effect was confirmed by the scattering of a laser beam in the colloidal solutions dispersed H-form powders, suggesting that the H-form nanoscroll powders have re-dispersibility. Additionally, the all solutions exhibit red emission, under UV light of 365 nm.

Fig. 2.9 shows the excitation and emission spectra of the solution dispersed the H-form powders into deionized water. Although the peak intensity of excitation and emission spectra of the phosphor solution was lower than that of the phosphor powder, similar to the results obtained for the H-form powder shown in Fig. 2.7. The excitation spectrum consisted of two broad band, corresponding to charge transfer (CT) transitions of Eu^{3+}-O^{2-} and O^{2-}-Mo^{6+}, respectively. Several strong narrow peaks were attributed to 4f-4f transitions of Eu^{3+}. Among these, the dominated sharp peak at 465 and 531 nm corresponded to the $^7F_0$-$^5D_2$ and $^7F_0$-$^5D_1$ transition of Eu^{3+}. In addition, the phosphor solution presents strong red-emission under excitation wavelength at 365 nm due to the 4f-4f transition of Eu^{3+}.

The solution exhibits another very unique and interesting property—*liquid crystallinity*. Liquid crystal is the material which has both of fluidity and anisotoropy. The behavior is one of the most important properties characteristic to anisotropic colloid particles and is fundamentally explained by the Onsager theory based on the excluded

volume effect [65, 66]. Liquid crystallinity of HK-form nanoscroll solution is confirmed by observing them between crossed polarizers by an optical microscope. The configuration of the optical microscope is shown in Fig. 2.10. When the polarized light, made by under-side polarizer, incidents on an anisotropic particle, the polarized light parts two refracting light—this phenomenon is called "birefringence". Each of two refracting light has different refractive index which is different with each domain, causing interference color. If the sample is isotropic material, the visual field shows dark part. Therefore, the bright or color part indicate the sample show liquid crystallinity. Fig. 2.11 shows a typical photograph of nanoscroll solution in capillary observed between crossed polarizers. The solution obviously shows birefringence and the bright and dark domain with the angle control made by the optical axis and polarization plane, as well as other inorganic liquid crystal materials [67-72]. This result indicates that HK-form nanoscroll solution have liquid crystallinity. There are only a few reports on inorganic liquid crystals, such as rod-like β-FeOOH [73], ribbon-like V_2O_5 gel [74] sheet-like $H_3Sb_3P_2O_{14}$ [75] and $[Nb_6O_{17}]^{4-}$ nanosheet [76], rod-like quantum dot CdSe [77], compared with organic liquid crystal materials. Up to now, to our knowledge, no emissive inorganic liquid crystal materials have been reported. The the solution dispersed HEu(MoO4)2 powders in de-ionized water, therefore, is the first case of the solution materials exhibits both liquid crystallinity and luminescence properties.

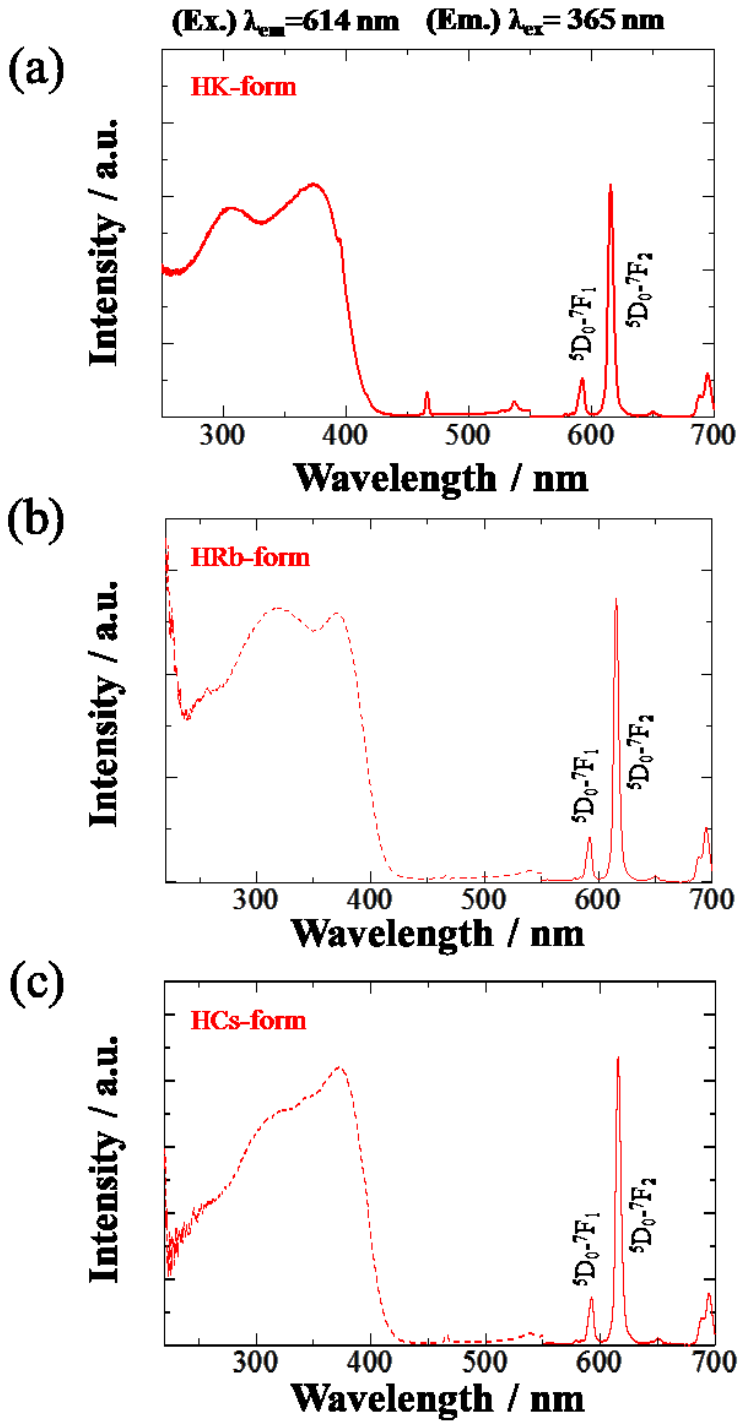

Fig. 2.9 The excitation (broken line) and emission (solid line) spectra of the suspension re-dispersed dried (a) HK-form, (b) HRb-form, and (c) HCs-form nanoscroll powders into deionized water after 1 h. Concentration of the H^+-form powder in the solution: 1.0×10^{-3} mol/dm^3.

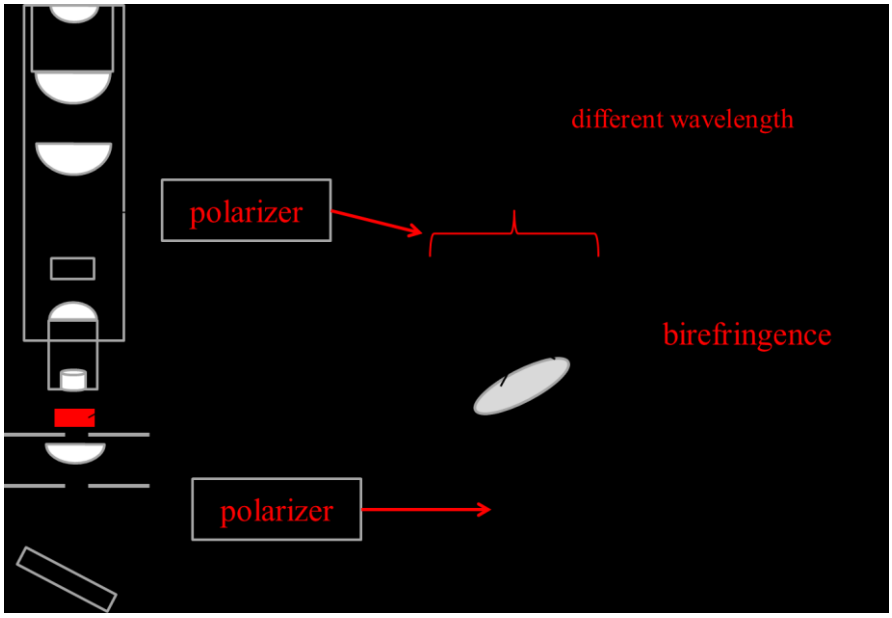

Fig. 2.10 The configuration of an optical microscope.

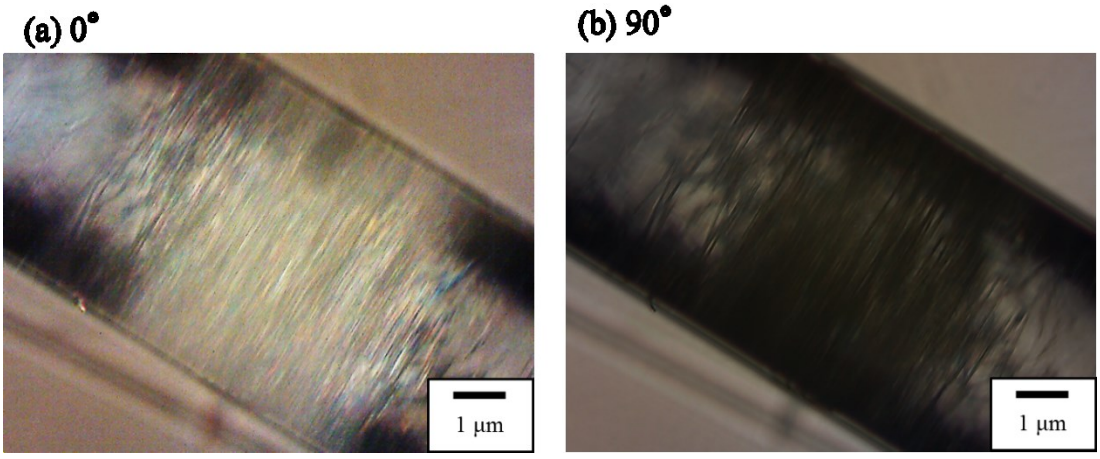

Fig. 2.9 An optical microscope image of the solution re-dispersed $HEu(MoO_4)_2$ nanoscroll powder derived from $KEu(MoO_4)_2$ (HK-form) in deionized water in a capillary under crossed polarizers at room temperature. Concentration of the HK-form powder in the solution: 1.0×10^{-3} mol/dm^3.

2.4 Summary

$KEu(MoO_4)_2$, $RbEu(MoO_4)_2$, and $CsEu(MoO_4)_2$ were successfully protonated by stirring in dilute HNO_3 aqueous solution (0.01 M) at room temperature for 7 day without organic compounds. The protonated powders have similar structure, morphology and optical properties, regardless of the structural difference of precursors. $HEu(MoO_4)_2$ could be synthesized under milder condition than other protonated materials, because the H^+ exchange procedure of $HEu(MoO_4)_2$ required diluter acid than other protonated materials. $HEu(MoO_4)_2$ has bundled nanoscroll morphology and the nanoscroll particle is below 20 μm in length, and have uniform outer diameters of about 20 nm suggesting that the way to roll up follows some sort of rules. The $HEu(MoO_4)_2$ nanoscroll shows excellent optical absorption below 450 nm and presents strong red emission due to the 4f-4f transition of Eu^{3+}. In addition, the $HEu(MoO_4)_2$ powders shows re-dispersibility in deionized water and the solution shows good luminescence efficiency under excitation at 396 nm and liquid crytalinity. Since the $HEu(MoO_4)_2$ nanoscroll solution is transparent and show good luminescent emission, it is expected to use in crystal Si solar cells as a down-conversion materials.

References

[1] Z. Zhang and Y. Wang, *J. Electrochem. Soc.*, **154** (2007) J62– J64.

[2] T.S. Chan, R.S. Liu, I. Baginskiy, N. Bagkar, and B.M. Cheng, *J. Electrochem. Soc.*, **155** (2008) J284– J286.

[3] Z.J. Zhang, S. Chen, J. Wang, X.X. Yang, J.T. Zhao, Y. Tao, H.H. Chen, and Y. Huang, *Opt. Mater.*, **32** (2009) 99– 103.

[4] P. Zhang, L.X. Li, M.X. Xu, and L. Liu, *J. Alloys Compd.*, **456** (2008) 216– 219.

[5] D.T.M. Huong, N.H. Nam, L.V. Vu, and N.N. Long, *J. Alloys Compd.*, **537** (2012) 54– 59.

[6] M.N. Huang, Y.Y. Ma, X.Y. Huang, S. Ye, and Q.Y. Zhang, *Spectrochim. Acta Part A: Mol. Biomol. Spectrosc.*, **115** (2013) 767– 771.

[7] U. Rambabu and S.D. Han, *Ceram. Int.*, **39** (2013) 1603– 1612.

[8] J.Y. Chen, C.K. Huang, W.B. Hung, K.W. Sun, and T.M. Chen, *Sol. Energy Mater. Sol. Cells*, **120** (2014) 168– 174.

[9] A. Luque and A. Martí, *Phys. Rev. Lett.*, **78** (1997) 5014– 5017.

[10] V. Sivakumar and U.V. Varadaraju, *J. Electrochem. Soc.*, **152** (2005) H168– H171.

[11] Y. Iso, S. Takeshita, and T. Isobe, *J. Electrochem. Soc.*, 159 (2009) J72–J76 .

[12] V.D. Rodríguez, J. Méndez-Ramos, V.K. Tikhomirov, J. del-Castillo, A.C. Yanes, and V.V. Moshchalkov, *Opt. Mater.*, **34** (2011) 179–182.

[13] S. Misra, L. Yu, M. Foldyna, and P.R.I. Cabarrocas, *Sol. Energy Mater. Sol.*

Cells, **188** (2013) 90–95.

[14] H. Hara, S. Takeshita, T. Isobe, T. Sawayama, and S. Niikura, *Mater. Sci. Eng. B*, **178** (2013) 311–315.

[15] H. Seo, Y. Wang, G. Uchida, K. Kamataki, N. Itagaki, K. Koga, and M. Shiratani, *Electrochem. Acta*, **95** (2013) 43–47.

[16] H. Lian, Z. Hou, M. Shang, D. Geng, and Y. Zhang, *J. Liu, Energy*, 57 (2013) 270–283.

[17] R.F. Klevtsova, L.P. Kozeeva, and P.V. Klevtsov, *Kristallografiya*, **19** (1974) 89–94.

[18] V.A. Morozo, A.V. Arakcheeva, P. Pattiso, K.W. Meert, P.F. Smet, D. Poelman, N. Gauquelin, J. Verbeeck, A. M. Abakumov, and J. Hadermann, Chem. Mater., 2015, 27 (16), 5519–5530.

[19]T. Wu, Y. Liu, Y. Lu, L. Wei, H. Gao, and H. Chen, *CrystEngComm*, **15** (2013), 2761–2768.

[20] C. Guo, S. Wang, T. Chen, L. Luan, and Y. Xu, *Appl. Phys. A*, **94** (2009), 365–371.

[21] P. Shi, Z. Xia, M.S. Molokeev, and V.V. Atuchin, Dalton Trans., 2014, 43, 9669–9676

[22] P.V. Klevtsov and R.F. Klevtsova, *J. Struct. Chem.*, **18** (1977) 339–355.

[23] O.D. Chimitova, V.V. Atuchin, B.G. Bazarova , M.S. Molokeev, and Z.G. Bazarova, *Proc. SPIE*, **3771** (2013) 87711A-1–9.

[24] G.B. Saupe, C.C. Waraksa , H.-N. Kim , Y.J. Han , D.M. Kaschak , D. M.

Skinner, and T.E. Mallouk, *Chem. Mater.*, **12** (2000) 1556–1562.

[25] R. Ma, Y. Bando, and T. Sasaki, *J. Phys. Chem. B*, **108** (2004) 2115–2119.

[26] Y.Omomo, T. Sasaki, L. Wang, and M. Watanabe *J. Am. Chem. Soc.*, **125** (2003) 3568–3575.

[27] T. Sasaki, M. Watanabe, H. Hashizume, H. Yamada, and H. Nakazawa., *J. Am. Chem. Soc.*, **118** (1996) 8329–8335.

[28] M. Fang, C.H. Kim, G.B. Saupe, H.-N. Kim, C.C. Waraksa, T.Miwa, A. Fujishima, and T.E. Mallouk, *Chem. Mater.*, **11** (1999) 1526–1532.

[29] R. E. Schaak and T. E. Mallouk, *Chem. Mater.*, **12** (2000) 3427–3434.

[30] T.Sasaki, Y. Ebina, M. Watanabe and G. Decher, *Chem. Commun.*, (2000) 2163–2164.

[31] T. Sasaki, Y. Ebina, T. Tanaka , M. Harada, and M. Watanabe, *Chem. Mater.*, **13** (2001) 4661–4667.

[32] N.A. Kotov, I. Dekany, and J.H. Fendler, *J. Phys. Chem.*, **99** (1995) 13065–13069.

[33] Zhenli, M.A. Horsch, M.H. Lamm, and S.C. Glotzer, *Nano Lett.*, **3** (2003) 1341–1346.

[34] M. Li, H. Schnablegger, and S. Mann, *Nature* **402** (1999) 393–395.

[35] A.K. Boal1, F. Ilhan, J.E. DeRouchey, T. Thurn-Albrecht, T.P. Russell and V.M. Rotello, *Nature* **404**, (2000) 746–748.

[36] Y. Lin, A. Böker, J. He, K. Sill, H. Xiang, C. Abetz, X. Li, J. Wang, T. Emrick, S. Long, Q. Wang, A. Balazs, and T.P. Russell, *Nature* **434** (2005) 55–59.

[37] M. Grzelczak, J. Vermant, E.M. Furst, and L.M. Liz-Marzan, *ACS Nano*, **4** (2010) 3591–3605.

[38] W. Shenton, S.A. Davis, and S. Mann, *Adv. Mater.*, **11** (1999) 449–452.

[39] T. Sasaki, M. Watanabe, H. Hashizume , H. Yamada, and H. Nakazawa, *J. Am. Chem. Soc.*, **118** (1996) 8329–8335.

[40] T. Sasaki and M. Watanabe, *J. Am. Chem. Soc.*, **120** (1998) 4682–4689.

[41] L. Pauling, *J. Am. Chem. Soc.*, **54** (1932) 3570.

[42] G.B. Saupe, C.C. Waraksa, H.-N. Kim, Y.J. Han, D.M. Kaschak, D. M. Skinner, and T.E. Mallouk, *Chem. Mater.*, **12** (2000) 1556–1562.

[43] R. Ma, Y. Bando, and T. Sasaki, *J. Phys. Chem. B*, **108** (2004) 2115–2119.

[44] L. Luan and Y. Xu, Appl. Phys. A 94 (2009) 365-371.

[45] A. Xie, X. Yuan, F. Wang, Y. Shi, J. Liu, and Z. Mu, *J. Alloys Compd.*, **501** (2010) 124–129.

[46] W.L. Feng, Y. Jin, Y. Wu, D.F. Li, and A.K. Cai, *J. Lumin.*, **134** (2013) 614–617.

[47] P.S. Dutta and A. Khanna, *ECS J. Solid State Sci. Technol.*, **2** (2013) R3153–R3167.

[48] S.P.S. Porto and J.F. Scott, *Phys. Rev.*, **157** (1967) 716–19.

[49] A.A. Kaminskii. A.V. Butashin, H.-J. Eichler, D. Grebe, R. Macdonald, K. Ueda, H. Nishioka, W. Odajima, M. Tateno, J. Song, M. Mush, S.N. Bagaev, and A.A. Pavlyu, *Opt. Mater.*, **7** (1997) 59–73.

[50] J. Hanuza, M. Mczka, J.H. Maas, *J. Mol. Struc.*, **348** (1995) 349–352.

[51] S.K. Sharma, A. Jayaraman, and S.Y. Wang, *J. Raman Spectrosc.*, **28** (1997) 39–44.

[52] F.D. Hardcastle and I.E.Wachs, *J. Raman Spectrosc.*, **21** (1990) 683–691.

[53] A. Jayaraman, S.Y. Wang and S.K. Sharma, *Solid State Commun.*, **93** (1995) 885–890

[54] V.V. Atuchin, O.D. Chimitova, M.S. Molokeev, T.A. Gavrilova, S.-J. Kim, N.V. Surovtsev, and J.G. Bazarov, *J. Crystal Growth*, **318** (2011) 683–686.

[55] V.V. Atuchin, O.D. Chimitova, S.V. Adichtchev, J.G. Bazarov, T.A. Gavrilova, M.S. Molokeev, N.V. Surovtsev, and Z.G. Bazarova, *Mater. Lett.*, **106** (2013) 26–29.

[56] B.A. Kolesov and L.P. Kozeeva, *Zh. Strukt. Khim.*, **34** (1993) 52–58.

[57] H. Tian, C. A. Roberts, and I.E. Wachs, *J. Phys. Chem. C*, **114** (2010) 14110–14120.

[58] B.C. Windom, W.G. Sawyer, and D.W. Hahn, *Tribol Lett.*, **42** (2011) 301–310.

[59] I.R. Beattie and T.R. Gilson, *J. Chem. Soc. A*, (1969) 23222–327.

[60] M.A. Py and K. Maschke **105** (1981) 370–374.

[61] L. Zhang, T. Xu, X. Zhao, and Y. Zhu, *Appl. Catal. B-Environ.*, **98** (2010) 138–146.

[62] G. Lakshminarayana, K.M. Kaky, S.O. Baki, A. Lira, P. Nayar, I.V. Kityk, and M.A. Mahdi, *J.Alloy. Compd.,* **690** (2017) 799–816.

[63] D. Philip, G. Aruldhas, and V. Ramakrishnan, *Pramana-J. Phys.*, **30** (1988) 129–133.

[64] L. Onsager, *Ann. N. Y. Acad. Sci.*, **51** (1949) 627–659.

[65] G.J. Vroege and H.N.W. Lekkerkerker, *Rep. Prog. Phys.,* **55** (1992) 1241–1309.

[66] O. Pelletier, C. Bourgaux, O. Diat, P. Davidson, and J. Livage, *Europ. Phys. J. B*, **12** (1999) 541–546.

[67] A. S. Sonin, **8**, (1998) 2557–2574.

[68] J.C.P. Gabriel, F. Camerel, B.J. Lemaire, H. Desvaux, P. Davidson, and P. Batail, *Nature*, **413** (2001) 504–508.

[69] T. Nakato and N. Miyamoto, *Adv. Mater.*, **14** (2002) 1267–1270.

[70] T. Nakato, N. Miyamoto, A. Harada, and H. Ushiki, *Langmuir*, **19** (2003) 3157–3163.

[71] F. M. van der Kooij, and H. N. W. Lekkerkerker, *J. Phys. Chem. B*, **102** (1998) 7829–7832.

[72] Q. Majorana, *Phys. Z.*, **4** (1902) 145.

[73] H. Zicher, Z. Anor. *Allg. Chem.*, **147** (1925) 91–110.

[74] L. Li, J. Walda, L. Manna, and A.P. Alivisatos, *Nano Lett.*, **2** (2002) 557–560.

Chapter 3

Improvement of luminescent efficiency of $HEu(MoO_4)_2$ nanoscrolls phosphor by suppression of concentration quenching

3.1 Introduction

Thin films with dispersed nanophosphor have been investigated for their use in displays, LEDs, and solar cells because of their excellent optoelectronic properties and low light-scattering intensity [1–5]. In particular, transparent displays with thin films containing dispersed nanophosphor attracted much attention in the context of next-generation displays [6]. Such transparent displays have been demonstrated mainly in the field of organic light-emitting devices [7]. In addition, stable low-scattering suspensions of inorganic phosphors in organic solvents have to be developed to improve the durability of flexible and transparent displays [8, 9]. However, almost all inorganic phosphors with high luminescence efficiency contain micron-sized particles, which have strong scattering characteristics. The desired insignificant scattering can be obtained for particles smaller than 50 nm [10]. Therefore, nano-sized inorganic phosphors are required for the fabrication of flexible and transparent displays. However, such nanophosphors agglomerate easily in organic solvents. Therefore, the fabrication of stable suspensions of nanophosphors is required.

Several wet chemical methods have been reported for the preparation of nanophosphors, such as the hydrothermal method [11], polymerized complex method

[12], sol-gel method [13], and others. These methods offer several advantages, such as homogeneity, phase purity, and narrow size distribution. However, these methods require a special reactor and special precursor materials to achieve complete dissolution in solvent solutions. In addition, methods for the synthesis of clear suspensions of nanophosphors have not been well established until now [14].

Red-emissive phosphors with Eu^{3+} have been widely used in color televisions, lamp. It is important to develop highly efficient phosphors with a high doping concentration (high absorption), because the excitation energy (blue or near UV light) in the conventional white LED is smaller than that of the fluorescent palm, PDP, and CRTs. $KEu(MoO_4)_2$ is one of the good candidate, because the lattice sites occupied by Eu are separated from each other by the K and MoO_4 layers, and a high luminescence efficiency is achieved even when all sits are occupied by activator ions (Eu). Such phosphors are called *stoichiometric phosphor*. The luminescence spectra of Eu^{3+}, however, have strong dependence on the concentration in the host lattice. This is because at higher concentrations, the higher emitting levels, $^5D_1$ of Eu^{3+} transfer its energies to neighboring ions of the same specie by the following cross-relaxations; that is:

$$^5D_1(Eu^{3+}) + {}^7F_0(Eu^{3+}) \rightarrow {}^5D_0(Eu^{3+}) + {}^7F_6(Eu^{3+}).$$

The emission, therefore, is often quenched by doping rare earth ions over an critical concentration—this phenomena is called *concentration quenching*.

The $HEu(MoO_4)_2$ nanoscrolls obtained from red-emissive $KEu(MoO_4)_2$ phosphor

via ion-exchange for preparing nanophosphors, in chapter 2, shows good luminescence property. In this chapter, we attempted to suppress the concentration quenching and to further enhance the emission efficiency of $HEu(MoO_4)_2$ nanoscrolls, by the substituting Eu^{3+} ions in $HEu(MoO_4)_2$ by smaller Gd^{3+} ions part of the Eu^{3+} ions in the $HEu(MoO_4)_2$ lattice were substituted by smaller Gd^{3+} ions. The morphological and luminescence properties of of $HEu_{1-x}Gd_x(MoO_4)_2$ were investigated.

3.2 Experimental

3.2.1 Synthesis of materials

$KEu_{1-x}Gd_x(MoO_4)_2$ ($0.00 \leq x \leq 1.00$) were synthesized by a conventional solid-state reaction method. K_2CO_3 (purity 99.95 %; Kanto Chemical Co. Inc.), Gd_2O_3 (purity 99.99 %; Shinetsu Chemical Co. Inc.), Eu_2O_3 (purity 99.99 %; Shinetsu Chemical Co. Inc.), and MoO_3 (purity 99.99 %; Kojundo Chemical Co. Inc.) were mixed using a mortar and pestle with acetone; the mixture was then calcined at 700 °C for 6 h in air. $HEu_{1-x}Gd_x(MoO_4)_2$ samples were obtained by the H^+ exchange of $KEu_{1-x}Gd_x(MoO_4)_2$ in HNO_3 solution (0.01 M, 100 mL) at room temperature for 7 days. The acid solution was refreshed once several days to complete H^+ exchange. After stirring, the solutions were isolated by suction filtration using a membrane filter (ADVANTEC MFS, INC., mixed cellulose ester, pore size: 0.45 μm, diameter: 47 mm). The samples were washed with deionized water at room temperature for 24 h and then dried at 50 ºC for 24 h. The obtained $HEu_{1-x}Gd_x(MoO_4)_2$ powder samples were redispersed in deionized water.

3.2.2 Materials characterization

The obtained samples were characterized by X-ray powder diffraction (XRD; Mac Science Ltd., MX-Labo) to identify the crystal structure and the sample composition was analyzed by X-ray fluorescence analysis (XRF; Seiko Instruments Inc., SEA 1200VX). Morphology of the samples was characterized by means of scanning electron microscopy (SEM; Hitachi Ltd., S-4300SD). The emission (PL) and excitation (PLE) spectra were measured at room temperature with a spectrofluorometer (Jasco

Corp., FP-6500/6600), where the emission spectra were obtained for excitation at 306 nm, and excitation spectra were obtained for emission at 612 nm

3.3 Result and discussion

The XRD patterns of the $KGd_xTb_{1-x}(MoO_4)_2$ ($0.00 \leq x \leq 1.00$) phosphors are shown in Fig. 3.1 The standard XRD pattern of $KGd(MoO_4)_2$ obtained from the inorganic crystal structure database (ICSD #6138) is also shown in Fig. 4.2 as a reference. The diffraction patterns were in good agreement with that of triclinic α-$KEu(MoO_4)_2$ type structure with the space group of *P*-1; diffraction peaks due to impurities corresponding to the starting materials were not observed in the patterns.

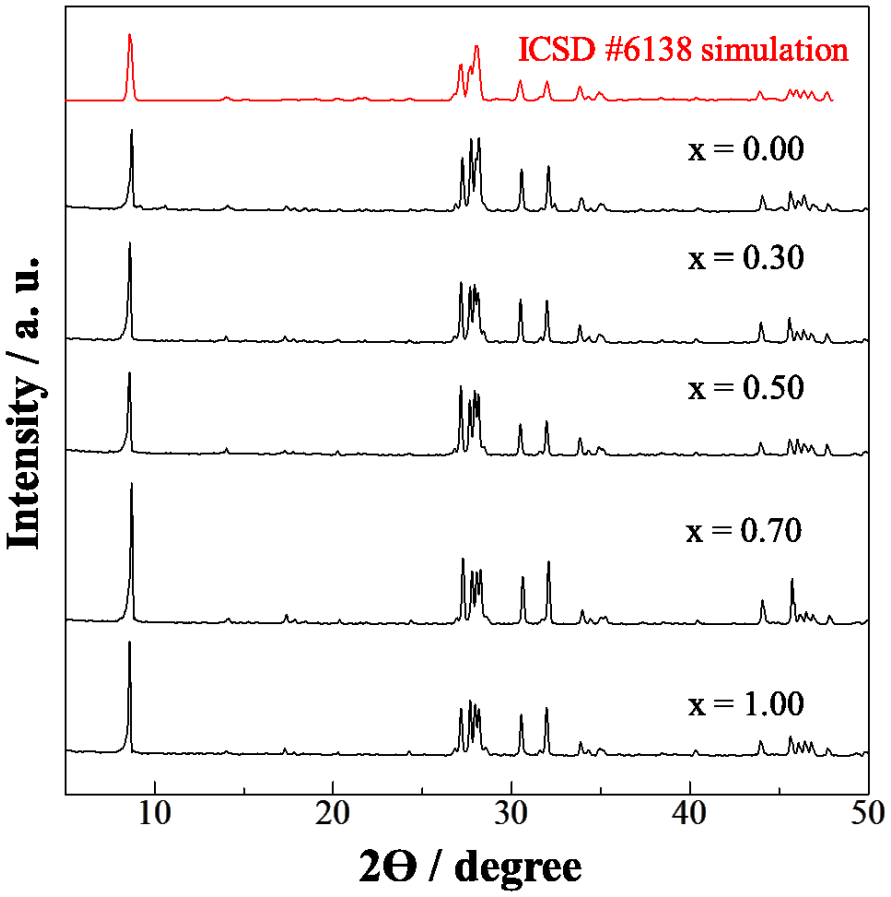

Fig. 3.1 The XRD pattern of $KEu_{x-1}Gd_x(MoO_4)_2$ ($0.00 \leq x \leq 1.00$) synthesized by the solid state reaction method at 700 ℃ for 6 h in air.

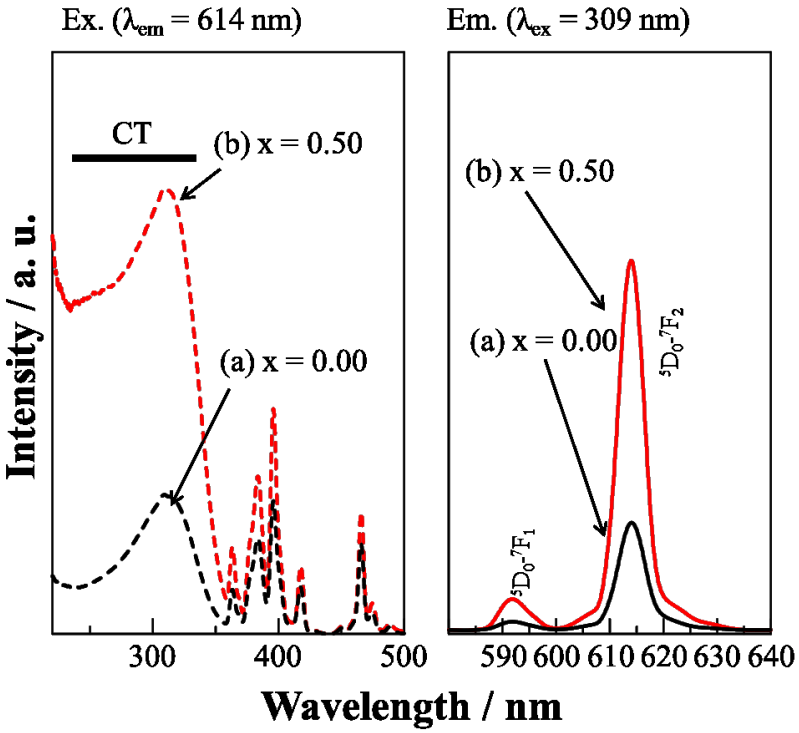

Fig. 3.2 Excitation (broken line) and emission (solid line) spectra at room temperature of $KEu_{1-x}Gd_x(MoO_4)_2$ (x = 0.00 ((a), black line) and x = 0.50 ((b), red line)) phosphors synthesized by the solid state reaction method at 700 ºC for 6 h in air.

Fig. 3.2 shows excitation and emission spectra of the precursor $KEu_{1-x}Gd_x(MoO_4)_2$ (x = 0.00 and 0.50) phosphors. The excitation spectra of all samples consisted of a strong broad band in the range from 220 to 350 nm, corresponding to the charge-transfer (CT) transition of O^{2-}–Mo^{6+}. Some strong narrow peaks are observed between 360 and 500 nm and are attributed to the 4f–4f transitions of the Eu^{3+} ion. On the other hand, the CT band of Eu^{3+}–O^{2-} is not clearly observed in the excitation spectra, possibly due to the overlap of the CT band with that of the molybdate group [15, 17–19]. In the emission spectra, all peaks corresponded to the Eu^{3+} 4f–4f transition. The emission peak intensity corresponding to the $^5D_0$–$^7F_2$ electric dipole transition at 614

nm is higher than that of the $^5D_0$–$^7F_1$ magnetic dipole transition at 592 nm, suggesting that the Eu^{3+} ions occupy sites in the $KEu(MoO_4)_2$ lattice without inversion symmetry. The ratio $I_{614nm}(^5D_0$–$^7F_2)/I_{592nm}(^5D_0$–$^7F_1)$ of $KEu(MoO_4)_2$ (12.5) decreased upon Gd^{3+} doping and was 10.8 in case of $KEu_{0.50}Gd_{0.50}(MoO_4)_2$. This result indicates that the symmetry of the Eu^{3+} site in the $KEu_{1-x}Gd_x(MoO_4)_2$ lattice was higher than that of the sample without the Gd^{3+} doping. It is well known that the $^5D_0$–$^7F_2$ electric dipole transition of Eu^{3+} is sensitively affected by the change of the site symmetry in the host lattice. The peak intensity corresponding to the $^5D_0$–$^7F_1$ transition is relatively higher than that of the $^5D_0$–$^7F_2$ transition when Eu^{3+} is located at a site having high symmetry (inversion symmetry site) in the host lattice, such as in case of $Ba_2GdNbO_5:Eu^{3+}$, $NaLuO_2:Eu^{3+}$, and $InBO_3:Eu^{3+}$ phosphors [20]. Concerning the presently studied $KEu_{1-x}Gd_x(MoO_4)_2$, since the ionic radius of Gd^{3+} (0.1193 nm for 8-fold coordination [21]) is smaller than that of Eu^{3+} (0.1206 nm for 8-fold coordination [21]), a lattice distortion is induced by doping of Gd^{3+} at the Eu^{3+} site of $KEu(MoO_4)_2$, which leads to a change of the local environment and symmetry of the Eu^{3+} site in the crystal lattice. On the contrary, the emission intensity of $KEu(MoO_4)_2$ was effectively enhanced by doping of Gd^{3+} into the host lattice. This can be explained by the suppression of the concentration quenching on decreasing Eu^{3+} concentration in $KEu_{1-x}Gd_x(MoO_4)_2$.

Fig. 3.3 shows the compositional dependence of the emission intensity excited at 309 nm of $KEu_{1-x}Gd_x(MoO_4)_2$ ($0.00 \leq x \leq 1.00$). The emission intensity initially increases with increasing amount of Gd^{3+} and reaches a maximum at $x = 0.50$. However, the emission intensity decreases on further increasing Gd^{3+} content beyond the optimum

concentration, which is attributed to the decrease of the Eu^{3+} concentration. To synthesize nanophosphors, the obtained $KEu_{1-x}Gd_x(MoO_4)_2$ phosphors were stirred in HNO_3 solution at room temperature. However, the $KEu_{1-x}Gd_x(MoO_4)_2$ powders were completely dissolved in highly concentrated HNO_3 solution above 0.05 M during the stirring process. In contrast, for the samples stirred in 0.01 M aqueous HNO_3 solution for 7 days, the K^+ ions of the $KEu_{1-x}Gd_x(MoO_4)$ phosphors were successfully exchanged by H^+ without particle dissolution. The composition of $KEu_{1-x}Gd_x(MoO_4)_2$ before and after H^+ exchange was analyzed by XRF. The amount of K^+ ions in the phosphors after H^+ exchange was reduced to about 30 % compared with the precursor materials $KEu_{1-x}Gd_x(MoO_4)_2$.

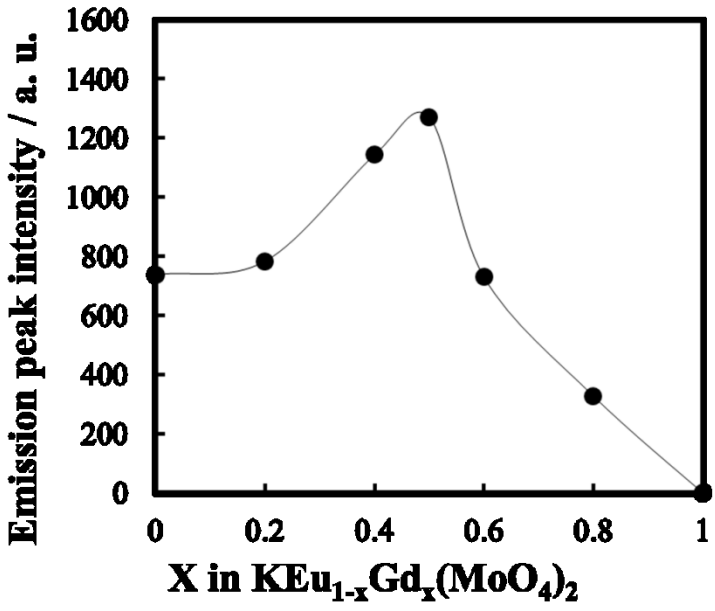

Fig. 3.3 Dependence of the emission intensity on the Gd^{3+} content in $KEu_{1-x}Gd_x(MoO_4)_2$ ($0.00 \leq x \leq 1.00$) phosphors

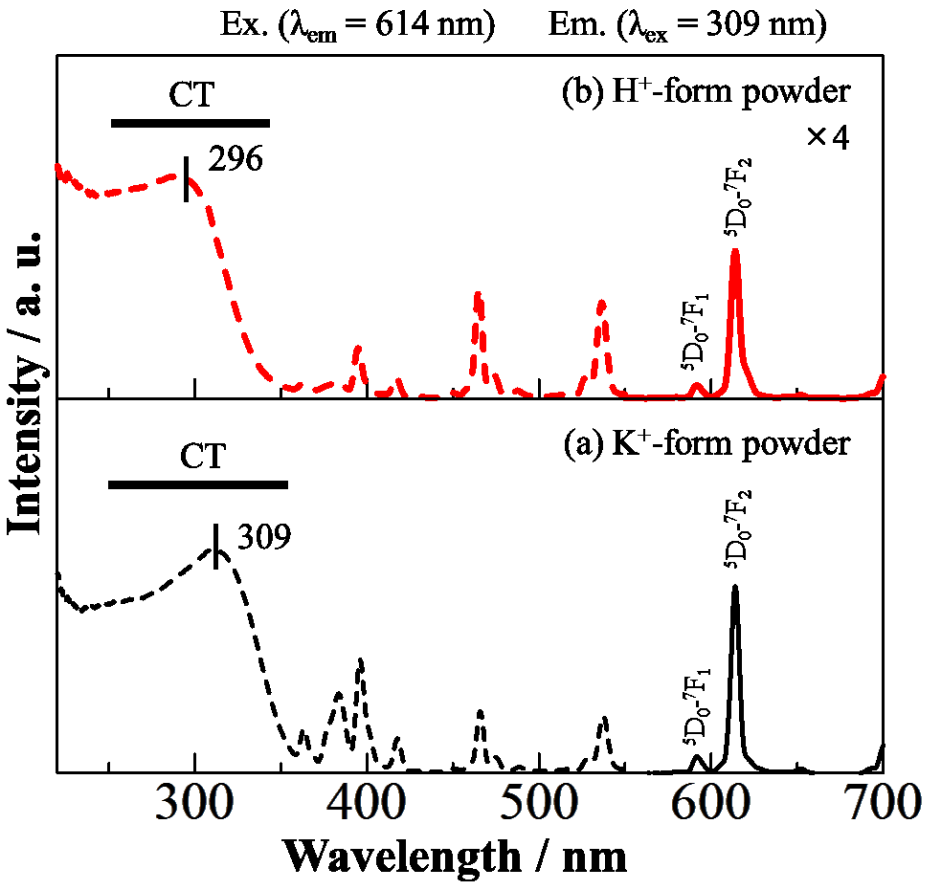

Fig. 3.4 Excitation (broken line) and emission (solid line) spectra at room temperature of (a) $KEu_{0.50}Gd_{0.50}(MoO_4)_2$ (K-form) and (b) dried $K_{0.3}H_{0.7}Eu_{0.50}Gd_{0.50}(MoO_4)_2$ (H-form) powders prepared by stirring in 0.01 M HNO_3 solution for 7 days.

To compare the photoluminescence property of $K_{0.3}H_{0.7}Eu_{1-x}Gd_x(MoO_4)_2$ (H-form) with that of $KEu_{1-x}Gd_x(MoO_4)_2$ (K-form), the H^+-form powders were washed with deionized water at room temperature for 24 h and then dried at 50ºC for 24 h. Fig. 3.4 shows excitation and emission spectra of dried K-form and H-form powders. The behavior observed in the excitation and emission spectra of all H^+-form powders was similar. The highest emission intensity was obtained for the H^+-form with x = 0.50.

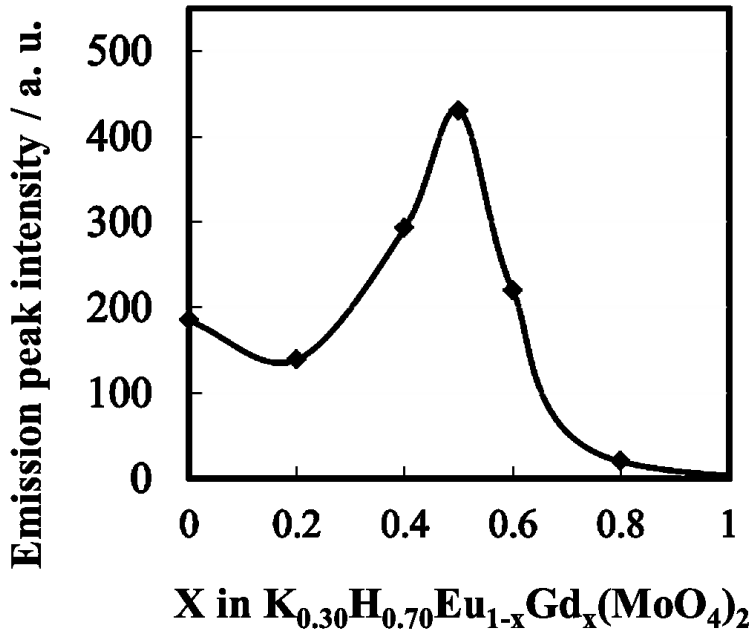

Fig. 3.5 Dependence of the emission intensity on the Gd^{3+} content of dried $K_{0.3}H_{0.7}Eu_{1-x}Gd_x(MoO_4)_2$ ($0.00 \leq x \leq 1.00$) phosphor powders prepared by stirring in 0.01 M HNO_3 solution for 7 days.

The peak wavelength of the CT bands of these phosphors depends on the excitation energy for electron transfer from O^{2-} to Mo^{6+}. Since the electronegativity of H^+ (2.1) is larger than that of K^+ (0.8), the electronic attractive force between O^{2-} and Mo^{6+} is increased by H^+ exchange which, in turn, is causative for the increase of the excitation energy for the electron transfer from O^{2-} to Mo^{6+}. As a result, the excitation absorption band corresponding to the CT transition of O^{2-}–Mo^{6+} is shifted toward shorter wavelength by H^+ exchange. In addition, the peak intensity of the CT transition of O^{2-}–Mo^{6+} decreased in comparison with that of the K^+-form. This is probably because H_2O persisted in the interlayers as a result of using dilute acid.

Fig. 3.6 shows the compositional dependence of the luminescence intensity excited at 309 nm of $K_{0.30}H_{0.70}Eu_{1-x}Gd_x(MoO_4)_2$ ($0.00 \leq x \leq 1.00$). Similar to the results

obtained for the K^+-form samples that are shown in Fig. 3.3, the emission intensity was effectively enhanced by doping of Gd^{3+} into the $K_{0.3}H_{0.7}Eu(MoO_4)_2$ lattice and the highest emission intensity was obtained for $K_{0.30}H_{0.70}Eu_{0.50}Gd_{0.50}(MoO_4)_2$.

Fig. 3.6 shows SEM images of dried K^+-form and H^+-form powders. The K^+-form powder has a granular particle morphology with average particle size of 10 μm. In contrast, although a small amount of granular particles remained, the dried H^+-form powders have rod-like particle morphology with 1–15 μm in length and outer diameters in the range of 50–500 nm. The morphology an size were similar to those of $HEu(MoO_4)_2$ derived from triclinic $KEu(MoO_4)_2$ phosphor with the same crystal structure, indicating the particle size and morphology of $KGd_{1-x}Tb_x(MoO_4)_2$ phosphors were successfully changed by H^+ exchange at the K^+ sites and obtained H-form nanoscrolls. Although the mechanism of the particle-morphology change remains unexplained in detail, it is possible to consider exfoliation of the $Eu_{1-x}Gd_x(MoO_4)_n$ layers by the substitution of K^+ by H^+ ions, which may has contributed to the change of the particle morphology. In addition, the rod-like particles formed larger aggregates, like fascicles of fibers. The dispersion of nanophosphors in solution is of high significance for their use in transparent displays. Fig. 3.6 (c) shows a SEM image of H^+-form powder redispersed in deionized water. A corresponding photograph of the suspension after 1 h is also shown in Fig 3.6. The concentration of the H^+-form powders were adjusted to 1.0×10^{-3} mol/dm^3. The Tyndall effect was confirmed by the scattering of a laser beam in the colloidal nanophosphor solution, suggesting that the H^+-form nanophosphors were fully suspended in deionized water without precipitation. From Fig. 7(b) and (c), the

aggregation of H^+-form nanophosphor particles was significantly reduced by the redispersion in deionized water and, as a result, the particles formed small units. These results suggest that $K_{0.3}H_{0.7}Eu_{0.50}Gd_{0.50}(MoO_4)_2$ might be used as a nanophosphor for transparent displays.

Fig. 3.7 exhibits the excitation and emission spectra of the suspension re-dispersed dried H-form nanoscrolls into deionized water. The concentration of the H-form phosphor powder is 1.0×10^{-3} mol/dm^{-3}. The solution shows green emission, corresponding to the 4f-4f transition of Tb^{3+} ion under UV light of 254 nm, as shown in inset photograph of Fig. 4.11. Although the peak intensity of excitation and emission spectra of the phosphor solution was lower than that of the phosphor powder, similar to the results obtained for the dried powder of $K_{0.4}H_{0.6}Gd_{0.50}Tb_{0.50}(MoO_4)_2$ nanoscroll phosphor. Fig. 3.4 shows the excitation and emission spectra of the $HEu_{0.50}Gd_{0.50}(MoO_4)_2$ nanophosphor solution, in which the concentration of the $HEu_{0.50}Gd_{0.50}(MoO_4)_2$ phosphor powder was adjusted to 1.01×10^{-2} mol/dm^3. Although the peak intensity of excitation and emission spectra of the phosphor solution was lower than that of the powdered phosphor, similar to the results obtained for the $HEu_{0.50}Gd_{0.50}(MoO_4)_2$ phosphor powder. The excitation spectrum consists of two broad band, corresponding to charge transfer (CT) transitions of O^{2-}–Mo^{6+}, respectively. Several strong narrow peaks were attributed to the 4f–4f transitions of Eu^{3+}.

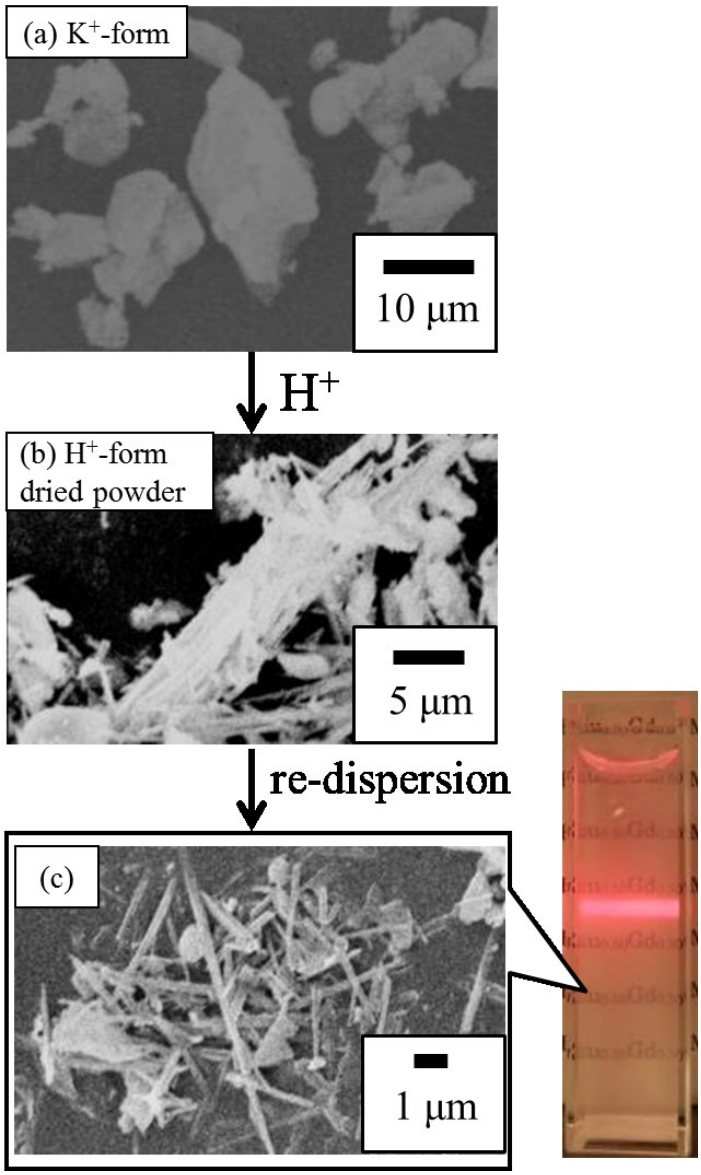

Fig. 3.6 SEM images of dried (a) $KEu_{0.50}Gd_{0.50}(MoO_4)_2$ (K^+-form) and (b) $K_{0.3}H_{0.7}Eu_{0.50}Gd_{0.50}(MoO_4)$ (H^+-form) powders and (c) H^+-form particles redispersed in deionized water (pH = 7) and corresponding photograph of the clear colloidal solution (the concentration of H^+-form powder was 1.0×10^{-3} mol/dm^3).

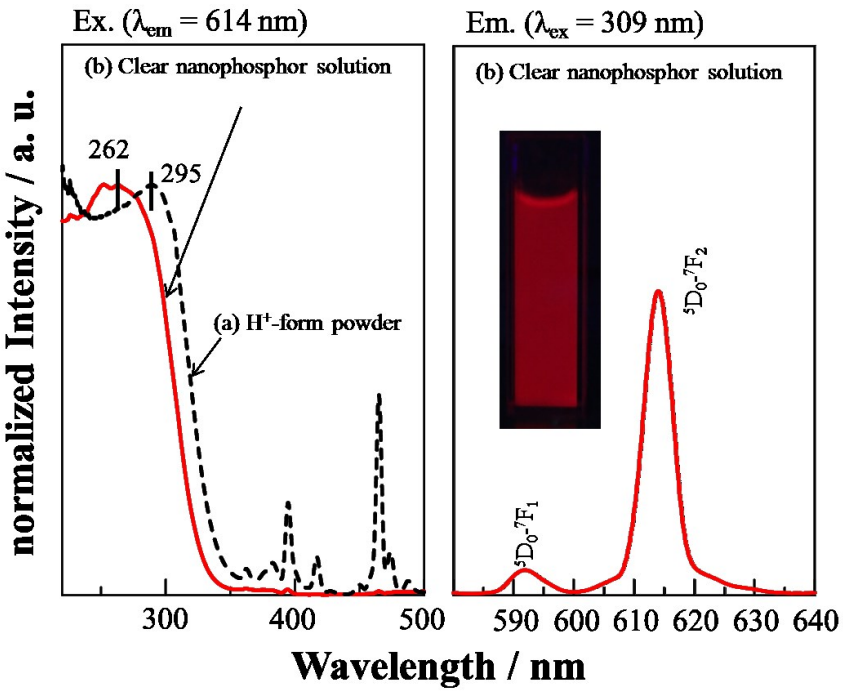

Fig. 3.7 Excitation spectra of (a) H^+-form dried powders and (b) the clear solution re-dispersed H^+-form nanophosphor. The excitation spectra were normalized in such way that the maximum intensity of the excitation spectrum is 1.

3.4 Summary

$HEu_{1-x}Gd_x(MoO_4)_2$ nanoscrolls were synthesized by one-step ion exchange achieved by stirring red-emissive $KEu_{1-x}Gd_x(MoO_4)_2$ phosphors in 0.01 M aqueous HNO_3 solution at room temperature for 7 days. The obtained $K_{0.3}H_{0.7}Eu_{1-x}Gd_x(MoO_4)_2$ nanophoscrolls have rod-like particle morphology with 0.5–15 μm in length and outer diameters in the range of 50 – 500 nm. The emission intensity of these phosphors was effectively enhanced by Gd^{3+} doping and the highest emission intensity was obtained for the samples with x = 0.50, both for $KEu_{1-x}Gd_x(MoO_4)_2$ and $K_{0.3}H_{0.7}Eu_{1-x}Gd_x(MoO_4)_2$ phosphors. We succeeded in improvement of the emission intensity of HEu(MoO4)2 nanoscroll by substituting Eu^{3+} with Gd^{3+} and suppression of concentration quenching. The aggregated dried nanoscroll powders could be redispersed in deionized water. Thus, it is expected that these phosphors can be applied as a transparent display material.

References

[1] M.V. Shestakov, V.K. Tikhomirov, D. Kirilenko, A.S. Kuznetsov, L.F. Chibotaru, A.N. Baranov, G.V. Tendeloo, and V. V. Moshchalkov, *Opt. express*, **19** (2011) 15955–15964.

[2] W.-T. Hsu, W.-H. Wu, and C.-H. Lu, *Mater. Sci. Eng. B*, 104 (2003) 40–44.

[3] Y. Iso, S. Takeshita, and T. Isobe, *Langmuir*, **30** (2014) 1465–1471

[4] A. Potdevin, G. Chadeyron, S. Therias, and R. Mahiou, *Langmuir,* **28** (2012) 13526–13535.

[5] A. Khetubol1, S. Van Snick, A. Hassinen, E. Fron, Y. Firdaus, L. Pandey, C.C. David, K. Duerinckx, W. Dehaen, Z. Hens, and M. Auweraer, *J. Appl. Phys.*, **113** (2013) 083507-1-12.

[6] C. W. Hsu, B. Zhen, W. Qiu, O. Shapira, B. G. DeLacy, J. D. Joannopoulos, and M. Soljačić, *Nat. Comm.*, **5** (2014) 1–6.

[7] S. Choi, S. W. Tae, J. H. Seo, and H. K. Jung, *J. Solid State Chem.*, **184** (2011) 1540–1544.

[8] C. Hilsum, *Phil. Trams. R. Soc. A*, **368** (2010) 1027–1082.

[9] V. Bulovic, G. Gu, P. E. Burrows, S. R. Forrest, and M. E. Thomposn, *Nature*, **380** (1996) 29, March.

[10] V. Buissette, D. Giaume, T. Gacoin, and J. -P. Boilot, *J. Mater. Chem.*, **16** (2006) 529–539.

[11] H. Yang, D. -K. Lee, and Y. -S. Kim, *Mater. Chem. Phys.*, **114** (2009) 665–669.

[12] J. Dhanaraj, R. Jagannathan, T. R. N. Kutty, and C. H. Lu, *J. Phys. Chem. B*, **105** (2001) 11098–11105.

[13] H. Hu, L. Xiong, J. Zhou, F. Li, T. Cao, and C. Huang, *Chem. Eur. J.*, **15** (2009) 3577– 3584.

[14] W.-S. Song, H.-N. Choi, Y.-S. Kim, and H. Yang, *J. Mater. Chem.*, 20 (2010) 6929–6934.

[15] C. Guo, S. Wang, T. Chen, L. Luan, and Y. Xu, *Appl. Phys. A*, **94** (2009) 365–371.

[16] R. F. Klevtsova, L. P. Kozeeva, and P. V. Klevtsov, *Sov. Phys. Crystallogr.*, **19** (1977) 339–355.

[17] M. Watanabe, K. Uematsu, S. Kim, K. Toda, and M. Sato, *J. Ceram. Proc. Res.*,**15** (2015) 173–176.

[18] A. Xie, X. Yuan, F. Wang, Y. Shi, J. Liu, and Z. Mu, *J. Alloys Compd.*, **501** (2010) 124–129.

[19] W. L. Feng, Y. Jin, Y. Wu, D. F. Li, and A. K. Cai, *J. Lumin.*,**134** (2013) 614–617.

[20] T. Kano, "Principal phosphor materials and their optical properties," in Phosphor Hand book, ed. S. Shionoya and W. M. Yen, pp. 178–300, CRC Press, New York, 1999.

[21] R. D. Shannon, *Acta Cryst.*, *Sect. A*, **32** (1976) 751–767.

Chapter 4

Synthesis and luminescence property of green-emissive $HGd_xTb_{1-x}(MoO_4)_2$ ($0.00 \leq x \leq 1.00$) nanoscrolls phosphor by soft-chemical H^+ exchange method

4.1 Introduction

Rare-earth doped compounds have been widely investigated because of their versatile application, including magnetic material [1], catalyst [2], solid electrolyte [3], phosphor [4], and so on. Among them, rare—earth doped phosphors for applications in photonic devices have attracted much attention due to the specific luminescence attributed to their f—f emission. Phosphors are commonly used in fluorescent lamps and luminescent displays [5] and are promising materials for applications in lasers [6] and X-ray imaging [7]. Nanophosphors improve the resolution of displays [8] and have promising applications as bioimaging probes [9], because of their transparency. The inorganic nanophosphors have advantage of photostability (no blinking or fading) and biocompatibility [10] over traditionally used organic dyes and semiconducting nanoparticles. Organic fluorescent dyes photobleach during bioimaging while semiconducting nanoparticles exhibit optical blinking [11]; they have toxic consequences [12]. Dispersible nanophosphors facilitate their employment in nanocomposite materials, such as thin films in flexible displays [5].

Tb^{3+}-doped nanomaterial have been widely used as green emitting phosphors due

to their intense $^5D_4 \rightarrow {}^7F_5$ emission in the green spectral region. Previous investigations have showed that Tb^{3+}-doped aluminates or phosphates exhibit relatively strong absorption in the near-UV region and intense green emission with good color purity [13-22].

Molybdates have been known to be important optical materials, because its central Mo metal ion is coordinated by four O^{2-} ions in tetrahedral symmetry (T_d), which makes MoO_4^{2-} is relatively stable and a good potential host material [23-29]. Tb^{3+}-doped $KGd(MoO_4)_2$ forming α-$KEu(MoO_4)_2$-type structure with the space group of *P*-1, to our knowledge, have been not reported, despite their layered structure which suppresses concentration quenching; A few report of their structural, optical-absorption and vibrational properties have been reported [30-32].

In this chapter, we attempted to synthesized triclinic $KGd_xTb_{1-x}(MoO_4)_2$ ($0.00 \leq x \leq 1.00$) forming α-$KEu(MoO_4)_2$-type structure with the space group of *P*-1 by the substituting Gd^{3+} ions in $KGd(MoO_4)_2$ by smaller Tb^{3+} ions and investigated their luminescence property. In addition, the morphological and luminescence properties of $HGd_xTb_{1-x}(MoO_4)_2$ ($0.00 \leq x \leq 1.00$) nanoscrolls obtained by H^+-exchange method were investigated.

4.2 Experimental

4.2.1 Synthesis of materials

$KGd_{x-1}Tb_x(MoO_4)_2$ ($0.00 \leq x \leq 1.00$) were synthesized by a conventional solid-state reaction (SSR) method. K_2CO_3 (purity 99.95 %; Kanto Chemical Co. Inc.), Gd_2O_3 (purity 99.99 %; Shinetsu Chemical Co. Inc.), Tb_4O_7 (purity 99.95 %; Kanto Chemical Co. Inc.), and MoO_3 (purity 99.99 %; Kojundo Chemical Co. Inc.) were mixed using a mortar and pestle with acetone; the mixture was then calcined at 600 °C for 6 h in air. $HGd_{1-x}Tb_x(MoO_4)_2$ samples were obtained by the H^+ exchange of $KGd_{1-x}Tb_x(MoO_4)_2$ in HNO_3 solution (0.01 M, 100 mL) at room temperature for 7 days. The acid solution was refreshed once several days to complete H^+ exchange. After stirring, the solutions were isolated by suction filtration using a membrane filter (ADVANTEC MFS, INC., mixed cellulose ester, pore size: 0.45 μm, diameter: 47 mm). The samples were washed with deionized water at room temperature for 24 h and then dried at 50 ºC for 24 h. The obtained $HGd_{1-x}Tb_x(MoO_4)_2$ powder samples were redispersed in deionized water.

4.2.2 Materials characterization

The obtained samples were characterized by X-ray powder diffraction (XRD; Mac Science Ltd., MX-Labo) to identify the crystal structure and the sample composition was analyzed by X-ray fluorescence analysis (XRF; Seiko Instruments Inc., SEA 1200VX). Morphology of the samples was characterized by means of scanning

electron microscopy (SEM; Hitachi Ltd., S-4300SD). The emission (PL) and excitation (PLE) spectra were measured at room temperature with a spectrofluorometer (Jasco Corp., FP-6500/6600), where the emission spectra were obtained for excitation at 288 nm, and excitation spectra were obtained for emission at 548 nm

4.3 Result and discussion

The XRD patterns of the $KGd_xTb_{1-x}(MoO_4)_2$ ($0.00 \leq x \leq 1.00$) phosphors obtained by the SSR method at 600℃ for 6 h are shown in Fig. 4.1. The standard XRD pattern of $KGd(MoO_4)_2$ obtained from the inorganic crystal structure database (ICSD #6138) is also shown in Fig. 4.1 as a reference. The diffraction patterns were in good agreement with that of triclinic α-$KEu(MoO_4)_2$ type structure with the space group of *P*-1; no diffraction peak corresponding to any impurity in the patterns was observed. A peak shift to higher angle in diffraction angle around 30 degree was observed with an increase in the Tb^{3+} content in the $KGd(MoO_4)_2$ lattice. This result indicates that Tb^{3+} ions successfully substituted the Gd^{3+} sites in the host lattice to form solid solutions, because the ionic radius of Gd^{3+} (0.1040 nm for eight coordination) [33] is smaller than that of Tb^{3+} (0.1053 for eight coordination) [33].

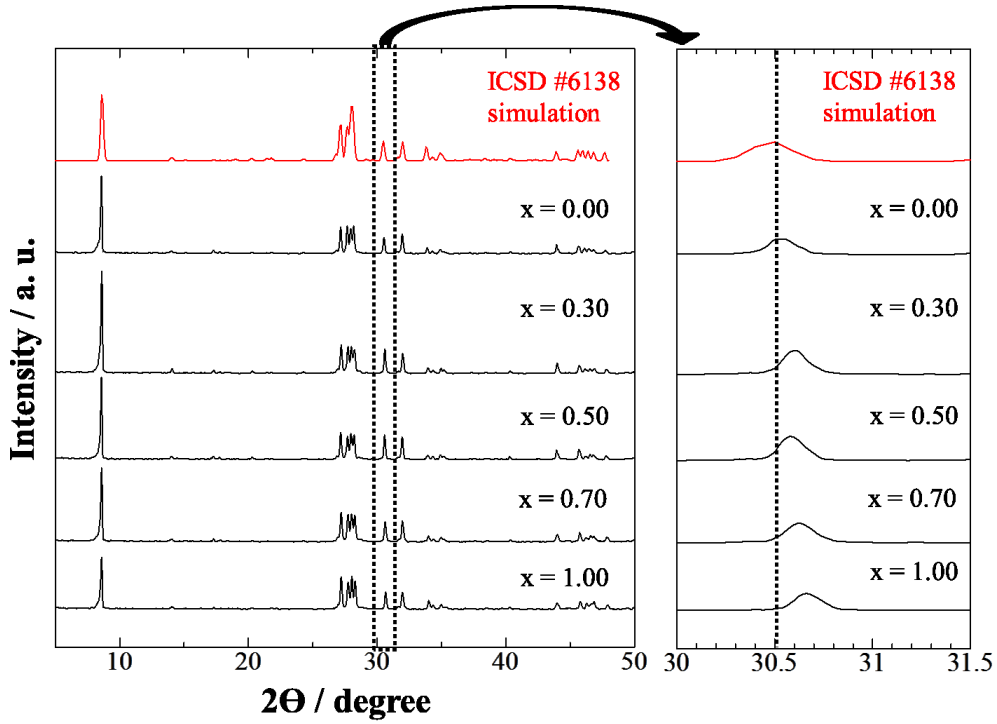

Fig. 4.1 The XRD pattern of $KGd_{x-1}Tb_x(MoO_4)_2$ ($0.00 \leq x \leq 1.00$) synthesized by the solid state reaction method at 600 ℃ for 6 h in air.

Fig. 4.2 shows excitation and emission spectra monitored at room temperature of the precursor green-emissive $KGd_{0.50}Gd_{0.50}(MoO_4)_2$ phosphors obtained by the SSR method at 600℃ for 6 h. The excitation spectra of all samples monitored at 548 nm consisted of a strong broad band in the range from 220 to 350 nm with a maximum at about 288, corresponding to the charge-transfer (CT) transition of O^{2-}–Mo^{6+} [34-36]. Some strong narrow peaks are observed between 350 and 500 nm and are attributed to the 4f–4f transitions of the Tb^{3+} ion. The emission spectra of the Tb^{3+} ions at 544 nm ($^5D_4$-$^7F_5$), 587nm ($^5D_4$-$^7F_4$) and 612 nm ($^5D_4$-$^7F_3$) were observed, corresponding 4f-4f transitions of Tb^{3+} ions and the all sample show green emission under UV-light excitation of 306 nm.

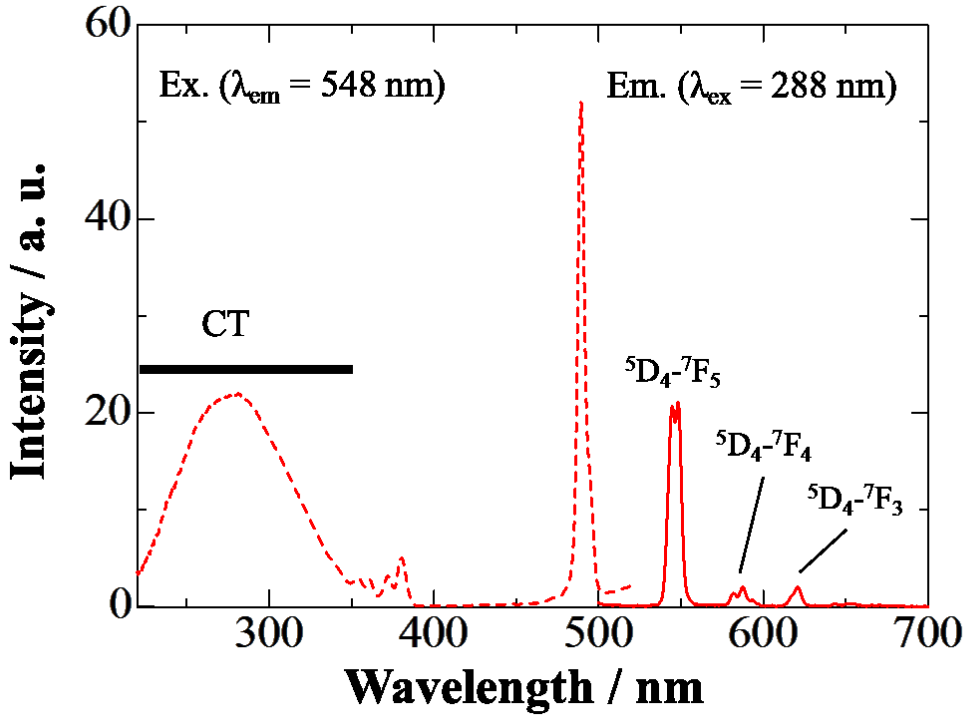

Fig. 4.2 The excitation (broken line) and emission spectra (solid line) at room temperature of $KGd_{0.50}Tb_{0.50}(MoO_4)_2$ synthesized by the solid state reaction method at 600 ºC for 6 h in air.

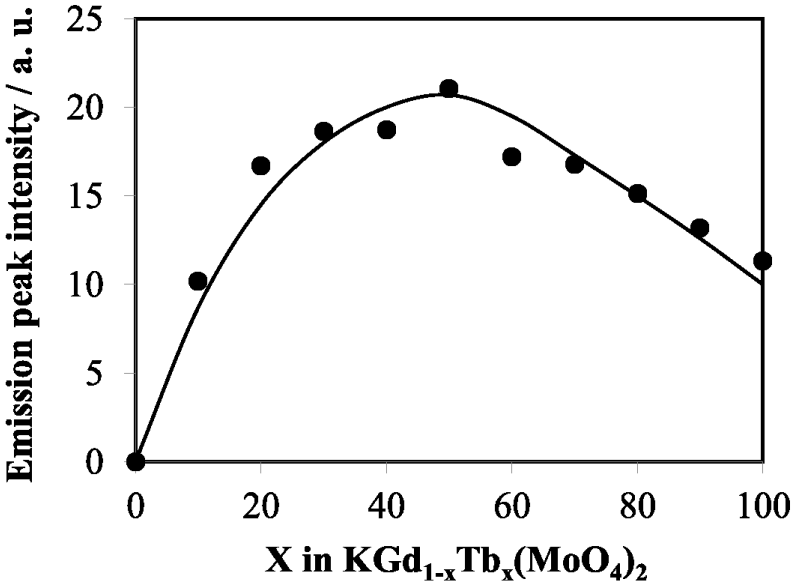

Fig. 4.3 The dependence of the emission intensity at 548 nm excited at 288 nm on the Tb^{3+} content in $KGd_{1-x}Tb_x(MoO_4)_2$ ($0.00 \leq x \leq 1.00$) phosphors.

The luminescence spectrum of Tb^{3+}, as well as that of Eu^{3+}, strongly depends on the concentration in the host lattice. This is because at higher concentrations, the higher emitting levels, $^5D_3$ of Tb^{3+} transfer its energies to neighboring ions of the same specie by the following cross-relaxations; that is $^5D_3(Tb^{3+})+^7F_6(Tb^{3+}) \rightarrow {}^5D_4(Tb^{3+})+^7F_0(Tb^{3+})$. Therefore, Tb^{3+} also exhibits concentration-quenching phenomena. Fig. 4.3 shows the compositional dependence of the emission intensity excited at 288 nm of $KGd_{1-x}Tb_x(MoO_4)_2$ ($0.00 \leq x \leq 1.00$). The emission intensity initially increases with increasing amount of Tb^{3+} and reaches a maximum at $x = 0.50$. However, the emission intensity decreases on further increasing Tb^{3+} content beyond the optimum concentration, which is attributed to the decrease of the Tb^{3+} concentration. This value is higher than other Tb^{3+}-doped phosphors. This result indicates that the phosphors possess a high critical value of Tb^{3+} quenching concentration.

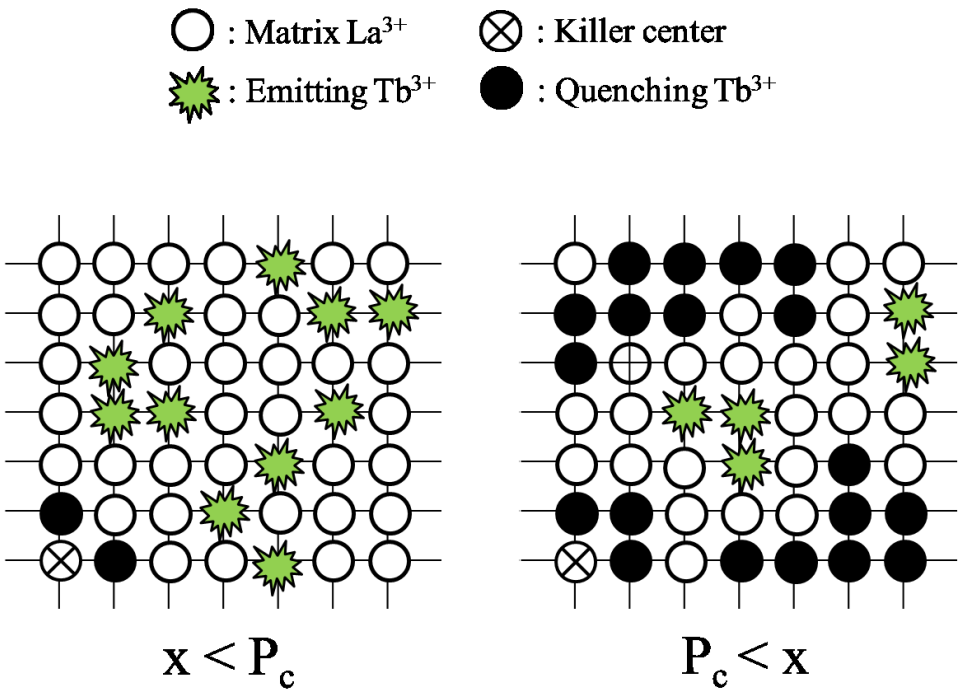

Fig. 4.4 The schematic representation of the percolation model.

The theoretical value of the optimum concentration in this compound is determined by a percolation model [37-39]. The percolation model has been used for describing the behaviors of many dilute physical systems. In the present study, the percolation model can be applied to the given compound based on two assumptions: (1) The interaction among Tb^{3+} ions occurs only among the nearest—neighbor sites in rare—earth sublattice and (2) The concentration quenching is due to the energy transfer from percolating clusters of the Tb^{3+} ions to killer centers. The the MoO_4—GdO_8 layer structure of the $KGd_{1-x}Tb_x(MoO_4)_2$ has a quasi—two—dimensional sublattice. In such a case, the optimum concentration is considered to be only dependent of the distance between the rare—earth ions. Fig. 4.4 shows a schematic representation of the percolation model. The filled circles in the lattice describe Tb^{3+} ions. When the Tb^{3+}

concentration is below the circle concentration, the Tb^{3+} ions exist in small cluster and emit individually. On the other hand, over the percolation threshold P_c, the cluster is connected with the other clusters. The percolating cluster increases the probability of contact with the killer centers, such as unknown defects or very small amounts of impurities. Vyssotsky et al. has reported an approximate expression of optimum concentration for the percolation model [37]:

$$z^*P_c = d/(d—1)$$

where z is the coordination number (the number of nearest—neighbor sites) of emission center, P_c the optimum concentration and d the number of dimensionality of the percolation lattice. The number of nearest Tb^{3+} sites z is 3 for the $KGd_{1-x}Tb_x(MoO_4)_2$, as shown in Fig. 4.5 . The calculated value P_c, the optimum Tb^{3+} concentration in the

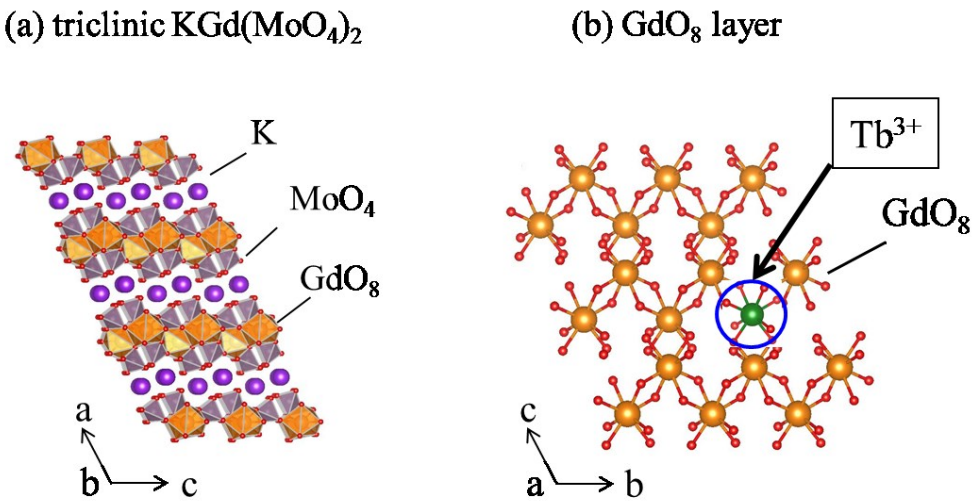

Fig. 4.5 The crystal structure of (a) the layered molybdate, triclinic $KGd(MoO_4)_2$ with triclinic α-$KEu(MoO_4)_2$ structure having the space group of P-1 and (b) the GdO_8 layer.

$KGd_{1-x}Tb_x(MoO_4)_2$ lattice is 0.67. The experimental date, however, was 0.50, disagreeing with the calculated value. This is, probably, because Tb^{4+}, non-luminous center ion, might remain in the host lattice; The raw material Tb_4O_7 contains bonth Tb^{3+} and Tb^{4+}.

To synthesize nanophosphors, the obtained $KGd_{1-x}Tb_x(MoO_4)_2$ phosphors were stirred in HNO_3 solution at room temperature. The composition of $KGd_{1-x}Tb_x(MoO_4)_2$ before and after H^+ exchange was analyzed by XRF. From XRF result, all $KGd_{1-x}Tb_x(MoO_4)_2$ retains the ratio of Gd, Tb, and Mo after H^+ exchange, suggesting the framework of $KGd_{1-x}Tb_x(MoO_4)_2$ precursor structure ware preserved. Fig. 4.6 shows the amount of remaining K^+ ions in the phosphors after H^+ exchange procedure. No H^+ exchange in the precursor with high concentration of Tb^{3+} ($0.80 \leq x \leq 1.00$) occurred. It is because surplus positive charge caused from remaining Tb^{4+} in the host lattice prevents H^+/H_3O^+ from inversion into interlayers and exchange K^+ ions.

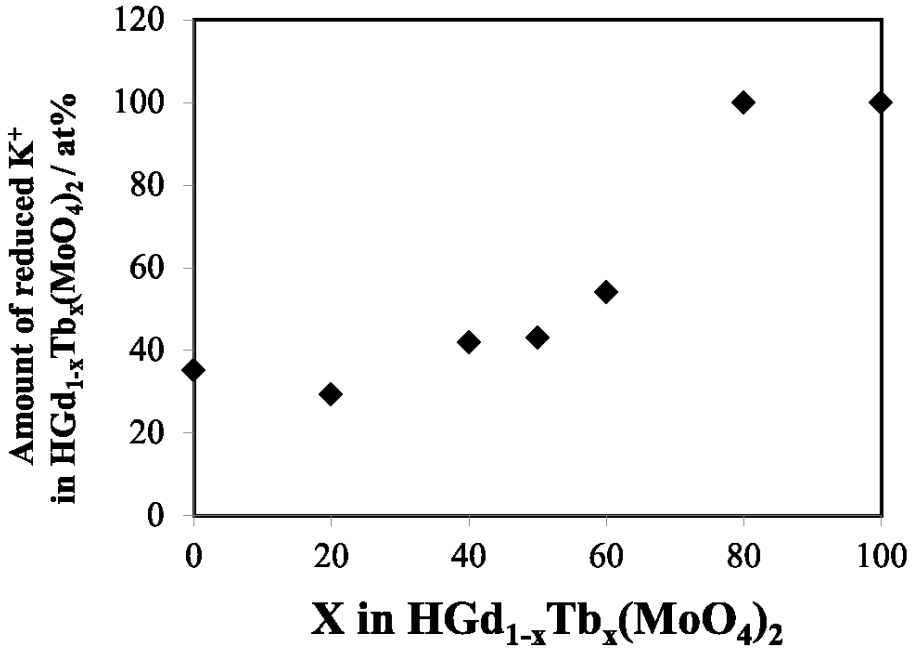

Fig. 4.6 The dependence of the amount of reduced K^+ in $HGd_{1-x}Tb_x(MoO_4)_2$ ($0.00 \leq x \leq 1.00$) phosphors after H^+-exchange procedure.

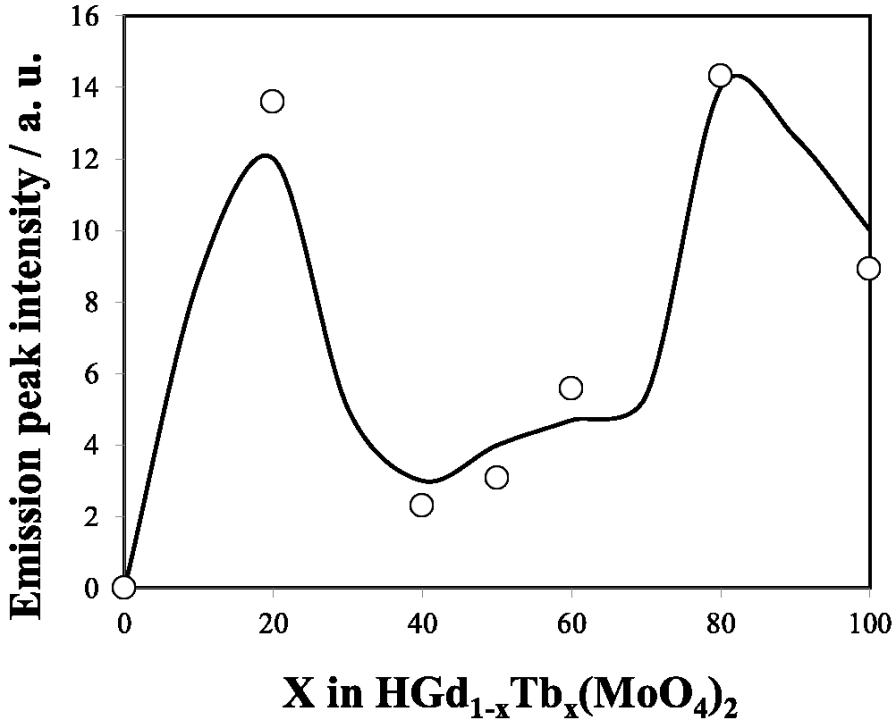

Fig. 4.7 Dependence of the emission intensity on the Tb^{3+} content in $HGd_{1-x}Tb_x(MoO_4)_2$ ($0.00 \leq x \leq 1.00$) phosphors.

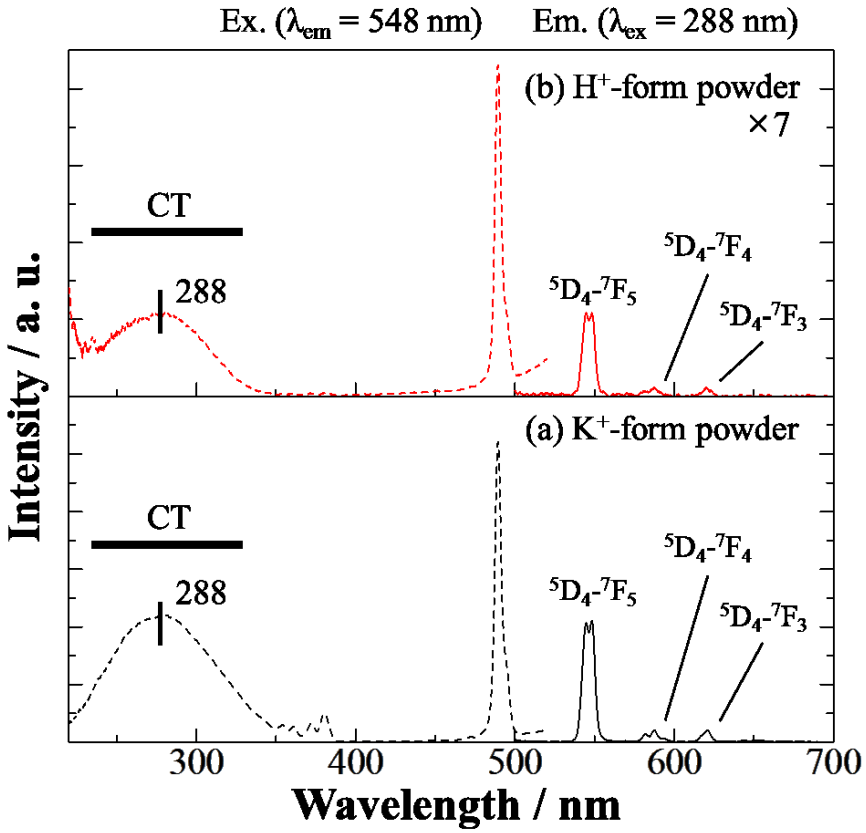

Fig. 4.8 Excitation (broken line) and emission (solid line) spectra at room temperature of (a) $KGd_{0.50}Tb_{0.50}(MoO_4)_2$ (K-form) and (b) dried $K_{0.4}H_{0.6}Gd_{0.50}Tb_{0.50}(MoO_4)_2$ (H-form) powders prepared by stirring in 0.01 M HNO_3 solution for 7 days.

Fig. 4.7 shows the compositional dependence of the luminescence intensity excited at 288 nm of $K_{0.40}H_{0.60}Gd_{1-x}Tb_x(MoO_4)_2$ ($0.00 \leq x \leq 1.00$) after H^+ exchange procedure. The emission intensity decreased with increasing the ratio of H^+ exchange. To compare the photoluminescence property of $K_{0.4}H_{0.6}Gd_{1-x}Tb_x(MoO_4)_2$ (H-form) with that of $KGd_{1-x}Tb_x(MoO_4)_2$ (K-form), the H-form powders were washed with deionized water at room temperature for 24 h and then dried at 50 ºC for 24 h. Fig. 4.8 shows

excitation and emission spectra of K-form and dried H-form powders. The behavior observed in the excitation and emission spectra of H^+-form powders ranging from x=0.40 to x=0.60 in $K_{0.4}H_{0.6}Gd_{1-x}Tb_x(MoO_4)_2$ was similar. It's noteworthy that the optimal concentration changes to x=0.20 after H^+ exchange in the same proton exchange ratio. It's probably because the coordination number (the number of nearest—neighbor sites) of emission center and the $Tb^{3+}-$Tb3+ nearest-neighbor distance change by the transformation into nanoscroll (shown in Fig. 4.9), resulting in change of environment of Tb^{3+}. The characteristic of excitation and emission spectra of H-form retains to that of K-form, although the emission intensity of H-form is lower than that of K-form.

Fig. 4.9 shows SEM images of $KGd_{0.50}Tb_{0.50}(MoO_4)_2$ and dried $K_{0.4}H_{0.6}Gd_{0.50}Tb_{0.50}(MoO_4)_2$ powders. The K-form powder has a granular particle morphology with average particle size of 3 μm. In contrast, although a small amount of granular particles remained, the dried H-form powders have bundled rod-like particle morphology with 1–15 μm in length and outer diameters in the range of 50–500 nm. The morphology an size were similar to those of $HEu(MoO_4)_2$ derived from triclinic $KEu(MoO_4)_2$ phosphor with the same crystal structure, indicating the particle size and morphology of $KGd_{1-x}Tb_x(MoO_4)_2$ phosphors were successfully changed by H^+ exchange at the K^+ sites and obtained H-form nanoscrolls.

Fig. 4.9 SEM images of (a) $KEu_{0.50}Gd_{0.50}(MoO_4)_2$ (K^+-form) and (b) dried $K_{0.4}H_{0.6}Eu_{0.50}Gd_{0.50}(MoO_4)$ (H^+-form) powders prepared by stirring in 0.01 M HNO_3 solution for 7 days.

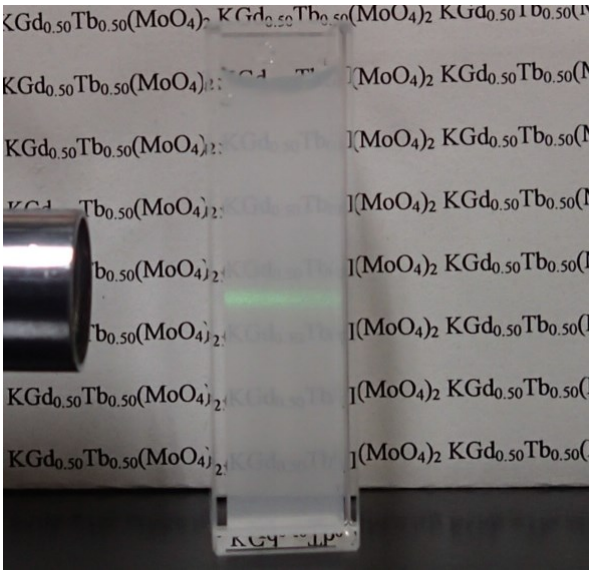

Fig. 4.10 Photograph of the suspension re-dispersed dried $K_{0.4}H_{0.6}Gd_{0.50}Tb_{0.50}(MoO_4)_2$ nanoscrolls into deionized water after 1 h (The concentration of the H-form powder was adjusted to 1.0×10^{-3} mol/dm^{-3}) and their Tyndall effect.

Fig. 4.10 shows the photograph of the suspension re-dispersed dried $K_{0.4}H_{0.6}Gd_{0.50}Tb_{0.50}(MoO_4)_2$ (H-form) nanoscrolls into deionized water after 1 h. The concentration of the H^+-form powder was adjusted to 1.0×10^{-3} mol/dm^{-3}. The Tyndall effect was confirmed by the scattering of a laser beam in the colloidal nanophosphor solution, suggesting that the H-form nanophosphors were fully suspended in deionized water without precipitation. Fig. 4.11 exhibits the excitation and emission spectra of the suspension re-dispersed dried H-form nanoscrolls into deionized water. The concentration of the H-form phosphor powder is 1.0×10^{-3} mol/dm^3. The solution shows green emission, corresponding to the 4f-4f transition of Tb^{3+} ion under UV light of 254 nm, as shown in inset photograph of Fig. 4.11. Although the peak intensity of excitation and emission spectra of the phosphor solution was lower than that of the phosphor

powder, similar to the results obtained for the dried powder of $K_{0.4}H_{0.6}Gd_{0.50}Tb_{0.50}(MoO_4)_2$ nanoscroll phosphor.

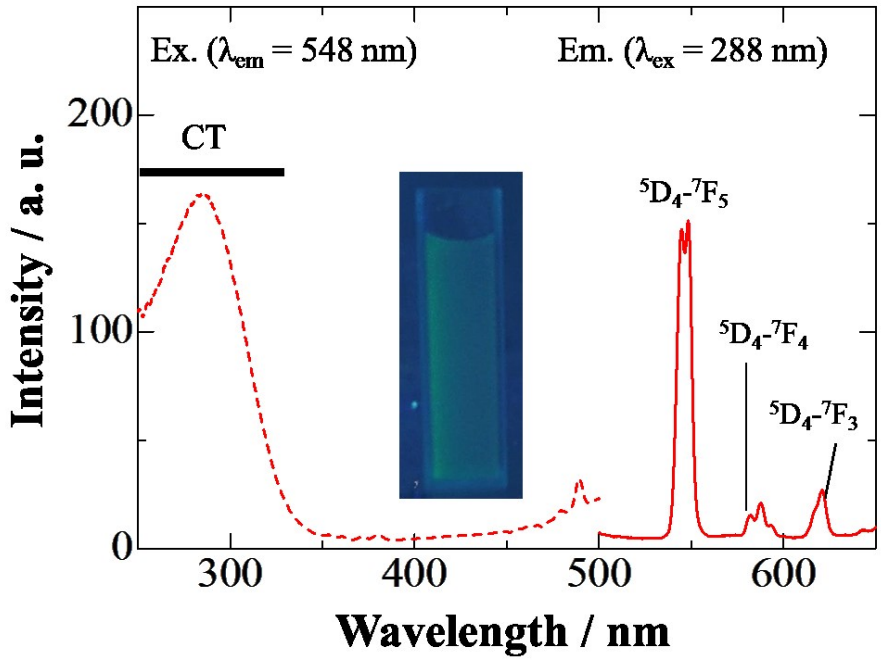

Fig. 4.10 Excitation (broken line) and emission (solid line) spectra of the suspension re-dispersed dried $K_{0.4}H_{0.6}Gd_{0.50}Tb_{0.50}(MoO_4)_2$ nanoscrolls into deionized water after 1 h. Concentration of the H^+-form powder in the solution: 1.0×10^{-3} mol/dm^3. The inset photograph shows green emission luminescence of $K_{0.4}H_{0.6}Gd_{0.50}Tb_{0.50}(MoO_4)_2$ solution illuminated by a UV light of 254 nm.

4.4 Summary

Green-emissive $HGd_{1-x}Tb_x(MoO_4)_2$ ($0.20 \leq x \leq 0.70$) nanoscroll phosphors were synthesized by one-step ion exchange achieved by stirring $KGd_{1-x}Eu_x(MoO_4)_2$ ($0.20 \leq x \leq 0.70$) phosphors in 0.01 M aqueous HNO_3 solution at room temperature for 7 days. The obtained $K_{0.4}H_{0.6}Gd_{1-x}Tb_x(MoO_4)_2$ nanophosphors have rod-like particle morphology with 0.5–15 μm in length and outer diameters in the range of 50 – 500 nm. The highest emission intensity was obtained for the samples with x = 0.50, both for $KEu_{1-x}Gd_x(MoO_4)_2$. After H^+ exchange, the optimal concentration change to x= 0.20. The excitation and emission of dried $K_{0.3}H_{0.7}Eu_{1-x}Gd_x(MoO_4)_2$ powder and the nanoscroll solution results similar to that of K-form powder. The dried nanophosphor powders could be redispersed in deionized water. These results suggest that $K_{0.4}H_{0.6}Eu_{0.50}Gd_{0.50}(MoO_4)_2$ is expected to be used as a nanophosphor for transparent thin film.

References

[1] J. M. D. Coey and H. Sun, *J. Magn. Magn. Mater.*, **87** (1990) L251–L254.

[2] H. Sasai, T. Suzuki, N. Itoh, K. Tanaka, T. Date, K. Okamura, and M. Shibasaki, *J. Am. Chem. Soc.*, **115** (1993) 10372–10373.

[3] K. Huang and J. B. Goodenough, *J. Alloy. Compd.*, **303–304** (2000) 454–464.

[4] E. Danielson, M. Devenney, D. M. Giaquinta, J. H. Golden, R. C. Haushalter, E. W. McFarland, D. M. Poojary, C. M. Reaves, W. Henry Weinberg, and X. D. Wu, *Science*, **279** (1998) 837–839.

[5] T. Jüstel, H. Nikol, C. Ronda, *Angew. Chem.-Int. Ed.*, **37** (1998) 3085–3103.

[6] Y. Mao, J.Y. Huang, R. Ostroumov, K.L. Wang, and J.P. Chang, *J. Phys. Chem. C*, **112** (2008) 2278–2285.

[7] S.L. Isslera and C.C. Torardi, *J. Alloys Compd.*, **229** (1995) 54–65.

[8] R. Kubrin, A. Tricoli, A. Camenzind, S.E. Pratsinis, and W. Bauhofer, *Nanotechnology*, **21** (2010) 2256603.

[9] .F Zhang and S.S. Wong, *ACS Nano*, **4** (2010) 99–112.

[10] G.K. Das and T.T.Y. Tan, *J. Phys. Chem. C*, **112** (2008) 11211–11217.

[11] M. Nirmal, B.O Dabbousi, M.G. Bawendi, J.J. Macklin, J.K. Trautman, T.D. Harris, L.E. Brus, *Nature*, **383** (1996) 802–804.

[12] I.L. Medintz, H.T. Uyeda, E.R. Goldman, H. Mattoussi, *Nat. Mater.*, **4** (2005) 435–446.

[13] B. Yan and H.-H. Huang, *J. Mater. Sci.*, **39** (2004) 3529–3531.

[14] G.A. Sotiriou, M. Schneider, and S.E. Pratsinis, *J. Phys. Chem. C*, **115** (2011) 1084–1089.

[15] D.P. Dutta, M. Roy, and A.K. Tyagi, *Dalton Trans.*, **41** (2012) 10238–10248.

[16] K.G. Tshabalala, S.-H. Cho, J.-K. Park, S.S. Pitale, I.M. Nagpure, R.E. Kroon, H.C. Swart, and O.M. Ntwaeaborwa, *J. Alloy. Compd.*, **509** (2011) 10115–10120.

[17] S. Som, S. Dutta, V. Kumar, V. Kumar, H.C. Swart, and S.K. Sharma, *J. Lumin.*, **146** (2014) 162–173.

[18] D.P. Dutta, R. Ghildiyal, and A.K. Tyagi, *J. Phys. Chem. C*, **113** (2009) 16954–16961.

[19] G.A. Sotiriou, M. Schneider, and S.E. Pratsinis, *J. Phys. Chem. C*, **116** (2011) 4493−4499.

[20] G.S. Raju, J.-Y. Park, H.-C. Jung, B.-K. Moon, J.-H. Jeong, and J.-H. Kim, *J. Electrochem. Soc.*, **158** (2011) J20–J26.

[21] D. Kumar, M. Sharma, D. Haranath, and O.P. Pandey, *J. Alloy. Compd*., **695** (2017) 726–736.

[22] D. P. Dutta, N. Manoj, and A.K. Tyagi, *J. Lumin.*, **131** (2011) 1807–1812.

[23] L. Li, D. Dong, J. Zhang, C. Zhang, and G. Jia, *Mater. Lett.*, **131** (2014) 298–301.

[24] M. Yang, Y. Liang, Q. Gui1, B. Zhao, D. Jin, M. Lin, Lu Yan, H. You, L. Dai, and Y. Liu, *Sci. Rep.*, **5** (2015) 1-12.

[25] L. Hou, S. Cui, Z. Fu, Z. Wu, X. Fu, and J.-H. Jeong, *Dalton Trans.*, **43** (2014) 5382–5392.

[26] J. Liao, D. Zhou, H. You, H.-R. Wen, Q. Zhou, and Bin Yang, *Optik*, **124** (2013)

1362–1365.

[27] Z. Xu, C. Li, G. Li, R. Chai, C. Peng, D. Yang, and J. Lin, *J. Phys. Chem. C*, **114** (2010) 2573–2582.

[28] Y. Tian, B. Chen, B. Tian, J. Sun, X. Li, J. Zhang, L. Cheng, H. Zhong, H. Zhong, Q. Meng, and R. Hua, *Physica B*, **407** (2012) 2556–2559.

[29] G. Li, L. Li, M. Li, W. Bao, Y. Song, S. Gan, H. Zou, and X. Xu, *J. Alloy.Compd.*, **550** (2013) 1–8.

[30] S.R. Shieh, S. Hemmi, L.C. Ming, A. Jayaraman, S. Endo, O. Shimomura, and T. Kikegawa, *J. Phys. Chum. Solids*, **l58** (1997) 2069-2077.

[31] A. Jayaraman, S.K Sharma, S.Y Wang, S.R Shieh, L.C. Ming, and S.-W. Cheong, P*ramana*, **47** (1996) 151-161.

[32] A. Jayaraman, S. K. Sharma, S. Y. Wang, S. R. Shieh, L. C. Ming, and S.-W. Cheong, *J. Raman, Spectrosc.*, **27** (1996) 485-490.

[33] R. D. Shannon, *Acta Cryst.*, *Sect. A*, **32** (1976) 751–767.

[34] Z. Wang, H. Liang, Q. Wang, L. Luo, and M. Gong, *Mater. Sci. Engineer. B*, **164** (2009) 120–123.

[35] Z. Hou, R. Chai, M. Zhang, C. Zhang, P. Chong, Z. Xu, G. Li, and J. Lin, *Langmuir*, **25** (2009) 12340–12348.

[36] A. Khanna and P.S. Dutta, *J. Solid State Chem.*, **198** (2013) 93–100.

[37] V.A. Vyssotsky, S.B. Gordon, H.L. Frisch, and J.M. Hammersley, *Phys. Rev.*, **123** (1961) 1566–1567.

[38] K. Toda, Y. Kameo, M. Ohta, and M. Sato, *J. Alloy. Compd.*, **218** (1995) 228–232.

[39] T. Honma, K. Toda, Z.-G. Ye, and M. Sato, *J. Phys. Chem. Solids*, **59** (1998) 1187–1193.

Chapter 5

Synthesis of HLn $(MoO_4)_2$ (Ln=Pr, Nd, Sm, Eu) nanoscroll derived from $RbLn(MoO_4)_2$ with orthorhombic $KY(MoO_4)_2$ type structure

4.5 Introduction

The $RbLn(MoO_4)_2$ have been of considerable interest from the crystal chemistry point of view, and the formation of $RbLn(MoO_4)_2$ phase with various structures have been reported [1, 2]. Nevertheless, the application and chemical and physical properties of the $RbLn(MoO_4)_2$ compounds are poorly investigated; the detail structural information and vibrational properties have been reported in a few investigate [3-6]. There, especially, are no reports for particle-size controlling. Therefore, synthesis of nanomatrial related to the $RbLn(MoO_4)_2$ phase is expected to achieve a new properties and application such as nano laser, nano magnetic material, and catalyst.

In this chapter, we focused on $RbLn(MoO_4)_2$ phase with $KY(MoO_4)_2$ type structure with the space group of *Pbcn* in order to synthesize nanoparticle related to $RbLn(MoO_4)_2$ phase; the formation of the phase can be observed for Ln=Pr-Eu. Therefore, it is expected to be synthesized $HLn(MoO_4)_2$ nanoscroll derived from them by H^+ exchange method. The structural and morphological of the nanoscrolls were evaluated.

5.2 Experimental

5.2.1 Synthesis of materials

Precursor powders $RbLn(MoO_4)_2$ (Ln=Pr, Nd, Sm), in previous study, were synthesized by conventional solid state (SSR) synthesis method, using a stoichiometric ratio mixture of Rb_2CO_3 (purity 97%; Wako Pure Chemical Industies, Ltd.), Pr_6O_{11} (purity 99.99%; Kojundo Chemical Co. Inc.), Nd_2O_3 (purity 99.99%; Kanto Chemical Co. Inc.), and Sm_2O_3 (purity 99.99%; Kanto Chemical Co. Inc.), and MoO_3 (purity 99.99%; Kojundo Chemical Co. Inc.) as starting materials [3, 4]. The multistage method with a step-by-step temperature increase is optimal for complex molybdates synthesis. Initially, rubidium and neodymium molybdates were prepared by the SSR method. Heat treatment of stoichiometric mixtures was started at T=450℃ and followed by a step-wise temperature increasing up to T=600℃ (Rb_2MoO_4) and 800℃ ($Pr_2(MoO_4)_3$, $Nd_2(MoO_4)_3$ and $Sm_2(MoO_4)_3$). The phase purity of intermediate products Rb_2MoO_4 and $Pr_2(MoO_4)_3$, $Nd_2(MoO4)_3$, and $Sm_2(MoO_4)_3$ was evaluated by powder XRD analysis. The XRD patterns were compared to the available structural characteristics of the molybdates obtained from ICSD. The powder mixture of the compounds in stoichiometric ratio was being preheated at T= 550℃ for about 24 h and then annealed at T=600℃ for 24 h to yield the $RbPr(MoO_4)_2$, $RbNd(MoO_4)_2$, and $RbSm(MoO_4)_2$ composition. $RbEu(MoO_4)_2$ was synthesized by the same way as chapter 2.

$HPr(MoO_4)_2$, $HNd(MoO_4)_2$, $HSm(MoO_4)_2$, $HEu(MoO_4)_2$, powders were obtained by stirring of $RbNd(MoO_4)_2$, $RbNd(MoO_4)_2$, $RbSm(MoO_4)_2$, $RbEu(MoO_4)_2$ (0.5 g) in 0.01 M aqueous HNO_3 solution (100 mL) at room temperature for 7 days, respectively,

in order to exchange alkali metal ions to proton. The acid solution was refreshed once several days to complete H^+ exchange. After stirring, the solution was isolated suction filtration with membrane filter (ADVANTEC MFS, INC., mixed cellulose ester, pore size: 0.45μm, diameter: 47 mm). The sample was washed with deionized water for 24 h and then dried at 50 °C for 24 h.

5.2.2 Materials characterization

The obtained samples were characterized by X-ray powder diffraction (XRD; Mac Science Ltd., MX-Labo) to identify the crystal structure and the sample composition was analyzed by X-ray fluorescence analysis (XRF; Seiko Instruments Inc., SEA 1200VX). Morphology of the samples was characterized by means of scanning electron microscopy (SEM; Hitachi Ltd., S-4300SD).

5.3 Result and discussion

To exchange Rb^+ to H^+ without dissolution of the precursors, the obtained $RbLn(MoO_4)_2$ (Ln=Pr, Nd, Sm, Eu) were stirred in dilute HNO_3 aqueous solution (0.01 M) at room temperature for 7 days. The Rb ions of the $RbLn(MoO_4)_2$ were successfully exchanged by H^+ without particle dissolution. The composition of $RbLn(MoO_4)_2$ before and after H^+ exchange was analyzed by XRF. The compositions are based on amount of Mo. In all sample powder, the amount ratios of Mo and Eu maintain after H^+ exchange procedure. On the other hand, there was remarkable change of amount of alkali metal ions. Fig. 5.1 shows the amount of Rb^+ ions in the precursors before and after H^+ exchange procedure. The ratio of remaining Rb^+ in protonated powders of $RbPr(MoO_4)_2$, $RbNd(MoO_4)_2$, $RbSm(MoO_4)_2$, and $RbEu(MoO_4)_2$ is 0.1, 0.0, 0.1 and, 0.1 %, respectively. In all sample, the amount of alkali metal ions in the protonated powders

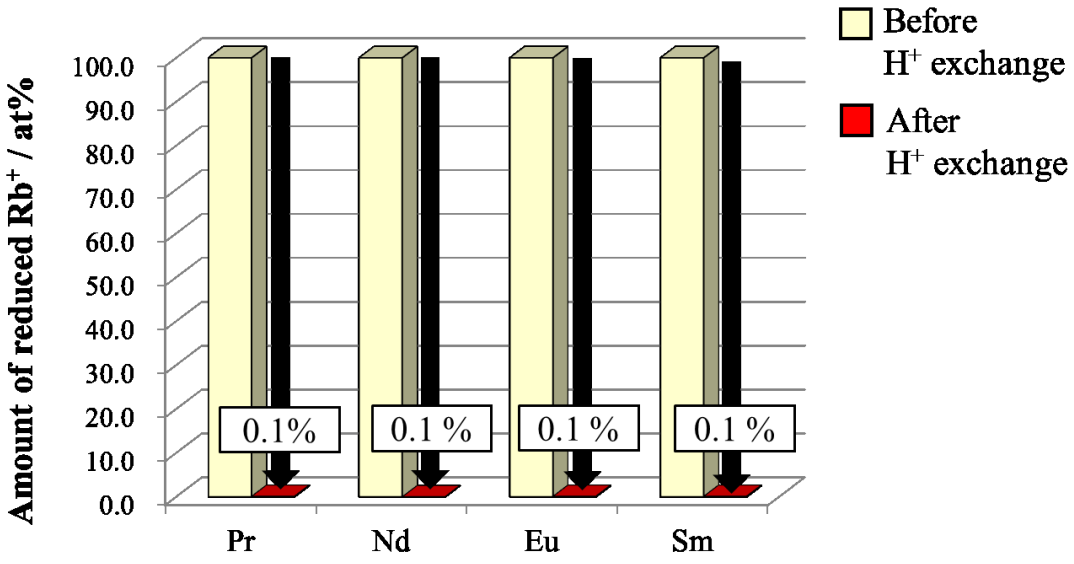

Fig. 5.1 XRF results of precursor powders synthesized by a conventional solid state method and dried protonated powder obtained by H^+-exchange method using 0.01 M HNO_3 for 7 d.

was reduced less 0.1 %. This result indicates that Rb ion in $RbPr(MoO_4)_2$, $RbNd(MoO_4)_2$, $RbSm(MoO_4)_2$, and $RbEu(MoO_4)_2$, respectively were completely exchanged by H^+, retaining their framework.

Fig. 5.2 shows the powder XRD patterns of the precursor $RbLn(MoO_4)_2$ powder and $HLn(MoO_4)_2$ powder obtained by the H^+ exchange of $RbLn(MoO_4)_2$. The precursor powders of $RbPr(MoO_4)_2$, $RbNd(MoO_4)_2$, $RbSm(MoO_4)_2$, and $RbEu(MoO_4)_2$ are described Pr-form, Nd-form, Sm-form, and Eu-form, respectively; the protonated powders are described HPr-form, HNd-form, HSm-form, HEu-form, respectively. All observed diffraction patterns of the precursor powder were well indexed the standard XRD pattern of orthorhombic $KY(MoO_4)_2$-type structure with the space group of *Pbcn*; the standard diffraction patterns were obtained from the inorganic crystal structure database (ICSD). In contrast, the XRD patterns of protonated powders were completely different from those of the precursor powders. This result indicates that the structures changed by H^+ exchange. All protonated powders have the new diffraction peaks which are not detected in the precursor powders; the new peaks are situated the similar area in all protonated powders. This result indicates that all protonated powders have similar structure by H^+ exchange. The peak below 10 degree in all protonated powders indicates that the layered structure related to precursor powders is still maintained after H^+ exchange and H^+/H_3O^+ with positive charge as counter cations was probably intercalated between MoO_4-LnO_8 layers with negative charge. In addition, this layered structure of protonated $HLn(MoO_4)_2$ powders is also similar to that of $HEu(MoO_4)_2$ powders obtained from triclinic $KEu(MoO_4)_2$ with the space group of *P*-1 and

monoclinic $CsEu(MoO_4)_2$ with the space group of $P12/c1$.

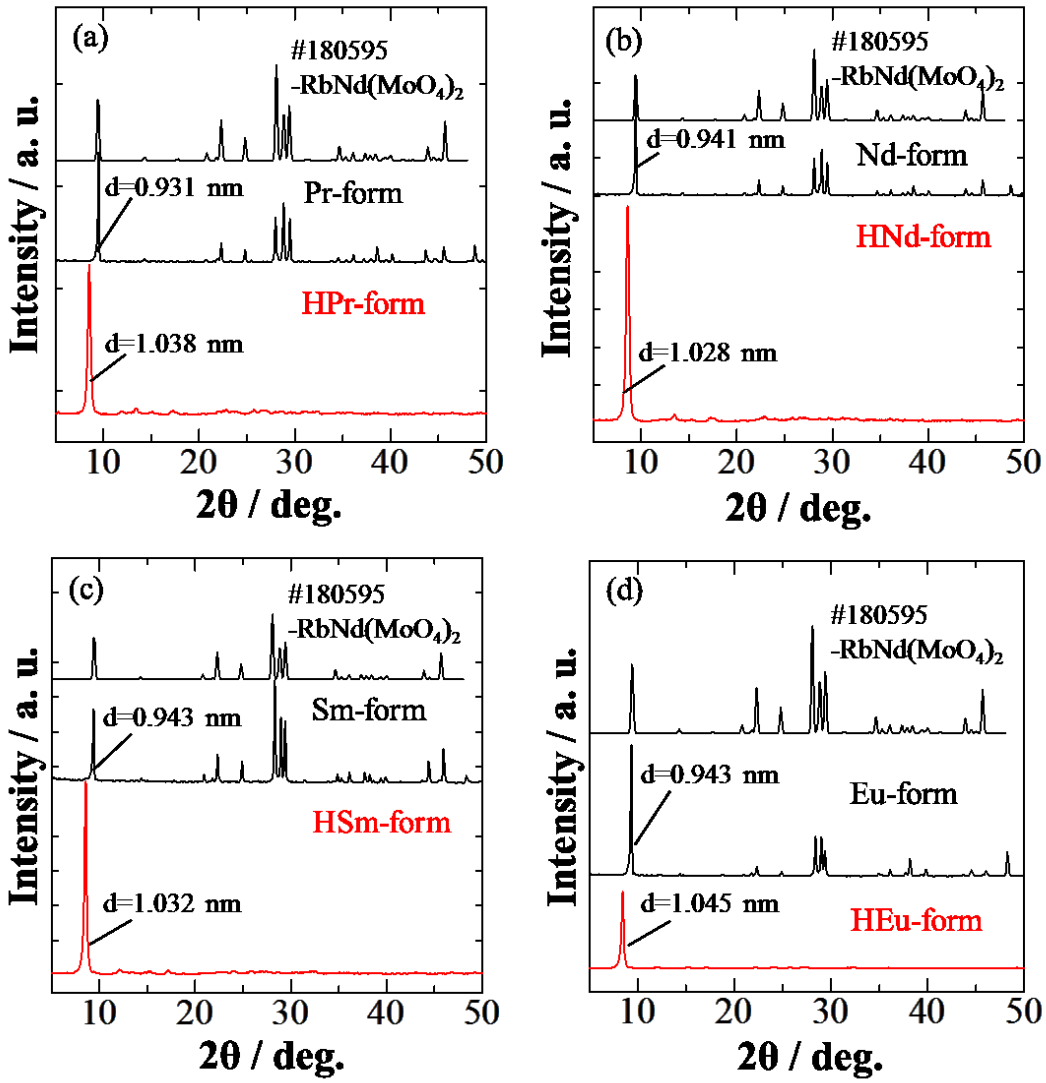

Fig. 5.2 the XRD patterns of (a) precursor $RbPr(MoO_4)_2$ (Pr-form) powder and protonated (HPr-form) powder, (b) precursor $RbNd(MoO_4)_2$ (Nd-form) powder and protonated (H-form) powder, (c) precursor $RbSm(MoO_4)_2$ (Sm-form) powder and protonated (HSm-form) powder, and (d) precursor $RbEu(MoO_4)_2$ (Eu-form) powder and protonated (HEu-form) powder. All A-form (A=K, Rb, Cs) powders were synthesized by a conventional solid state method. All dried H-form powders were obtained by stirring in 0.01 M HNO_3 at room temperature for 7 d and drying.

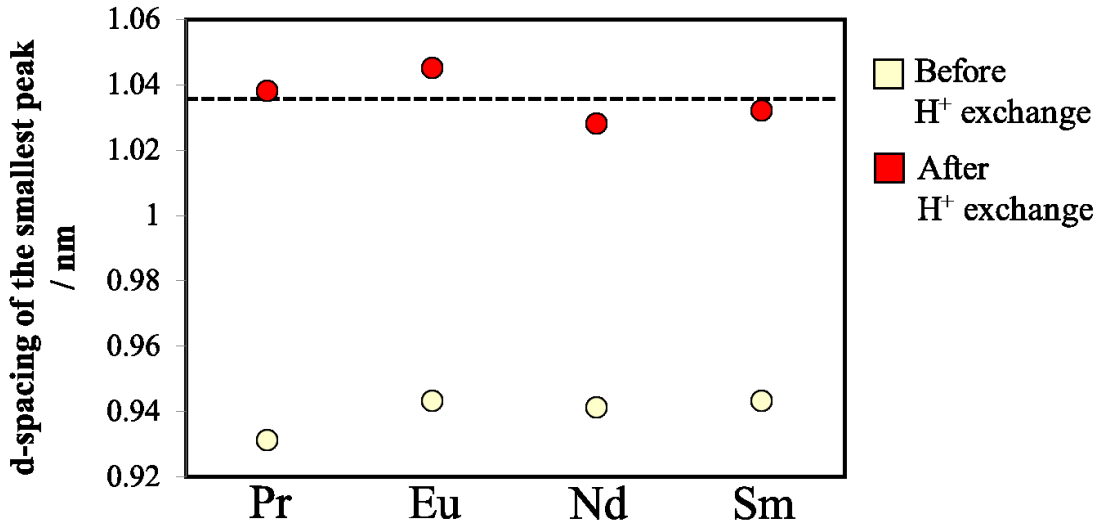

Fig. 5.3 the *d*-spacing of the smallest peak in the precursor and protonated powders, indicating the interlayer distance. The broken line shows the average *d*-spacing (1.036 nm) after H^+ exchange.

The *d*-spacing of peaks at the smallest angle reflect the interlayer distances of precursor powders with layered structure. Fig. 5.3 exhibits the value of *d*-spacing of the smallest peak in the precursor and protonated powders. Although the *d*-spacing of the smallest peak of precursor powders were different, those of protonated powders were similar, indicating that all protonated powders form similar interlayer distance by H^+ exchange regardless of that of precursors.

Fig. 5.4 shows the SEM images of the precursor $RbLn(MoO_4)_2$ powders and $HEu(MoO_4)_2$ powder prepared by the H^+ exchange of $RbLn(MoO_4)_2$. The particles of precursor Pr-form, Nd-form, Sm-form and Eu-form have a granular particle morphology; the particle sizes in all samples were over 10 μm. On the contrary, the protonated powders show different result from the precursor powders. HPr-from,

HNd-form, HSm-form and HEu-form have rod-like particle morphology. The rod-like particles contained smaller rod-like particles and formed bundles. These results indicate that the particle size and morphology of $RbLn(MoO_4)_2$ were successfully changed by the H^+-exchanging in the alkali metal site and the samples after H^+-exchanging maintain layered crystal structure. However, the length and width of HPr-from and HNd-form are clearly different from those of HSm-form and HEu-form. The rod-like particle in HPr-from and HNd-form 10 μm in average length, and most have outer average diameters ranging from 560 to 580 nm, while rod-like particle in HSm-form and HEu-form is less 20 μm in average length, and most have outer average diameters ranging from 300 to 360 nm; the aspect ratio of length/width of HPr-from and HNd-form, ranging from 17 to 18—is smaller than that of HSm-form and HEu-form (55–67). This result suggested that the different of rare-earth ion in the LnO_8 site cause the difference of morphology and size. The difference might relate to basic characteristics of rare-earth ions, such as electronegativity, and ion radius. However, the detail has been revealed.

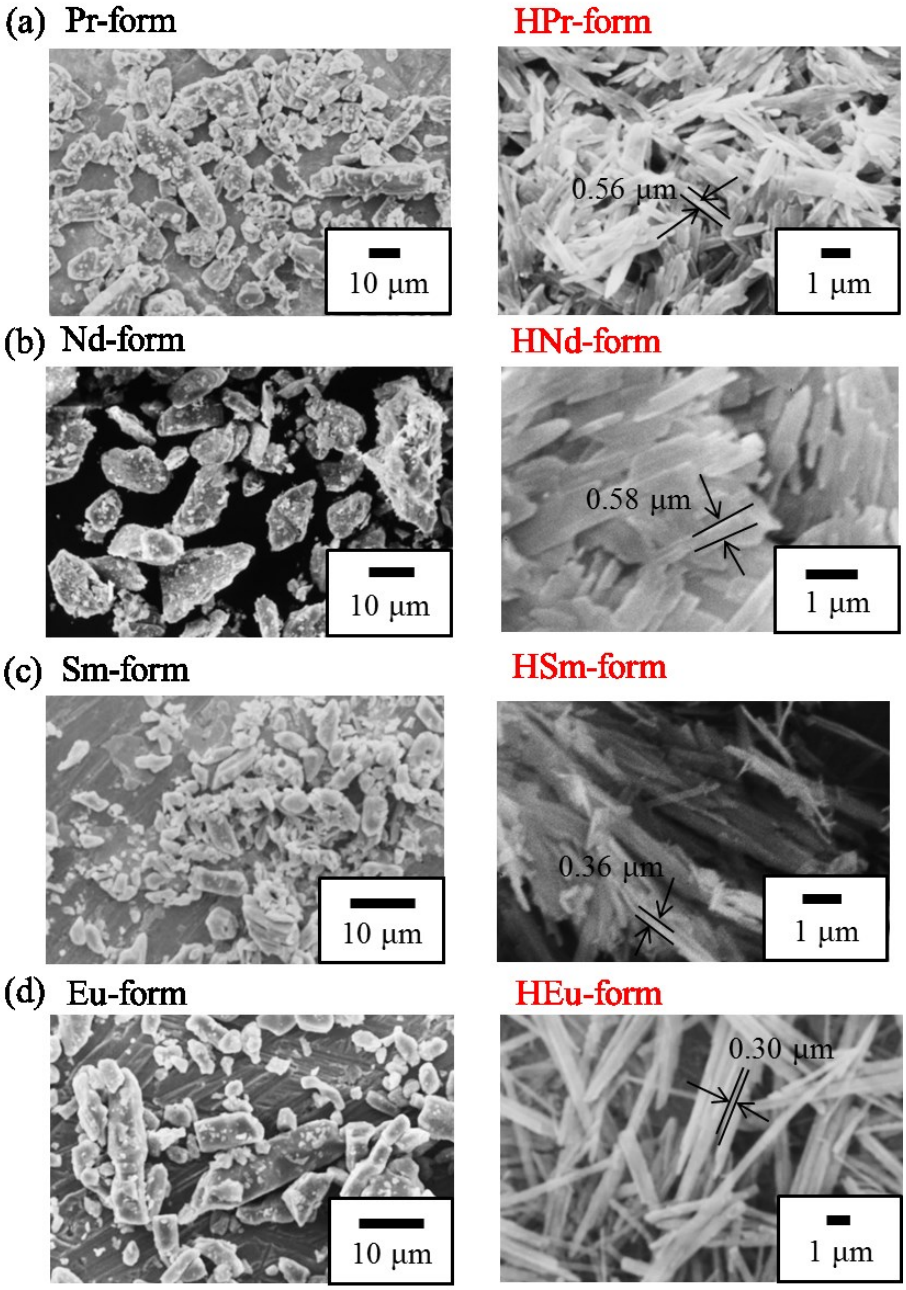

Fig. 5.2 the SEM images of (a) precursor $RbPr(MoO_4)_2$ (Pr-form) powder and protonated (HPr-form) powder, (b) precursor $RbNd(MoO_4)_2$ (Nd-form) powder and protonated (H-form) powder, (c) precursor $RbSm(MoO_4)_2$ (Sm-form) powder and protonated (HSm-form) powder, and (d) precursor $RbEu(MoO_4)_2$ (Eu-form) powder and protonated (HEu-form) powder. All A-form (A=K, Rb, Cs) powders were synthesized by a conventional solid state method. All dried H-form powders were obtained by stirring in 0.01 M HNO_3 at room temperature for 7 d and drying.

5.4 Summary

$HLn(MoO_4)_2$ (Ln= Pr, Nd, Sm, Eu) rod-like particles were synthesized by one-step ion exchange achieved by stirring orthorhombic $RbLn(MoO_4)_2$ (Ln= Pr, Nd, Sm, Eu) with the space group of *Pbcn* in 0.01 M aqueous HNO_3 solution at room temperature for 7 days. The obtained $HLn(MoO_4)_2$ protonated have rod-like particle morphology with 10-20 μm in length and outer diameters in the range of 300 – 580 nm. The aspect ratio of the rod-like particle of $HLn(MoO_4)_2$ (Ln= Pr, Nd) is smaller than that of $HLn(MoO_4)_2$ (Ln= Eu, Sm), although the *d*-spacing is similar in all sample. By using orthorhombic $RbLn(MoO_4)_2$ (Ln= Pr, Nd, Sm, Eu) with different rare-earth ions as precursor, therefore, the protonated $HLn(MoO_4)_2$ powder with different size and morphology and same structural property could be obtained. Bundled one-dimensional nanoscrolls, $HLn(MoO_4)_2$ are expected as laser materials and so on.

References

[1] P. V. Klevtsov and R. F. Klevtsva, *J. Struct. Chem.*, **18** (1977) 419–439.

[2] O.D. Chimitova, V.V. Atuchin, B.G. Bazarova, M.S. Molokeev, and Z.G. Bazarova, *Proc. of SPIE*, **3771** (2013) 87711A-1–9.

[3] V.V. Atuchin, O.D. Chimitova, M.S. Molokeev, T.A. Gavrilova, S.-J. Kim, N.V. Surovtsev, and J.G. Bazarov, *J. Crystal Growth,* **318** (2011) 683-686.

[4] V.V. Atuchin, O.D. Chimitova, S.V. Adichtchev, J.G. Bazarov, T.A. Gavrilova, M.S. Molokeev, N.V. Surovtsev, and Z.G. Bazarova, *Mater. Lett.*, **106** (2013) 26–29

[5] V.V. Atuchin O.Y. Khyzhun, O.D. Chimitova, M.S. Molokeev, T.A. Gavrilova, B.G. Bazarov, and J.G. Bazarova, *J. Phys. Chem. Solids*, **77** (2015) 101–108.

[6] V.V. Atuchin, A.S. Aleksandrovsky, O.D. Chimitova, C.-P. Diao, T.A. Gavrilova, V.G. Kesler, M.S. Molokeev, A.S. Krylov, B.G. Bazarov, J.G. Bazarova, and Z. Lin, *Dalton Trans.*, **44** (2015) 1805–1815.

Chapter 6

Concluding remarks

Scroll-type oxide nanotube is a very rare material and its property is so limited. Especially, there is no report on the molybdate-based nanoscroll with rare-earth ions. In this study, we could obtain molybdate-based nanoscroll with rare-earth ions which shows various functional properties by H^+ exchange at room temperature without organic compound and investigated its luminescence property under no organic compound. In addition, several nanoascroll materials with luminescence property could be obtained by design of crystal structure of the precursors. We could add a new page to the history of protonated oxides and oxide nanoscrolls. The summary of results is described as follows:

1. From chapter 2 to chapter 5, it is described that $ALn(MoO_4)_2$ (A= K, Rb, Cs, Ln= Pr, Nd, Sm, Eu, Gd, Tb) with layered structure are successfully protonated in dilute acid at room temperature and have faster proton exchange rate compared to other layered oxide materials, such as $K_4Nb_6O_{17}$, $KCa_2Nb_3O_{10}$ and $K_2La_2Ti_3O_{10}$. The detail TEM observation revealed that the transform of $ALn(MoO_4)_2$ into $HLn(MoO_4)_2$ nanoscroll with the H^+ exchange procedure. All crystal structure of the precursors, α-$KEu(MoO_4)_2$, $KY(MoO_4)_2$, and $RbLu(SO_4)_2$, could be protonated and transformed into the nanoscroll. This result suggests that the $(Ln(MoO_4)_2)_n$ layer is most important element for rolling up

of layer.

2. In chapter 2, the luminescence property of red-emissive $HEu(MoO_4)_2$ nanoscroll and the solution dispersed protonated powders were explained. The excitation spectra obviously shift to higher wavelength, causing by environment of Mo^{6+} — the coordination number of Mo^{6+} change higher coordination number by H^+ exchange and morphological change. In addition, the solution dispersed protonated powders shows both red emission and liquid crystallinity.

3. In chapter 3, the luminescence property of $HEu(MoO_4)_2:Gd^{3+}$ was explained. By the substitution Eu^{3+} with Gd^{3+} in the precursor crystal structure $KEu(MoO_4)_2$, the concentration quenching of Eu^{3+} could be suppressed and the luminescence intensity of $HEu(MoO_4)_2$ nanoscroll enhanced. The proton exchange ratio of $KEu(MoO_4)_2:Gd^{3+}$ is lower than that $KEu(MoO_4)_2$

4. From chapter 2 to chapter 4, the luminescence property of $HLn(MoO_4)_2$ nanoscroll phosphor was described. The luminescence property is completely originated to pure nanoscroll without organic compound.

5. In chapter 4, luminescence property of green-emissive $HGd(MoO_4)_2:Tb^{3+}$ nanoscrolls was described. It's noteworthy that the optimal concentration changed after H^+ exchange. In addition, in chapter 5, the structural and morphological properties of

$HLn(MoO_4)_2$ (Ln= Pr, Nd, Sm, Eu) was described. The morphology of the nanoscroll changes by change of rare-earth ions, suggesting that we can control morphology by changing rare-earth ions in precursor materials. These results indicate that $ALn(MoO_4)_2$ with layered structure could broaden the area of application by change the alkali ion and rare-earth ions.

As demonstrated above, the objectives of this this were achieved. A novel nanoscroll material was successfully synthesized by H^+ exchange without organic compound. The materials were freshly included on a list of nanoscrolls as the first example molybdate with rare-earth ions. In contrast, the properties of this material will abundantly extend depending on design of the crystal structure of the precursor.

Acknowledgement

The author would like to express is sincere gratitude to my supervisor, Associate Professor Dr. Kenji Toda, Graduate School of Science and Technology, Niigata University, for giving him this precious study opportunity as a Ph. D candidate student in Toda's research group.

The author would deeply like to thank Professor Dr. Mineo Sato, Assistant Professor Dr. Atsushi Itadani, Research Assistant Professor Dr. Sun-wook Kim, Dr. Research Assistant Professor Kazuyoshi Uematsu, and Postdoctoral researcher. Dr. Dai Okada, Niigata University, for their great advise, suggestions and encouragements. The author would also like to thank. Associate Professor Dr. Naoki Kano, Niigata University, for their kind informative suggestions in this thesis.

The author also thanks the co-workers, Dr. Takuya Hasegawa, Mr. Ryota Yamanashi, Mr. Shota Kumagai, Mr. Masaru Muto, and Mr. Yusuke Abe for their assistance, and all other members of Toda's and Sato's research groups for their helpful and valuable experimental suggestions.

The author also thanks for support by office administrator, Ms. Junko Takahashi, members of N-luminescence, Ms. Masako Toda, Ms. Mieko Kawakami, and Ms. Junko Koide, PragNotes Dr. Shigeki Shirakura.

Finally, the author has sincerely grateful to his family, Mitsuru Watanabe, Michiyo Watanabe, and Takanori Watanabe, for providing him a chance to study again at Niigata University.